SEVERE CONVECTIVE MESOSYSTEMS IN NEW ENGLAND

by

JAMES ELBERT KESTER

S.B., Massachusetts Institute of Technology
1966

SUBMITTED IN PARTIAL FULFILLMENT

OF THE REQUIREMENTS FOR THE

DEGREE OF MASTER OF

SCIENCE

at the

MASSACHUSETTS INSTITUTE OF

TECHNOLOGY

February, 1974

Signature of Author_____
Department of Meterology, February 5, 1974

Certified by_____
Thesis Supervisor

Accepted by_____
Chairman, Departmental Committee on Graduate Students

ABSTRACT

Title: Severe Convective Mesosystems in New England

Author: James Elbert Kester

Submitted to the Department of Meteorology on February 5, 1974 in partial fulfillment of the requirements for the degree of Master of Science.

This study of convection over New England is divided into two parts. Part I is a search for a consistent mesoscale pressure pattern associated with severe convective storms over southern New England during the summers of 1971 and 1972. Such a pattern was found in four of the ten cases studied, but due to data problems was not well defined. In Part II a numerical model was derived from the budget equations for heat and water vapor and was used to determine if the effects of small scale convection are detectable in the synoptic radiosonde network in the New England area. The effects of both convection and radiation were detected in large sample statistical analyses of the model output parameters. The variances of the model parameters were too large to permit detection of the effects of convection on a day-to-day basis.

Thesis Supervisor: Frederick Sanders

Title: Professor of Meteorology

TABLE OF CONTENTS

TABLE OF CONTENTS, Continued

LIST OF TABLES

LIST OF FIGURES

LIST OF FIGURES, Continued

1. Introduction:

Rules of thumb are often the product of long years of experience and careful scrutiny of all available weather data. This thesis is an attempt to study two rules of thumb involving thunderstorm activity in the southern New England area.

Part I concerns itself with Professor Frederick Sanders' tentative rule, formulated in the summer of 1971, that a certain common pattern of mesoscale activity was associated with occurrences of severe convective weather in New England.

Part II is a numerical study of the hunch of many meteorologists that convective activity results in a stabilizing of the atmosphere in an area by cooling at low levels and heating and moistening aloft. This is a crude statement of the refined question being studied by cumulus parameterization researchers: "How does convective activity, at its very small scale, influence meteorological parameters on the much larger synoptic scale?" Part II is directed at the basic assumption of this question: "Is the influence of convective activity detectable in the synoptic-scale observing network and if so, to what degree?"

PART I:

2. Preliminary Studies:

As just stated, this part of my research was a search for a consistent mesostructure associated with severe convective weather in New England.

This investigation began as a preliminary study of several synoptic situations during the summer of 1971 which showed promise of stronger-than-normal convective activity in the New England area. Professor Sanders had plotted surface charts of the Service "A" teletype reports for each hour from mid-afternoon into the evening on days when strong convection was expected. Table I is a list of these preliminary cases.

When analyzed for pressure, these charts showed a tentative pattern: a mesoscale high forming along the east slopes of the Appalachians in the late afternoon. In conjunction with this the pressure at Concord, New Hampshire, seemed to jump just after the passage of a thunderstorm at Concord and prior to the arrival of heavy thunderstorm activity in the Boston area.

3. Selection of Cases:

As the beginning of my research, I attempted to reconstruct the thinking which led Professor Sanders to select these few days as having severe thunderstorm potential. I checked all available facsimile maps on file for each case and noted the consistent features. Each case was characterized by passage of a northeast - southwest oriented cold front through New England. This cold front trailed from an eastward moving low centered, at 0000Z on the evening of the case, in northern New England, the St. Lawrence Valley, or eastern Canada. The front in each case was tilted to the east far enough that the surface pressure at Boston prior to frontal passage was lower than the pressure at New York (Kennedy International) for the same time. This is not usual for north-south oriented fronts. Examination of teletype sequences showed passage of the cold front at New England coastal stations to have occurred within a few hours after 0000Z.

Having determined these common characteristics of the Sanders cases, I went back to the map files and screened all the surface charts available (only 0000Z and 1200Z are archived at M.I.T.) for the months of June, July, and August of 1971 and 1972. A list was made of days exhibiting the characteristics above; cases for more detailed study would be selected from this list.

As a first check, however, the Boston synoptic six-hourly observations were scanned for thunder in the current and past weather blocks,

and a list of thunder occurrences for the same periods (June through August, 1971 and 1972) was compiled and compared with the case list. Neither list matched the other completely. It was found that Boston always had at least rain showers with each case on the list, however.

The initial list contained some 24 frontal passage cases, a number too large to allow detailed study of each in the time available. It was decided to limit arbitrarily the cases studied to around ten. The list was thinned out based on the following facts:

Film strips of the MIT WR-66 radar scope were not available for many of the cases.

Concurrent teletype reports of surface or upper air observations were missing from the MIT Meteorology Department archives in some cases.

Although fewer cases occurred in 1972 than 1971, it was desirable to have study cases from both years.

One case with a morning (after 12Z) frontal passage was retained to study any differences between the mesoscale phenomena occurring during daytime heating and during nighttime cooling.

The ten cases finally selected are listed in Table II.

4. Area of Study and Time Intervals:

Figure I shows the area of study and the surface observing stations within this area. The area was selected to be larger by a factor of four or more than the primary area of study, i.e. New England east of the Appalachian divide. This size of analysis area allows the analyst to distinguish those features which advect or move into an area from those that develop there. Further, in statistical analysis of station parameters, the influence of a mesoscale variation will be smaller the larger the area over which the statistics are derived. When one is looking at a feature in terms of its deviation from larger scale norms, it is undesirable to have it bias the norms to any great degree.

The analysis interval is as crucial as area in mesoscale analysis. Bosart, et. al. (1972) speak of mesoscale features in terms of not only tens of nautical miles, but fractions of hours as well, with lifetimes of mesoscale features of only a few hours. Thus it behooved me to examine data with the capability of resolving features of very short time duration.

5. Data Collection:

Two types of data were finally selected for study: surface observations and films from the M.I.T. radar.

Surface Data:

Mesoscale features appear in the fields of surface wind, temperature, and pressure. Wind and temperature are noticeably influenced by station altitude, local topography, and other smaller-than-mesoscale influences. Pressure thus seemed the best parameter to study, particularly since both the sea level pressure and altimeter setting are "corrected" to sea level for station altitude.

I decided to use altimeter settings for this study for two reasons: First, not all observing stations compute a sea-level pressure every hour, and as mentioned before, it is important here to have parameters observed at short intervals. Furthermore, stations such as New Bedford do not report sea level pressures at all. Since most weather observing stations are located at airports, altimeter settings are reported at least hourly for aircraft operations.

Second, the correction applied to the altimeter setting is not subject to meteorological influence as is the correction to sea-level pressure. The correction to sea level pressure is computed based on the current station temperature and the temperature twelve hours before. As such, the temperature and hence the correction are subject to both meso- and synoptic-scale influences. The altimeter correction

assumes a fixed temperature-pressure relationship and is thus a constant regardless of time of day or year, or synoptic situation. It was anticipated that considerable noise would appear in the pressure observations; the inclusion of the temperature influence would have added still more noise.

The decision to use altimeter settings (ALSTGs) did give away some advantages. First, ALSTG is only measured to four significant digits (± .005 in.) versus five digits (± .05 mb) for sea level pressure. Also, some stations (climatological and synoptic reporters only) never compute altimeter settings. I decided in these cases to compute an "ALSTG" simply by multiplying the sea level pressure by a constant (29.92 in/1013.25 mb = .0295 in/mb). In these few cases the temperature noise would intrude.

The map area selected was searched for all available surface observations for 1971 and/or 1972. In addition to National Weather Service first order stations, which operate 24 hours per day, all stations at which surface parameters were observed were researched even if only four or five observations per day were available. I obtained microfilm or xerox copies of observation logs for all stations which were not available on archived Service "A" teletype sequences for the cases listed in Table II. I did not attempt to obtain from Service "A" stations those observations which were missing occasionally on the teletype sequences. Figure 1 shows all the stations used.

Radar

The sole available radar film for my cases was from the M.I.T. WR-66 weather radar. Characteristics of this radar are shown in Table IV. A range circle of 100 nautical miles, shown on Figures 3 and 8 through 16, is the approximate effective range of this radar set.

Tracings of these radar films were made. For each case, the frames closest to five minutes of each hour were traced, plus the initial and final frame of each series, if within the case time frame. Tracings were done on the same scale as the maps used for the pressure analyses (described later). Levels traced were 2, 5, 7, 8, 9, and 10 decibels.

6. Pressure Reduction Program:

The surface pressure at any given station may be viewed as the sum of several influences

$P = P_{syn}$ (synoptic and larger scale variations)

$+ P_{sub}$ (sub-synoptic scale variations)

$+ B$ (systematic errors - "bias" in measurement and computation)

$+ D$ (diurnal variation)

$+ N$ (microscale "noise" and random errors)

Denoting a time average over a long period (more than several days) by an overbar,

$$\overline{B} \approx B$$

$$\overline{D} \equiv \phi$$ if Δt is large or an integral number of days

$$\overline{N} \equiv \phi$$

If we further hypothesize that Δt is large enough that

$$\overline{P}_{SUB} \approx \phi$$

then

$$\overline{P} \approx \overline{P}_{SYN} + B$$

Turning for a moment to an average of pressures at different stations over a "large" area (denoted by $\overline{X}^A$)

$$\overline{D}^A \approx D$$

and

$$\overline{P}^A_{SUB} \approx \phi$$

Now subtracting:

$$P - \overline{P} \approx (P_{SYN} - \overline{P}_{SYN}) + P_{SUB} + D + N \tag{6.1}$$

and further:

$$(P - \overline{P}) - \overline{(P - \overline{P})}^A \approx (P_{SYN} - \overline{P}_{SYN}) - \overline{(P_{SYN} - \overline{P}_{SYN})}^A + P_{SUB} + N \tag{6.2}$$

Thus we see from (6.1) that subtracting off the long term mean removes any systematic error from the observations of pressure. This is necessary in mesoanalysis if stations with different biases are to be used in the analysis.

In (6.2) the effects of diurnal variation have been removed by subtracting off the area mean, assuming the area is small in the east-west direction compared to (one hour)$\cdot\Omega\cdot a$, where Ω is the angular

velocity of the earth's rotation and a is the mean radius of the earth. This distance is 1672 km or about 870 N.M. If the area is comparable in span to this number, the diurnal wave will be detectable between the east and west boundaries, and $\overline{D}^A$ at any one time will not be equal to the D at any given station.

D, the diurnal variation, need not be removed in any event, since in an hour by hour map analysis of pressure it will merely represent a constant (approximately) added to the value of all isobars, if the map is over a small enough area.

Note that while the synoptic and larger scale influence is reduced in some sense by the subtraction of averages, it is never removed completely. The smaller the scale of these influences the more will remain after this calculation.

Due to the large number of cases (10), hours (12-15), and stations (100), a FORTRAN program was written to reduce the pressure data according to (6.1) and (6.2).

Pressure data from all available station logs and teletype sequences were extracted for each case and entered on punched cards by station number and hour of observation. Where the (preferred) altimeter setting was not available, the sea level pressure was used if available, and flagged for conversion by the program. Missing data were ignored.

The program reads in the card data for

each case, performs a check for wrong case number on each card, and converts any sea level pressure encountered to a bogus altimeter setting. All pressures are then stored in a two-dimensional array by station number and time (to the nearest hour), where the averaging over time and area can be done.

The results of this simple data reduction were printed for each case by time and station number. Hourly maps were plotted from this reduced data and analyzed at intervals of .02 inches of mercury. Some results are shown as Figures 8 through 16.

Before discussing these results, a look at the effects of the program reduction is in order.

First, it can be shown that if the typical synoptic variation is simply a pressure fall followed by a rise (for the cold fronts I am studying), then the largest values of the processed p will occur at stations near the east and west edges of the analysis area at the earliest and latest map times. These stations will experience either a continuous fall or continuous rise over most of the case period, while stations near map center will experience a fall and a rise, each of about half the amplitude of the edge fall or rise. This effect is shown graphically in Figures 2a through 2c.

Second, any time average corresponds in real time to a specific map time at a given station. That is, since pressure is a continuous variable and a function of time, there will be at least one time in the

case period where the observed (or interpolated) pressure will be equal to the time mean. This means that for stations which are close together on the synoptic scale, that time will occur at very nearly the same map time, and at this map time the $p - \overline{p}$ values will all be nearly zero. Hence there will be very little synoptic gradient in this small area except for the mesoscale and other subsynoptic gradients. (This is somewhat the inverse of the first effect mentioned.)

Finally, the effects of missing data cannot be ignored in the analysis process. Figure 2d shows the effect of data missing due to a station's being closed at night. Since most of our cases have the lowest pressure (frontal passage) occurring near 00Z, and day-only stations are closed from roughly 01Z to 09Z, a batch of low pressures will be missing, and the time mean will be artificially high. This effect was empirically allowed for in the analysis of the plotted maps.

7. Results:

The overall results of these pressure-radar analyses are summarized in Table III.

In four of the ten cases, a strong mesoscale pattern of highs and lows was evident well ahead of the synoptic scale front. These cases (numbers 2, 3, 5, and 7) are discussed later. In five of the remaining cases, some pressure mesostructure was evident, but was weak or could not be easily followed from hour to hour. The remaining case was the nighttime case (number 8) and failed to show any mesoscale pattern: this was probably due to the absence of a large number of observing stations, those not operating during the night. The widely spaced nighttime stations, predominantly National Weather Service first - order stations, were too widely spaced to define any mesoscale pattern ahead of the strong cold front. This does not imply that no mesostructure was present, only that the analysis technique with the data used did not resolve any. Any mesostructure should still be evident in, for example, the barograph traces for the first-order observing stations.

The radar tracing sequences show more similarity than the pressure analyses. In all but one of the ten cases the radar showed distinct lines of shower and thunderstorm echoes oriented parallel to the cold front and also parallel to the predominant upper flow. (For example, the echoes shown in Figures 9 through 12 for Case 7 are aligned roughly

along the upper winds which were 240° at 40kt at 500mb and 240° at 35kt at 700mb at 12Z 11 August 1971, changing to 230° at 50kts at 500mb and 250° at 35kts at 700mb at 0000Z 12 August 1971.) Echo coverage over southern New England varied from widely scattered cells (<1%) to areas and lines covering 30 - 40%.

Severe weather occurrences for each case were extracted from the Department of Commerce/National Weather Service publication Storm Data and plotted on the same scale chart as the pressure analyses. This data is also summarized in Table III. In general, severe weather occurrences correlated well with percent of echo coverage. The more cells, the better the odds of having some cells in the area spawn severe weather.

To check the results for validation of the theory on which the pressure program was written, station (time) mean pressures and map (area) mean pressures were plotted for each case.

Figure 3 is the time mean pressure analysis for Case #7, and is typical of most of the time mean maps analyzed. As expected, higher pressures appear at the southeast and western map extremes, with the lowest pressures in the north where the case criteria low was situated. The most prominent and common feature among the cases is the double trough pattern over New York and southern New England. In this case the troughs are more pronounced than in the other cases, where the troughs extend along the New England coast from Bangor to Boston, and

over southern New England from Providence to New York City.

These features cannot be completely or adequately explained by a single synoptic scale cold front transiting the area, nor by a consistent pattern in the observing bias (B), since this pattern is not located in exactly the same place in any two cases.

A possible explanation might be that these troughs are meso-scale equivalents of the "lee-side trough" observable in the 500mb climatological charts downwind of the Rocky Mountains. Two reservations limit the credibility of this explanation. First, one of the troughs is probably associated with the synoptic cold front. Second, it is debatable whether the time and space distribution of observations is adequate to define an effect of this character in my analyses. Comparing Figures #1 and #3, it seems obvious that the ridge between the double troughs is defined more by stations bordering the ridge than by one or more stations under the ridge itself. It is possible that a fortuitous conjunction of bias errors at the surrounding stations in this case "defined" a feature that really isn't there. The variations of these bias errors from case to case might also be responsible for the differences in strength and location of the trough pattern from case to case.

Geographical variation is evident in the bias (B) from several of these mean maps. Highs appear distinctly over the Catskills of New York and Poconos of Pennsylvania in all cases and over the Green Mountains of Vermont and Adirondacks of Northern New York in Cases 4 and 9.

I should mention that these analyses were not easy to draw. The station to station variation of B was considerable in each case, and isolines of mean pressure could be placed only approximately in some areas. The variations mentioned above were strong enough to stand out over this random variation of B. The random variations on the Case 7 chart, for example, were spread over about 30 of the observing stations. The mean magnitude of the difference between analyzed and observed mean pressure was 3 hundredths (3/100) of an inch over the "reliable" stations with a maximum difference of 12/100. Over the ten least reliable stations the mean difference was 13/100 with a maximum of 45/100. These variations occurred primarily at those stations which reported infrequently, although even some 24-hour reporting stations participated in these considerable deviations.

The plotted curves of the map (area) mean pressures are shown in Figures 4 through 7. With the exception of Case 8 (Figure 7), all curves show the influence of the diurnal variation, although in the latter half of Case #1 (Figure 4) the diurnal variation is washed out. The synoptic variation of pressure in 24 hours is seen to be about 8 to 12 hundredths of an inch of mercury, roughly twice the diurnal variation.

The Case 8 curve (Figure 7) does show some influence of the diurnal variation between 1600Z and 2000Z where the strong rise due to the synoptic high moving in is almost cancelled by the drop in the diurnal

pressure curve during this period. On the whole, however, the synoptic variation of the pressure in Case 8 seems to be so strong as to wash out the diurnal effects completely. Here the 24 hour variation of pressure is three times the diurnal peak-to-trough variation.

The Mesostructures:

Cases 2, 3, 5, and 7 exhibited a pronounced mesostructure with several features similar among the cases. It is interesting to note that all of these are listed in Table I as preliminary cases selected by Professor Sanders. Another of his cases corresponds to case number 6 and his remaining two were not selected under my criteria. This tends to confirm, to some extent, the correctness of Professor Sanders' original thinking in selecting these dates for study, as well as confirming the criteria by which my cases were selected.

In Cases 2, 3, 5, and 7 a meso-high formed in the Concord, New Hampshire area (in Case 7, the Lebanon-Montpelier area) and moved southeastward to off the coast, varying in size and intensity with the echoes around it. These highs were occasionally preceded by a corresponding meso-trough. The highs tended to lie under or behind lines or cells of strong radar echoes. Highs formed around 19Z in the afternoon, usually rapidly, and dissipated offshore after 02Z. The history of these highs, once past the coast, is in doubt since the mesoscale observing capability tends to end at the water's edge except south of

Cape Cod. Thus it was not possible to follow highs (or anything else) far over water.

We will now take a closer, blow-by-blow look at Cases 7 and 2.

Combined pressure and radar charts for Case 7 are shown in Figures 8 through 12. In Figure 8, the 15Z mesoscale pressure pattern is relatively flat with isobars roughly parallel and oriented northeast-southwest. The synoptic scale frontal trough is still well northwest of the St. Lawrence River. A line of convective echoes is evident beyond the 100 NM circle in the northwest quadrant of the M.I.T. radar. By 16Z this line of echoes had moved to within 100 NM of M.I.T. and acquired more detail. A flat high-pressure area had formed over Lebanon, New Hampshire and Montpelier, Vermont with a weak ridge extending south to Worcester. By 17Z this ridge had intensified and rotated to lie northeast-southwest from Berlin to Keene. The line of echoes continued to move southeast, spawning tornadoes at Fryeburg, Maine (1730Z), Bridgton, Maine (1745Z), and, beyond radar range, at Bingham, Maine (1800Z). Figure 9 at 18Z shows the continued advance of high and echo line. The small high near New York City apparently developed there after 17Z or moved in undetected at Stewart or Poughkeepsie. The scattered echoes in Massachusetts and Connecticut at 18Z developed into a separate line extending from Worcester to Bridgeport by 19Z. (It is possible that the mini-high at New York

in Figure 9 was associated with a line of echoes which grew northeastward to form this Connecticut line; however, the New York City area is completely beyond the range of the M.I.T. radar, so this must remain merely conjecture.)

At 19Z the ridge behind the main line of echoes was visible all the way from Caribou to Keene, and the synoptic trough had just moved into western New York and the St. Lawrence Valley. By 20Z the ridge had reached the coastline and the echoes had weakened. A third line of echoes, weaker than the first, formed from Keene to Poughkeepsie. At 21Z (Figure 10) this line had moved southeastward while the main ridge (now near Pease) had weakened on the coast and the advance echoes had dissipated into weak areas and isolated cells. The synoptic front across New York State is amorphous. At 22Z the third echo line extended from Pease Air Force Base to Bradley with a remnant of the high-ridge over Boston. By 24Z (Figure 11) the ridge was almost gone except near Presque Isle, and a fourth echo line, tied to the synoptic frontal trough, had moved into western Massachusetts. This line, weaker still than the first three, continued eastward with the synoptic frontal trough, shown (at 0300Z) in Figure 12 lying down the Connecticut Valley and along the south coastal waters.

Case 2, shown in Figures 13 through 16, was notable for its exceptionally strong radar weather. The pressure patterns at 15Z

and 16Z were flat except for a weak low over southeastern Massachusetts, which may reflect measurement errors. The 17Z picture (Figure 13) is remarkably similar to Figure 8 for Case 7. The synoptic front is just east of the St. Lawrence Valley. By 18Z the echo area had moved over Lebanon into the 100 NM radar circle with no pronounced pressure pattern change. At 19Z the pressure at Concord jumped rapidly after a heavy thunderstorm struck. By 20Z (Figure 14) the strong echoes had passed Manchester with the strong high behind it and a trough ahead of it from Boston to western Massachusetts. A second area of echoes was forming over the northwest corner of Massachusetts. The first echo area, which had been moving to the right of the upper winds since passing Manchester, passed over Cape Ann by 21Z, striking Essex, Massachusetts, with 77 mph (64 knots) winds out of heavy thunderstorms. Meanwhile the second echo area in western Massachusetts grew rapidly northeastward to Portsmouth into a line of strong echoes with the pressure ridge under it. This line moved southeastward to the Portsmouth-Bradley line with a wavelike feature near Worcester. At 23Z (Figure 15) heavy thunderstorms struck Norwood and South Weymouth, Massachusetts, as this Line Echo Wave Pattern (LEWP) moved rapidly eastward along the echo line. Pressure made extreme jumps at both South Weymouth and Norwood behind this LEWP. The synoptic trough at this point extended from Oldtown to Wilkes-Barre. From 23Z onward

the pressure and echo patterns continued to move southeastward, weakening as they neared the coast. By 02Z (Figure 16) the synoptic trough dominated the pattern with the remainder of the meso-high south of Rhode Island and weak echo areas scattered over the southern coastal waters. The passage of the frontal trough offshore cleared these echoes completely.

Case 2 was noted, surprisingly, not for many isolated occurrences of severe weather such as large hail or tornadoes, but for widespread reports of heavy rain, strong winds, and hail. The Storm Data summaries show statewide severe weather in all New England states but only a few instances of localized storm damage.

Case 7 differs from the other three mesostructure cases in that the initial meso-high formed further to the northwest, over Lebanon-Montpelier, rather than in the southern New Hampshire area. Figure 8 does show the associated echo line detectable at about 115 NM from the M.I.T. radar; to appear as a line at this distance the line of convection must have been exceptionally strong and well-organized, leading to the suspicion that it did not develop over the mountains but moved in from further out-of-range. It is also possible that the mesohigh was misplaced in the analysis due to the relatively sparse observing net over the Green Mountains; neither Rutland or Berlin reported around this time.

Note that the synoptic-scale trough is difficult to follow or

find in some figures. This is a feature common to all ten cases, and is undoubtedly due to the fact that there is some mesostructure to the front (trough) itself regardless of whether a consistent meso-structure precedes it. The "trough" associated with the cold front looked more like a string of amorphous low pressure areas than an actual trough on most maps. My study was more concerned with the pre-frontal structure. Perhaps a separate study could be done of the frontal structure itself.

8. Conclusions:

These pressure analyses need more work. The primary limitations on the analysis of these are the noise introduced by poor and missing data. As previously discussed, data missing can make a 24-hour station mean pressure spuriously low or high, with resultant noise in the plotted difference of station pressure minus station mean pressure. In six cases this noise was a serious problem. A better algorithm is needed for correcting for missing data. This algorithm should include a means for use of data from infrequent reporters such as the Coast Guard stations, which report only every three hours, and stations such as Laconia and Saranac Lake, which report three or four times daily.

It also appears from the results discussed that subtracting off the synoptic- and larger-scale variations was not very successful. The impact of missing data is particularly severe. A better method of analysis might be to examine the fields of pressure change by plotting and analyzing the hour-to-hour pressure changes at all stations. Missing data would still be a problem, but would not contaminate the analysis for times other than the times which would have used the missing data. Naturally stations with observations more than an hour apart (e.g. synoptic-only reporters and Coast Guard stations) could not be used.

More definite results would also entail better observing coverage.

Mesoscale features were seen to appear suddenly over areas of good station density when it was apparent they had actually moved in from an area of sparse coverage. This was noticeable in Maine, where the interior is sparsely populated while the coastal region has a dense observing net. Also some systems moved into the southern New York-Long Island area from the sparsely observed Catskills-Poconos area. Vermont and New Hampshire are not densely observed either. Meso-studies in New England will require more 24 hour observing stations in the nether regions.

PART II:

9. The Convective-Synoptic Interaction: Review of the Literature:

The study of the interaction of convective scales of motion has been increasing in recent years. The recent review by Ogura (1972) covers the field quite adequately. While many workers (e.g. Ogura and Cho [1973], Yanai, et al [1972]) are concerned with the interaction of cumuli with the large scale tropical air masses, others, including Ninomiya (1968, 1971), have attempted studies of budgets of parameters in the mid-latitudes.

The case study of Ninomiya (1971) is a good example of the work currently being undertaken. Ninomiya first does a descriptive analysis of a severe thunderstorm situation in the eastern United States using ATS-III pictures and conventional meteorological observations. He then proceeds to study budgets of heat and moisture in an area bounded by Pittsburgh, Washington D. C., Greensboro, North Carolina, and Huntington, West Virginia. The numerical analysis of the budgets for this area, derived from the rawin observations of these four stations, yields various insights into the processes accompanying the severe convection taking place there.

The first point to be raised in this study and others like it is a fundamental one: Does the data have the capability of supporting the conclusions being drawn? Would the budget calculations look any

different for a period when the area studied contained only clear subsiding air? Do the vertical profiles found in one case have similarity to those from other cases of severe convective weather--that is, are the results repeatable?

The objective of Part II of this thesis is to examine these questions for an area over New England. I begin by deriving my own set of budget equations.

10. Derivation of Equations:

First I will examine the budgets of various quantities in a volume of the atmosphere. Imagine a frame of reference fixed at the earth's surface near New England with coordinates x, y, and z in the north, east, and vertical directions. For the moment, assume that the fields of $\underset{\sim}{V}$, T, q, l, and i are known over a defined volume. (Symbols are defined in Table V.) For convenience, I will use p as the vertical coordinate instead of z, using the hydrostatic approximation:

$$\frac{\partial p}{\partial z} = -\rho g \tag{10.1}$$

A knowledge of the $\underset{\sim}{V}$ field and a vertical boundary condition (e.g. at the earth's surface or some level aloft) then completely specifies the ω field through the equation of continuity:

$$\nabla \cdot \underset{\sim}{V} + \frac{\partial \omega}{\partial p} = \phi \tag{10.2}$$

which implies:

$$\omega(p) = \omega(p_0) - \int_{p_0}^{p} \nabla \cdot \underset{\sim}{V}\, dp \tag{10.3}$$

For a small parcel of air in my volume the change of any variable f is defined as:

$$\frac{df}{dt} \equiv \frac{\partial f}{\partial t} + \underset{\sim}{V} \cdot \nabla f + \omega \frac{\partial f}{\partial p}$$

and, for any f:

$$\frac{df}{dt} = \sum \text{(sources of f)} + \sum \text{(sinks of f)}$$

Deriving the heat equation first, I start with the first law of thermodynamics, stated as:

$$Q = \frac{dI}{dt} + \frac{dW}{dt}$$

where Q is defined, after the manner of Lorenz (1967), as a net rate of heating from all sources and sinks.

For gases:

$$I = C_v T$$

and

$$dW = p\, d\alpha$$

so

$$Q = C_v \frac{dT}{dt} + p \frac{d\alpha}{dt} \tag{10.4}$$

I introduce here the simple equation of state:

$$p\alpha = RT$$

from which

$$p = \frac{RT}{\alpha} \tag{10.5}$$

and

$$\frac{1}{p}\frac{dp}{dt} + \frac{1}{\alpha}\frac{d\alpha}{dt} = \frac{1}{T}\frac{dT}{dt} \tag{10.6}$$

Combining (10.4) and (10.5):

$$Q = C_v \frac{dT}{dt} + \frac{RT}{\alpha} \frac{d\alpha}{dt}$$

and using (10.6):

$$Q = C_v \frac{dT}{dt} + RT\left(\frac{1}{T}\frac{dT}{dt} - \frac{1}{p}\frac{dp}{dt}\right)$$
$$= (C_v + R)\frac{dT}{dt} - \frac{RT}{p}\frac{dp}{dt}$$

So:
$$Q = C_p \frac{dT}{dt} - \frac{RT\omega}{p} \qquad (10.7)$$

Formulations in terms of the dry static energy s are possible, as used by Yanai, et. al. (1972), Ogura and Cho (1973), and Arakawa (1971). From (10.4) and (10.5):

$$Q = C_v \frac{dT}{dt} + \frac{RT}{\alpha}\frac{d\alpha}{dt}$$
$$= C_v \frac{dT}{dt} + RT\left(\frac{1}{T}\frac{dT}{dt} - \frac{1}{p}\frac{dp}{dt}\right)$$
$$= C_p \frac{dT}{dt} - \frac{RT}{p}\frac{dp}{dt}$$
$$= C_p \frac{dT}{dt} - \alpha\left(\frac{dp}{dz}\right)\frac{dz}{dt} \quad *$$
$$= C_p \frac{dT}{dt} - \frac{1}{\rho}(-\rho g)\frac{dz}{dt}$$
$$= C_p \frac{dT}{dt} + g\frac{dz}{dt}$$
$$= \frac{d}{dt}\left(C_p T + gz\right)$$
$$= \frac{ds}{dt}$$

This formulation is limited to somewhat restricted situations since the substitution of $-\rho g$ for $\frac{dp}{dz}$ at * is only rigorously correct if:

$$\frac{dp}{dz} \equiv \frac{\partial p}{\partial z} \tag{10.8a}$$

To find when this is true, I expand the total derivative:

$$\begin{aligned}\frac{dp}{dz} &= \frac{dp}{dt}\frac{dt}{dz} \\ &= w^{-1}\frac{dp}{dt} \\ &= w^{-1}\left(\frac{\partial p}{\partial t} + \underset{\sim}{V}\cdot\nabla p + w\frac{\partial p}{\partial z}\right) \\ &= w^{-1}\left(\frac{\partial p}{\partial t} + \underset{\sim}{V}\cdot\nabla p\right) + \frac{\partial p}{\partial z}\end{aligned} \tag{10.8b}$$

This reduces to (10.8a) only when

$$\frac{\partial p}{\partial t} \equiv \phi$$

and

$$\underset{\sim}{V}\cdot\nabla p \equiv \phi \,.$$

These conditions are satisfied in the formulations of Yanai, et. al. (1972), and Ogura and Cho (1973) since these authors deal with averages of p, u, v, and ω over large areas and long time periods in the tropics.

Having formulated (10.7) as my heat equation, the forms of Q must be defined. The chief sources of heating in the atmosphere are through release of latent heats of vaporization and fusion of water, and radiation, both solar and long-wave. Other sources and sinks will be dictated by specified boundary conditions. Quantitatively:

$$Q = L_v(C-E) + L_f(F-M) + \mathcal{R}$$

(10.7) then becomes

$$C_p \frac{dT}{dt} - \frac{R\omega T}{p} = L_v(C-E) + L_f(F-M) + \mathcal{R} \qquad (10.9)$$

Leaving the heat equation in this form for a moment, I will deal with the conservation equations for q, l, and i. The only significant source and sink for water vapor are evaporation and condensation. Thus:

$$\frac{dq}{dt} = (E-C) \qquad (10.10)$$

For liquid water, condensation of vapor and melting of ice are sources, and evaporation and freezing are sinks. In addition, another significant source/sink is fall in/out of drops for whatever volume is being discussed. Thus:

$$\frac{dl}{dt} = (C-E) + (M-F) + \omega_{fl} \frac{\partial l}{\partial p} \tag{10.11}$$

assuming liquid transports across the sides of the volume are negligible. (ω_{fl} is defined in Table V.)

For ice, freezing and melting are the primary source and sink, but the fall in/out cannot be neglected. Thus:

$$\frac{di}{dt} = (F-M) + \omega_{fi} \frac{\partial i}{\partial p} \tag{10.12}$$

An important modification can be made to the representation of the time derivative $\frac{d}{dt}$ in (10.9) - (10.12). This operator has been defined as:

$$\frac{df}{dt} = \frac{\partial f}{\partial t} + \underset{\sim}{V} \cdot \nabla f + \omega \frac{\partial f}{\partial p}$$

where f is any scalar quantity. If we multiply the equation of continuity

$$\nabla \cdot \underset{\sim}{V} + \frac{\partial \omega}{\partial p} = \phi$$

by f and add to the equation containing $\frac{df}{dt}$, the terms combine as:

$$\frac{df}{dt} = \frac{\partial f}{\partial t} + \underset{\sim}{V}\cdot\nabla f + \omega\frac{\partial f}{\partial p} + f\,\nabla\cdot\underset{\sim}{V} + f\frac{\partial \omega}{\partial p}$$

$$= \frac{\partial f}{\partial t} + \left(\underset{\sim}{V}\cdot\nabla f + f\,\nabla\cdot\underset{\sim}{V}\right) + \left(\omega\frac{\partial f}{\partial p} + f\frac{\partial \omega}{\partial p}\right)$$

$$= \frac{\partial f}{\partial t} + \nabla\cdot\left(\underset{\sim}{V}f\right) + \frac{\partial}{\partial p}(\omega f)$$

It is this form that I will use henceforth. To avoid confusion let

$$\frac{\delta f}{\delta t} \equiv \frac{\partial f}{\partial t} + \nabla\cdot\left(\underset{\sim}{V}f\right) + \frac{\partial}{\partial p}(\omega f) \tag{10.13}$$

So my four equations become:

$$C_p\frac{\delta T}{\delta t} - \frac{R\omega T}{p} = L_v(C-E) + L_f(F-M) + \mathcal{R} \tag{10.14a}$$

$$\frac{\delta q}{\delta t} = (E-C) \tag{10.14b}$$

$$\frac{\delta \ell}{\delta t} = (C-E) + (M-F) + \omega_{f\ell}\frac{\partial \ell}{\partial p} \tag{10.14c}$$

$$\frac{\delta i}{\delta t} = (F-M) + \omega_{fi} \frac{\partial i}{\partial p} \qquad (10.14d)$$

At this point it is time to face reality. Through the conventional rawinsonde network we have a fair handle on $\underset{\sim}{V}$, T, and q. Radar can give some idea of the distribution of l and i, but only for concentrations of large drops or flakes (the lower size threshold depending on the wavelength of the radar), with accuracy decreasing directly as distance from the radar antenna increases. Further, most radars are operated only when foul weather is impending within their view, so records are not as continuous in time as are the rawinsonde records.

Hence the best records are only of $\underset{\sim}{V}$, T, and q. The equation set (10.14) must thus be simplified to involve only these parameters. If the presence of ice is neglected the term involving (F-M) in equation (10.14a) drops out. Equations (10.14a) and (10.14b) can then be added if (10.14b) is multiplied by L_v:

$$C_p \frac{\delta T}{\delta t} - \frac{R\omega T}{p} + L_v \frac{\delta q}{dt} = R \qquad (10.15)$$

Perturbation

(10.15) is a total heat budget equation for an atmospheric volume,

with the presence of ice neglected, independent of scales of variation of $\underset{\sim}{V}$, T, and q. I will now examine those scales.

Imagine a grid of observing points occupying a volume of the atmosphere. Assume a more or less continuous record in the vertical, but only a knowledge of variable values at discreet points in the horizontal, separated from each other by grid distances Δx and Δy. Over a horizontal section of the volume the average value of the variable f is defined as $\overline{f}$.

Define the value of f at a grid point as:

$$f = \overline{f} + \widetilde{f} + f'$$

The symbol $\widetilde{f}$ represents that part of the deviation of f from its area mean on a constant pressure surface that is due to variations detectable by the grid of observation points. The symbol f' denotes the part due to smaller-than-grid-scale variations. For example, $\widetilde{T}$ might be due to the increase of temperature as one moves toward the equator, easily detectable in even a coarse grid. A large value of q' might be due to fog or very localized cumulus cloud at one grid point. It is obvious that

$$\overline{(\widetilde{f} + f')} \equiv \emptyset$$

since

$$(\tilde{f} + f') = (f - \bar{f}) .$$

Using this symbolism for T, q, w, and $\underset{\sim}{V}$ in (10.15):

$$C_p\left[\frac{\partial}{\partial t}\left(\bar{T}+\tilde{T}+T'\right) + \nabla\cdot\left(\left(\bar{\underset{\sim}{V}}+\tilde{\underset{\sim}{V}}+\underset{\sim}{V}'\right)\left(\bar{T}+\tilde{T}+T'\right)\right) + \frac{\partial}{\partial p}\left(\left(\bar{\omega}+\tilde{\omega}+\omega'\right)\left(\bar{T}+\tilde{T}+T'\right)\right)\right] - \frac{R\left(\bar{\omega}+\tilde{\omega}+\omega'\right)\left(\bar{T}+\tilde{T}+T'\right)}{p}$$

$$+ L_v\left[\frac{\partial}{\partial t}\left(\bar{q}+\tilde{q}+q'\right) + \nabla\cdot\left(\left(\bar{\underset{\sim}{V}}+\tilde{\underset{\sim}{V}}+\underset{\sim}{V}'\right)\left(\bar{q}+\tilde{q}+q'\right)\right) + \frac{\partial}{\partial p}\left(\left(\bar{\omega}+\tilde{\omega}+\omega'\right)\left(\bar{q}+\tilde{q}+q'\right)\right)\right] = \mathcal{R} \qquad (10.16)$$

Now ω is known only through the continuity equation from our knowledge of $\tilde{\underset{\sim}{V}}$. To avoid complicated calculation, I will compute only $\bar{\omega}$. Thus

$$\tilde{\omega} \equiv \phi$$

is assumed.

Dropping $\tilde{\omega}$ out and averaging both sides of the equation over the horizontal area:

$$C_p\left[\frac{\partial \bar{T}}{\partial t} + \nabla\cdot\left(\bar{\underset{\sim}{V}}\bar{T}\right) + \frac{\partial}{\partial p}\left(\bar{\omega}\bar{T}\right)\right] - \frac{R\bar{\omega}\bar{T}}{p}$$

$$+ L_v\left[\frac{\partial \bar{q}}{\partial t} + \nabla\cdot\left(\bar{\underset{\sim}{V}}\bar{q}\right) + \frac{\partial}{\partial p}\left(\bar{\omega}\bar{q}\right)\right]$$

$$+ C_p\,\overline{\nabla\cdot\left(\tilde{\underset{\sim}{V}}\tilde{T}\right)} + L_v\,\overline{\nabla\cdot\left(\tilde{\underset{\sim}{V}}\tilde{q}\right)} +$$

$$+ C_p\left[\nabla\cdot(\overline{\underset{\sim}{V}'T'}) + \frac{\partial}{\partial p}(\overline{\omega'T'})\right] - \frac{R\overline{\omega'T'}}{p}$$

$$+ L_v\left[\nabla\cdot(\overline{\underset{\sim}{V}'q'}) + \frac{\partial}{\partial p}(\overline{\omega'q'})\right] = \overline{R}$$

(10.17)

(10.17) has been simplified in several ways. First, some product terms, when averaged, are identically zero; those involving only one factor of the form $(\widetilde{f} + f')$ are in this category. Second, I have assumed that the averages of terms involving products of $\widetilde{f}_1$ and f_2' are nearly zero compared to the other terms in the equation. This is equivalent to assuming that there is very little correlation between the grid scale variation of one parameter (for example, $\widetilde{\underset{\sim}{V}}$) and the sub-grid scale variation of another (e.g. T' or q'). Since convective activity can be at least descriptively linked with synoptic variations, this assumption is a bit shaky, but is necessary here.

Examining (10.17), the terms $\nabla\cdot(\overline{\underset{\sim}{V}}\,\overline{T})$ and $\nabla\cdot(\overline{\underset{\sim}{V}}\,\overline{q})$ are zero since the terms in parentheses are constants. The terms $\nabla\cdot(\overline{\underset{\sim}{V}'T'})$ and $\nabla\cdot(\overline{\underset{\sim}{V}'q'})$ will be neglected; it will be assumed that the sub-grid variations of $\underset{\sim}{V}$, q, and T are not strongly correlated compared to the variations of ω with T and q. Thus (10.17) becomes:

$$C_p\left[\frac{\partial \bar{T}}{\partial t} + \overline{\nabla\cdot(\tilde{\underset{\sim}{V}}\tilde{T})} + \frac{\partial}{\partial p}(\bar{\omega}\bar{T})\right] - \frac{R\bar{\omega}\bar{T}}{p}$$

$$+ L_v\left[\frac{\partial \bar{q}}{\partial t} + \overline{\nabla\cdot(\tilde{\underset{\sim}{V}}\tilde{q})} + \frac{\partial}{\partial p}(\bar{\omega}\bar{q})\right]$$

$$\approx \bar{\mathcal{R}} + \frac{R\overline{\omega'T'}}{p} - C_p\frac{\partial}{\partial p}(\overline{\omega'T'}) - L_v\frac{\partial}{\partial p}(\overline{\omega'q'}) \qquad (6.18)$$

The terms $\overline{\nabla\cdot(\tilde{\underset{\sim}{V}}\tilde{T})}$ and $\overline{\nabla\cdot(\tilde{\underset{\sim}{V}}\tilde{q})}$ represent the grid-scale-detectable horizontal divergences of fluxes of T and q. These are identical (within errors of $\nabla\cdot(\overline{\underset{\sim}{V}'T'})$ and $\nabla\cdot(\overline{\underset{\sim}{V}'q'})$) to $\overline{\nabla\cdot(\underset{\sim}{V}T)}$ and $\overline{\nabla\cdot(\underset{\sim}{V}q)}$ since the differences are $\nabla\cdot(\bar{\underset{\sim}{V}}\bar{T})$ and $\nabla\cdot(\bar{\underset{\sim}{V}}\bar{q})$; that is, zero.

These terms are equal to the integral, around the boundary of the horizontal area, of the component of $\underset{\sim}{V}$ T and $\underset{\sim}{V}$ q normal to the boundary.

That is:

$$\iint \nabla\cdot\underset{\sim}{E}\, dS = \oint \underset{\sim}{E}\cdot d\underset{\sim}{l}$$

which leads to

$$\overline{\nabla\cdot\underset{\sim}{E}} \iint dS = \oint F_n\, dl$$

where $d\underset{\sim}{l}$

is an element of boundary.

So

$$\overline{\nabla \cdot \underset{\sim}{F}} = \frac{1}{\iint dS} \oint F_n \, dl$$

Letting $A = \iint dS$, the horizontal area of the volume:

$$\overline{\nabla \cdot \underset{\sim}{F}} = A^{-1} \oint F_n \, dl$$

The right hand side of (10.18) will be referred to as the RESIDUE:

$$Res \equiv \overline{R} + \frac{R\overline{\omega' T'}}{p} - C_p \frac{\partial}{\partial p}(\overline{\omega' T'}) - L_v \frac{\partial}{\partial p}(\overline{\omega' q'}) \qquad (10.19)$$

Now assume a knowledge of our parameters only at discrete pressures in the vertical instead of as a continuum. Also assume a knowledge of them only at discrete intervals in time. Integrating (10.18) over a layer between pressures p_1 and p_2 of thickness

$$\Delta p = p_2 - p_1 \; ;$$

$$\int_{p_1}^{p_2} C_p \left[\frac{\partial \overline{T}}{\partial t} + A^{-1} \oint (\underset{\sim}{V} T)_n \, dl \right] dp + \left(C_p \overline{\omega}\, \overline{T} \right)_{p_1}^{p_2}$$

$$- \int_{p_1}^{p_2} \frac{R\overline{\omega}\,\overline{T}}{p} \, dp +$$

$$+ \int_{p_1}^{p_2} L_v \left[\frac{\partial \bar{q}}{\partial t} + A^{-1} \oint (\chi q)_n \, dl \right] dp$$

$$+ \left(L_v \bar{\omega} \bar{q} \right) \Big]_{p_1}^{p_2} = \int_{p_1}^{p_2} \overline{Res} \, dp$$

Assuming a linear variation of all parameters between pressure levels and defining the average of a quantity over the interval p_1 to p_2 as $\overline{f}^p$:

$$C_p \left[\frac{\partial}{\partial t} \overline{\overline{T}}^p + A^{-1} \overline{\oint (\chi T)_n \, dl}^p \right] \Delta p + C_p \left(\bar{\omega} \bar{T} \right) \Big]_{p_1}^{p_2}$$

$$- \overline{\left(\frac{R \bar{\omega} \bar{T}}{p} \right)}^p \Delta p$$

$$+ L_v \left[\frac{\partial}{\partial t} \overline{\bar{q}}^p + A^{-1} \overline{\oint (\chi q)_n \, dl}^p \right] \Delta p + L_v \left(\bar{\omega} \bar{q} \right) \Big]_{p_1}^{p_2}$$

$$= \overline{Res}^p \, \Delta p$$

Dividing this by Δp on both sides, averaging over a time interval defined by two observing times, (t_2 and t_1)

$$\Delta t = t_2 - t_1$$

and assuming all parameters vary linearly in time over Δt (with time average denoted by $\overline{f}^t$):

$$C_p \left[\overline{\overline{T}}^p \right]_{t_1}^{t_2} + A^{-1} \Delta t \, \overline{\overline{\oint (\chi T)_n \, dl}^p}^t + C_p \overline{\left[\left(\bar{\omega} \bar{T} \right) \Big|_{p_1}^{p_2} \Delta \bar{p}^{-1} \right]}^t$$

$$- \overline{\left(\frac{R\bar{\omega}\bar{T}}{p}\right)'^{p}}^{t} \Delta t$$

$$+ L_v \left[\overline{\bar{q}'^{p}}^{t} \Big|_{t_1}^{t_2} + A^{-1} \Delta t \; \overline{\oint (\underset{\sim}{V} q)_n \, dl'^{p}}^{t} \right]$$

$$+ L_v \overline{\left[(\bar{\omega}\bar{q}) \Big|_{p_1}^{p_2} \Delta p^{-1} \right]}^{t} = \overline{Res'^{p}}^{t} \Delta t$$

Dividing by Δt:

$$C_p \left[\overline{\bar{T}'^{p}} \Big|_{t_1}^{t_2} \Delta t^{-1} + A^{-1} \overline{\oint (\underset{\sim}{V} T)_n \, dl'^{p}}^{t} + \overline{(\bar{\omega}\bar{T}) \Big|_{p_1}^{p_2} \Delta p^{-1}}^{t} \right]$$

$$- \overline{\left(\frac{R\bar{\omega}\bar{T}}{p}\right)'^{p}}^{t}$$

$$+ L_v \left[\overline{\bar{q}'^{p}} \Big|_{t_1}^{t_2} \Delta t^{-1} + A^{-1} \overline{\oint (\underset{\sim}{V} q)_n \, dl'^{p}}^{t} + \overline{(\bar{\omega}\bar{q}) \Big|_{p_1}^{p_2} \Delta p^{-1}}^{t} \right]$$

$$= \overline{Res'^{p}}^{t} \qquad (10.20)$$

which is the finite difference form of (10.15). It should be noted that the residue for the finite difference form will also include a noise component due to the errors in measuring and computing the terms on the left-hand sign of (10.20), as well as due to assumptions such as linearity of variation in p and t and neglect of the variation of L_v with temperature. The size of this noise component, compared to the "signal" variation in the residue due to the variations of radiation,

$\left(\frac{\partial}{\partial p}\overline{\omega' T'}\right)$, $\left(\overline{\omega' T'}\right)$ and $\left(\frac{\partial}{\partial p}\overline{\omega' q'}\right)$, will be a measure of how much can be said about the effects of convective scale activity on a large scale using only rawinsonde data.

An examination of (10.19) or (10.20) shows the units of the residue to be (energy) $(\text{mass})^{-1}$ $(\text{time})^{-1}$. I have chosen to use the meter-ton-second system of units as defined by Phillips (1972). The values of the several constants in this system are given in Table V. This makes the units of the residue: (kilojoules) $(\text{metric ton})^{-1}$ $(\text{sec})^{-1}$.

Several standards of comparison are available when examining computed residues. The solar constant of 2 Ly/minute, when converted to my units, is: 1.394 kj m^{-2} sec^{-1}. Applied to a mass equivalent to the weight of the whole atmosphere (10.3 metric $tons/m^2$) this is .139 kj ton^{-1} sec^{-1}.

The long wave radiative flux to space from the atmosphere is 470 Ly/day at 40 degrees North after Vonder Haar and Suomi (1969). In my units, applied to the mass of the atmospheric depth, this is .023 kj ton^{-1} sec^{-1}.

Examining individual parameter changes, a residue of .1 kilojoule/ton/sec can be equivalent to a net increase or decrease in temperature (T) or mixing ratio (q) in a layer of the atmosphere. A residue of .1 kj ton^{-1} sec^{-1} over a twelve hour period is equivalent to a temperature change of 4 degrees K or a mixing ratio change of 1.6 g/kg.

Note that (10.20), and indeed (10.15), contain no pressure units, since every ω is divided by p or differentiated by p. I have chosen to express all pressures in millibars (mb), converting to other units only where necessary to do a computation (such as calculation of q from pressure, temperature, and relative humidity).

11. The Data:

I decided to examine the behavior of the Residue as defined in (10.20) over an area of New England corresponding roughly to the areas of convective weather in the cases of Part I. The four National Weather Service rawinsonde stations in this area are located at Albany, New York, Portland, Maine, Chatham, Mass., (formerly located at Nantucket, Mass.) and Kennedy Airport, New York, New York. I also decided to use the objective analysis method of Sanders (1970) to simplify divergence and wind calculations by use of strict north-south and east-west boundaries on the volume to which (10.20) would be applied. Sanders' analysis program determined the objective analysis regression equations for a grid of fixed points, so it seemed convenient to choose a grid bounded by a set of these points. The volume finally chosen was that bounded in the horizontal by 41.0°N, 44.3°N, 69.5°W, and 74.0°W. The upper boundary of the volume was chosen at 50 mb since this level would be above the top of even the largest convective cells over New England and would assure that the inflows of both heat and water vapor through the upper boundary were negligible at all times.

The regression equations for the sixteen (16) points defining this volume are shown in Table VI along with pertinent identification numbers for the stations involved in each equation. Due to the non-

availability of data for 1972 for Maniwaki, Ontario, a Maniwaki observation was "made up" using another regression equation involving other stations north, south, and west of Maniwaki.

Having determined what rawinsonde data was needed and for which stations, I obtained this data in the 645 card deck format on magnetic tape from the National Climatic Center (NOAA), Asheville, North Carolina. The taped data covered the summers (June, July, and August) of both 1971 and 1972. The 645 card deck format includes data for each sounding at the surface, 1000 mb (if present), 950 mb, and at 50 mb increments up to 200 mb, at 25 mb increments up to 100 mb, and at 50 mb. This made it convenient to use a pressure interval (layer thickness) of 50 mb for the evaluation of (10.20).

Due to time restrictions I decided to limit the time periods that would be examined in this portion of the research. The question at hand was not "Can the variations of the residue in the vertical be correlated with known convective activity?" (cf. Ninomiya [1971]) but "Is the variation of the residue large enough compared to the noise level of the observations to distinguish between convective and benign weather regimes in the volume?" With this in mind I sought to examine long spans of time, broken up into 12 hour periods (the frequency of rawin obs), encompassing both fair weather and foul. To limit the number of these periods to a manageable size, I chose to look at the

time spans of June 1971, July 14 to 24, 1972, and August 1 to 6, 1972. These periods cover Cases 1 through 4, Case 9, and Case 10, respectively, of Part I.

I found that the Asheville tape had some gaps in station data. The M.I.T. teletype archives were resorted to here, each missing observation being hand plotted and the data for the appropriate pressure levels extracted and hand-punched using the 645 card deck format. The problem of units implicit here was left to the analysis program; the winds in the Asheville archives are in meters per second, while those reported by teletype are in knots. The hand-punched data was flagged to indicate that a knots-to-m/sec conversion was necessary.

After obtaining the missing observations in this manner, the hand-punched data was merged with the data on the Asheville tape, sorted by time and station and reduced to the selected time spans named above. This final batched data was now ready for processing.

12. The Residue Program:

The evaluation of (10.20) using the data just described was accomplished with the aid of M.I.T.'s IBM 360/370 computer through a straightforward FORTRAN program.

The program began by reading in the limits of the time span to be analyzed. The batched data was then searched for the first RAOB for the start time of that span. Each RAOB for that time was then read in and passed to a subroutine for translation of the appropriate fields of the 645 card format into wind components, temperature (degrees Kelvin), and mixing ratio. Missing data was flagged for interpolation; the details of interpolation will be discussed in a moment. Winds flagged as being in knots were converted to m/sec before reduction to u and v (south and west) components. Mixing ratio was computed from the given pressure, temperature, and relative humidity using the formulae:

$$v_{sat} = (6.11 \text{ mb}) \cdot \left(\frac{T_o}{T}\right)^5 \cdot \exp\left(24.84573 \cdot \left(1 - \left(\frac{273.16}{T}\right)\right)\right)$$

(after Phillips-1972)

$$\text{and} \quad q = \frac{\epsilon v_{sat}}{p - v_{sat}} \quad \text{where} \quad \epsilon = 0.622$$

The interpolation methods, seen at second hand, were chosen primarily for programming convenience. As a result, most of the soundings involving interpolated data had to be discarded later due to

obvious noise introduced into the calculation. For missing data at levels between the surface and 100 mb, a linear interpolation was performed between the parameter values at the adjacent levels, regardless of whether either was missing also. Mixing ratio was automatically interpolated when the temperature was interpolated since the missing temperature was needed to compute the mixing ratio (as above). Any RAOB requiring more than 20 interpolations was discarded.

The surface, 100 mb, and 50 mb levels were specially treated. The surface wind, if missing, was assumed equal to half the 950 mb wind. The surface temperature and mixing ratio were set equal to the 950 mb temperature and mixing ratio if missing. At the 100 mb and 50 mb levels, where the bulk of missing data occurred, three fallbacks were provided. First, if only 50 mb data was missing, the wind was set equal to half the 100 mb wind and/or the temperature set equal to the 100 mb temperature. If both levels were missing, the data was set equal to the values from twelve hours before. If that sounding was missing also, then the final fallback was to calm winds and dry air ($q = 0.0$ gm/kg) with a temperature of -60°C (213°K).

A count was kept as the RAOB's for each sounding time were read in. Only if all required RAOB's (six for 1971, seven for 1972) were read in would the program continue.

With all RAOB data read in, the program began the objective

analysis process. My objective analysis technique used regression equations derived by Sanders (1970) based on theory developed by Eddy (1967). These equations were previously employed by Williams (1972) in another study.

Sanders' equations (for values of a parameter at points on a grid covering the Gulf of Mexico, Caribbean Sea, western North Atlantic, and eastern United States) were based on a correlation function derived as part of a study to be used in forecasting tropical storm movements. The regression coefficients in these equations were derived specifically to determine the departures, from the zonal average for a particular synoptic time, of the zonal and meridional components of the wind averaged from 1000 mb to 100 mb, derived from a data sample over North America, the Gulf of Mexico, and the Caribbean for several hurricane-season months. The zonal average of u is large and varies strongly with latitude, while the zonal average of v is small and varies less drastically. Thus there were derived two correlation functions (for u and for v) and two regression equations at each point on the grid.

Thus, for each of the grid points in my study area I had two equations, one each for the deviations of u and v from certain averages. Each equation expressed the deviation of u or v as a linear combination of the deviations of u or v at selected observing

points "near" the grid point. I also had similar equations for parameter deviations at the six main rawinsonde stations in terms of deviations at other rawin stations; these allowed the calculation of a "bogus" observation from other stations whenever a given station was missing.

Of the four parameters used in my budget equations, (u, v, T, and q), only v does not exhibit the properties of large mean (with respect to deviations) and strong variation with latitude. With this in mind I decided to use the u-equation for all four parameters rather than program specially for v apart from u, T, and q.

Of course, the question arises of the validity of using Sanders' techniques, strictly applicable to the 1000-100 mb mean wind components in the hurricane season, to u, v, T, and q on constant pressure surfaces in summer. My defense is that in the New England area the data points are dense with respect to the prevailing major scales of variation of u, v, and T, and hence almost any objective analysis scheme will do. The scale of variation of q, being the smallest, places the most doubt onto the analysis of q with this technique. Again, I hoped for the best and pressed on.

As was mentioned previously, Maniwaki observations were "bogused" in all the 1972 analyses using the regression equation for that station and the observations from other surrounding stations. The

required observations for Moosinee in this regression equation were not available for this bogusing and were omitted as not contributing greatly to the objective analysis at the 16 grid points.

In lieu of the zonal mean of each parameter (u, v, T, and q), I decided that the means of the parameters over the six (or seven) RAOB stations would be a close enough approximation for this study. The program thus averaged all the read-in values as a first step and subtracted these mean values from the RAOB's, leaving deviations from the means to be passed to the next step. The values of the parameters were then objectively determined at the twelve boundary points by multiplying each deviation by the appropriate regression coefficient and summing, then adding back onto the mean value of the parameter. The area mean, taken as the mean value of a parameter over all sixteen points, was similarly found using coefficients derived by summing the sixteen regression equations and dividing by 16.

Having thus determined the necessary grid values of u, v, T, and q, as well as the area means of these parameters, the next step in the program was to find the area mean of ω using the equation of continuity:

$$\frac{\partial \omega}{\partial p} = -\nabla \cdot \underset{\sim}{V}$$

from which

$$\omega(p) = \omega_0 - \int_{p_0}^{p} \nabla\cdot\underset{\sim}{V}\, dp$$

or

$$\overline{\omega}(p_k) = \omega_0 - \sum_{i=1}^{k} \overline{(\nabla\cdot\underset{\sim}{V})}_i \Delta p$$

My chosen Δp was 50 mb and ω_0 at p_0=50 w_0 was assumed equal to zero.

A subroutine (DIVERG) was written which computed the area average divergence $\overline{\nabla\cdot\underset{\sim}{F}}$ of any vector quantity $\underset{\sim}{F}$ given the components of $\underset{\sim}{F}$ at the 12 boundary grid points of my chosen area. This subroutine was used not only to compute $\overline{\nabla\cdot\underset{\sim}{V}}$ but also the terms $\overline{\nabla\cdot(\underset{\sim}{V}T)}$ and $\overline{\nabla\cdot(\underset{\sim}{V}q)}$ required in (10.20). The subroutine used the relation:

$$\iint(\nabla\cdot\underset{\sim}{V})\, dS = \oint \underset{\sim}{V}\cdot d\underset{\sim}{\ell}$$

to compute the in- or outflow on each of the four sides of the area, assuming a linear variation of u and v between grid points along each side.

To determine ω at each level, this subroutine was used to compute the divergence at each of the 20 levels in the volume. Then layer average divergences were computed by averaging the divergences at the levels bounding the layer. Finally, the layer divergences were finite

difference integrated from p_o = 50 mb downward to obtain a value of the area mean omega for each level down to the surface. In general the surface omega would be non-zero due to errors in the wind measurements and divergence computations. This is a loathsome occurrence at a solid boundary and can be remedied in several ways. O'Brien (1970) gives an excellent discussion of the possible correction schemes. I chose to assume the surface ω to be zero always, and to distribute the net divergence error (uncorrected surface ω divided by the depth of integration) uniformly over the depth of the atmosphere. Thus the program computed DIVCOR (the divergence correction) as:

$$\text{DIVCOR} = \frac{\text{uncorrected surface } \omega}{(\text{surface pressure} - 50 \text{ mb})}$$

and subtracted this from all layer average divergences. Omega was then recomputed at all levels to yield values of omega corrected for the divergence error.

Once this area mean omega ($\overline{\omega}$) had been computed the program computed the terms $\overline{\nabla\cdot(\underline{V}T)}$ and $\overline{\nabla\cdot(\underline{V}q)}$. This was done by multiplying u and v by T or q at each of the twelve boundary points, and using the divergence subroutine (DIVERG) on the parameter pairs (uT, vT) and (uq, vq) instead of the pair (u, v) as was done in the omega computation. These terms must also be corrected for measurement and computational errors as the divergence was in the omega computation. The error in $\overline{\nabla\cdot(\underline{V}T)}$ is roughly:

$$\overline{[\nabla\cdot(\underset{\sim}{V}T)]}' \simeq \overline{T}\,\overline{[\nabla\cdot\underset{\sim}{V}]}' + \overline{\underset{\sim}{V}}\cdot\overline{[\nabla T]}'$$

Since ∇T is resolved on the large scale by my grid, I here assumed that $(\nabla T)'$ was randomly distributed over the area under study and hence that its area average is zero. Thus $\overline{\nabla\cdot(\underset{\sim}{V}T)}$ can be corrected by subtracting off the area mean temperature ($\overline{T}$) multiplied by the divergence correction (DIVCOR = $\overline{[\nabla\cdot\underset{\sim}{V}]}'$) at each pressure level. Similarly, $\overline{\nabla\cdot(\underset{\sim}{V}q)}$ was corrected at each level by subtracting off the product $\overline{q}(\overline{[\nabla\cdot\underset{\sim}{V}]}')$.

At this point all the parameters in (10.20) had been computed for each pressure level from 50 mb down to 950 mb and the surface. Before proceeding further, the handling of the boundary layer must be discussed.

The boundary layer in this simple model is defined as the layer of air below the 950 mb level. To keep the boundary layer physics, and consequently the programming, as simple as possible, the effects of the extremely variable topography in the area to which the model was applied must be neglected. Due to the varying release elevations of the RAOBs used in the objective analysis, this is a good idea since the surface (release level) data may not apply at the distinctly non-objective actual surface elevations at each of the grid points.

The bottom of the boundary layer was assumed to be at the lowest objectively analyzed release pressure among the twelve boundary points. The objectively analyzed data at this level was based on the surface (release level) data at the source RAOBs. The boundary layer was treated in the same manner as the layers above it except that its thickness was not a fixed 50 mb but might vary from time to time due to the variable pressure at the lowest level. No effects due to the orographically induced vertical motions near the ground were assumed, and the effects of evaporation from the earth's surface were neglected. Any neglected effects would appear in any case in the boundary (lowest) layer computational results in any case, and be distinguishable by comparison with other layers.

Once all area and divergence terms were obtained at each pressure level, pressure averages and derivatives were computed over each layer assuming a linear variation of each term with pressure. The adiabatic lift term in (10.20), $\frac{R\overline{\omega}\overline{T}}{p}$, was computed at each level and then averaged between levels. After the terms involving q were averaged in each level, they were multiplied by a value of L_v, the latent heat of vaporization for water, appropriate to the layer average temperature ($\overline{T}^p$). While the variation of L_v is only on the order of one per cent per degree Kelvin, the variation of $\overline{T}^p$ is considerable between the boundary layer and the tropopause layer

(a variation of about 70° K!) and this variation had to be taken into account at this point if meaningful comparisons between widely-separated layers are to be made.

This completed all computations over the study volume at a specific time t_o. The terms and parameters thus computed were stored and the set of RAOBs for the time t_o + 12 hours were read in and similarly processed. When all terms for this time had been calculated, the terms were used to compute time means and derivatives as required for equation (10.20). These time terms were then summed to obtain the layer Residues defined in (10.20). The Residues were then finite-difference integrated from 50 mb to the surface. Also computed were averages of the values and magnitudes of the layer residues, omegas, and divergences for use in statistical analysis of the results.

The final stage of the program printed out the computed residues and their integral as well as the terms composing the residues and the area mean parameters which went into those terms. A sample of the area mean parameter output is shown in Figure 17; Figure 18 is a sample of the residue output. After all numbers had been printed, the program stored the second time parameters and terms in the first time (t_o) storage area, zeroed out the second time storage and residue storage, and returned to read in the RAOBs for the end time of the next twelve hour period. This cycle of read-in, computation, and

output was continued until the end time of the desired time span was encountered or a gross error was discovered during read-in.

13. Results:

The Residue computations were performed by this program over the previously-cited time spans. Each completed computation was scanned by sounding time and period for significant weather, missing data, and gross errors. The current and past weather from the synoptic observations by Concord, New Hampshire, and Logan Airport, Boston, were annotated for the applicable time periods on each Area Mean sheet and each Residue computation. Where doubts existed as to the weather the Service "A" airways observation achives were scanned for convective weather (rain showers or thunder) in the computation area.

Each sounding time was also scanned for data missing from the component RAOBs which had been interpolated by the program. Where this caused visible gross errors in the level divergences or the residue terms in which the level participated, the sounding time was flagged and the results of the computations using that time were discarded. This process was necessary to keep program-induced error to a minimum.

To establish a baseline for errors and the sizes of various terms, the model was run for each of the objective analysis "years" with two bogus sets of RAOBs, one set having a constant west wind (270°) at 10 m/sec at all levels and stations and the other set having a constant south (180°) wind at 10 m/sec at all levels and stations. If

the objective analysis equations were exact, the west wind RAOBs would produce no divergence and hence no vertical velocity (ω). The south wind would produce a divergence, given the north and south boundary lengths chosen, of -3.84×10^{-7} sec^{-1} due to the longer length of the southern boundary. And obviously the objectively analyzed u and v components at the grid points should be exactly 10 m/sec.

Table VII shows the actual results of these tests. While the error in analyzed wind speed is substantial in 1971, the largest error in divergence is in the south-wind test for 1972. This is no doubt due to the absence of data for Moosinee, one of the stations needed to "bogus" Maniwaki. Moosinee contributes from 5.6% to 13.6% of the variance at four of the points on the northern boundary of the model area.

Since we correct for the divergence error in the omega computation and in the calculation of $\overline{\nabla \cdot (\underset{\sim}{V} T)}$, and $\overline{\nabla \cdot (\underset{\sim}{V} q)}$, the impact of the u and v error is forgiveable. The error in divergence is another matter since it could materially affect the validity of my computed omegas. Two checks were made on this. First, of 43 RAOB times in the final results for 1971, 22 had positive uncorrected omegas and 21 negative. For 1972, of eleven cases only two were negative, with nine positive. A feel for vertical velocities would indicate that a

50-50 split around zero is desirable if the model is not to have an unwanted bias in the omegas.

Second, one can compare the magnitudes of these test divergences with the actual uncorrected level divergences from the results. It would be undesirable to have the error in the objective analysis itself constitute most of the error in actual uncorrected divergences. A screening of the Area Mean sheets revealed that for the 1971 cases this analysis error rarely exceeded 10% of any uncorrected divergence. For the 1972 cases, this threshold was exceeded at roughly one third of the levels. By either standard, the 1972 results must be looked at with a somewhat jaundiced eye.

Of the 29 periods left after culling out bad data, 23 had perfect data, i.e. no missing parameters at any level except humidity (mixing ratio) at high levels. These 29 cases were divided into the categories of Weather (showers or thundershowers in the twelve hour period) and No Weather (all other), and further into the subcategories of Day (1200Z to 2400Z) and Night (0000Z to 1200Z). This breakdown allows the examination of parameters, most particularly the Residues, for the effects of convective-scale motions, using the No Weather cases as a control or baseline to determine the noise level.

The first check on reasonableness of the actual results is to look at the area mean parameters as composites of the periods as

broken into categories. Vertical composites of ω, T, q, u, and v are tabulated in Table VIII and shown pictorially in Figures 19 through 22.

Figure 19, showing the omega profiles, is perhaps the most definitive. The most negative omegas, and hence the strongest ascents, are for the Weather cases, with Day-Weather stronger than Night-Weather. For the No Weather cases, Night cases show slight ascent, while the Day cases show strong descent with some ascent above the tropopause (level 5, 250 mb).

The temperature profiles (Figure 20) are a bit less intuitive. There seems to be little if any discrimination between the Day and Night cases within the No Weather category, and only in the layer from 950 to 800 mb in the Weather category, where Day is one to one-and-a-half degrees warmer than Night. This small Day-Night distinction is probably due to the fact that both 0000Z and 1200Z soundings were averaged to obtain both Day and Night profiles; had 0000Z been used for one type and 1200Z for the other a greater distinction would have resulted.

As for differences between Weather and No Weather temperature profiles, the Weather soundings are not obviously more stable than the No Weather. The Weather soundings are warmer than the No Weather by two or three degrees below 500 mb increasing to four degrees near

300 mb; they then become cooler than No Weather at the tropopause (200 mb).

A look at the mixing ratio profiles (Figure 21) does not improve this much immediately. These show the obvious; one expects days with convective activity to be wetter than days without. But this extra moisture is significant for stability. Computing a Showalter Stability Index for each of the categories, using the 850 mb mixing ratios and the temperature profiles in Figure 20, the stabilities for No Weather cases are: Day +8, Night +7.5; the Weather case stabilities are: Day +2.5, Night +4.5. The surprise here is the slightly less stable No Weather-Night condition compared to No Weather-Day cases. This parallels the slight ascent noted for No Weather-Night omegas in Figure 19. No immediate explanation presents itself for this phenomenon.

The u and v profiles are less easily anticipated. The v profiles seem to show no real differences among the categories. The v component is northerly (negative) for all levels except for the lowest in the Day-Weather cases, where a southerly component is expected for convective weather. The u components divide sharply between Weather and No Weather, with little distinction between Day and Night cases. Weather cases have a consistently stronger westerly component (u) at all levels below level 8 (400 mb) over No Weather cases. The significance of the No Weather-Day peak at level 4 (200 mb), being larger than the other three categories, is uncertain and is close enough to

be due to random chance.

The reason for the predominance of negative v components for all categories is also uncertain. However, an examination of the NWS publication Climatological Data for 1971 and 1972 shows that winds in the area of my study were westerly or north of westerly at most stations and levels during these years. Thus the model is just indicating a real climatic trend in this instance.

Before examining the Residue output, I should review the physical significance of the terms that make up the Residue. (10.19) states, with (10.18):

$$Res = C_p\left[\frac{\partial \bar{T}}{\partial t} + \nabla\cdot(\underset{\sim}{V}T) + \frac{\partial}{\partial p}(\bar{\omega}\bar{T})\right] - \frac{R\bar{\omega}\bar{T}}{p}$$
$$+ L_v\left[\frac{\partial \bar{q}}{\partial t} + \nabla\cdot(\underset{\sim}{V}q) + \frac{\partial}{\partial p}(\bar{\omega}\bar{q})\right]$$

or

$$Res = C_p\left[\frac{\partial \bar{T}}{\partial t} + \nabla\cdot(\underset{\sim}{V}T) + \frac{\partial}{\partial p}(\bar{\omega}\bar{T}) - \gamma\frac{\bar{\omega}\bar{T}}{p}\right]$$
$$+ L_v\left[\frac{\partial \bar{q}}{\partial t} + \nabla\cdot(\underset{\sim}{V}q) + \frac{\partial}{\partial p}(\bar{\omega}\bar{q})\right]$$

Now

$$\nabla\cdot(\underset{\sim}{V}f) + \frac{\partial}{\partial p}(\bar{\omega}f)$$

is just the three-dimensional divergence of the transport of f; the rate of flow of f into or out of the volume, if you will. For a conservative quantity (where $\frac{df}{dt} = 0$) this term should be exactly balanced by $\frac{\partial f}{\partial t}$. Looking first at the case f = q, we note that $\overline{q}$ is actually measured, as are the terms $\nabla\cdot(\underset{\sim}{V}q)$ and $\frac{\partial}{\partial p}(\overline{\omega}\overline{q})$. Hence the sum of all three may not be zero, real data as being perverse as it is, and allowing for the possibility of evaporation and condensation. The non-zero result will include added q due to evaporation of cloud in the volume, any errors in the measurements of q and $\underset{\sim}{V}$ and in the calculation of $\overline{\omega}$, and any error introduced by the assumptions used to calculate these terms, plus the effects of sub-grid-scale motions.

The same argument applies for the f = T case, except that the added term $-\frac{R}{c_p}\frac{\overline{\omega}\overline{T}}{p} = \gamma\frac{\overline{\omega}\overline{T}}{p}$ accounts for the known changes in temperature due to changing pressure, by ascent or descent primarily. $\frac{\partial\overline{T}}{\partial t}$ is the measured change in $\overline{T}$ while $\nabla\cdot(\underset{\sim}{V}T) + \frac{\partial}{\partial p}(\overline{\omega}\overline{T})$ is the measured three-dimensional divergence of the transport of T. The sum of these four terms multiplied by C_p is a measure of the imbalance of the four; it would be zero if the atmosphere behaved exactly as my physics describe it and my assumptions require. (Perfectly accurate observations would also be required.) As it stands, this temperature term includes not only the errors in T and $\underset{\sim}{V}$, but the effects of solar and longwave radiation acting in the volume and the effects of sub-grid-scale motions.

The sum of the T and q halves of the Residue equation should cancel given perfect observations and all the previous assumptions, even in the presence of condensation or evaporation, since any loss of q (condensation) will cause a corresponding increase in T due to release of latent heat. Again, this is not likely to balance exactly due to sub-grid-scale motions and errors in measurements and calculations.

Thus the Residue will reflect the errors in all parameters measured plus radiation plus the sub-grid effects plus all those troublesome terms I threw out after (10.16).

Examination of the actual Residue output shows the following characteristics:

- Generally the q terms are small compared to the resultant Residue. In a very few cases the individual q terms reached the order of magnitude of the Residue; the net sum of the q terms was still small compared to the Residue.
- The largest magnitudes are those of the vertical and horizontal elements of the divergence of the transport of T.
- The adiabatic term $-\frac{R\bar{\omega}\bar{T}}{p}$ was next in size after the divergence of T transport.
- The balance of terms is very close. The residue is generally less than 10% of the largest terms in the sum. Hence a great deal of the residue is apt to be the noise in the computation

of these large terms. In the case of $\nabla \cdot (\underset{\sim}{V} f)$ these terms are themselves computed as differences of still larger numbers. Hence, more noise.

The categorized cases are shown in Table IX with means of the layer Residues and omegas over the twelve-hour period. Both the algebraic means and mean magnitudes of both parameters are shown. Finally, means over the categories have been computed and listed.

Note that certain cases are set apart due to some minor flaw in the data. In most of these cases the wind was missing for one or two levels in one of the input RAOBs, but the interpolation for this missing data caused no obvious flaw in the results. I will discuss the results both excluding and including these "bummers," with the convention that a statistic normally stated will be for the clean data cases, while the same statistic with "bummers" included will be shown in parentheses.

My first hope would be for a clear demarcation, by residue size, between the Weather and No Weather cases. An examination of Table IX shows that is not to be. The overlap in the residues between the two categories is considerable. The (algebraic) means seem to divide more clearly between Day and Night than between Weather and No Weather.

To test out the assumption that the sub-scale activity is larger during periods of convective weather, let's look at the computed

magnitudes of the Residues. Again, unfortunately, the overlap is considerable, more so than for the algebraic values of the Residues. But perhaps there is still some statistical separation even if there is no absolute separation. The mean for the Weather cases is .12237 (.12472) kj sec^{-1} ton^{-1}; the mean for the No Weather cases is .09093 (.08924). Since the computed variance of the whole lot is .0321 (.0330), this is a separation of about one standard deviation. A test for significance shows this would happen by chance with this sample size (23 or (29)) less than 1% (.005%) of the time. So the assumption looks fairly good, at least in a large sample.

The possibility exists, however, that we are merely seeing an increase in the noise level. It has already been shown that omegas and u's are larger for convective cases, and a higher level of fine-scale turbulence can be expected with these higher bulk-air motions. To check this possibility out, Figure 23, a scattergram of the average magnitude of the residues versus the average magnitude of omega, was plotted. The Weather-No Weather and Day-Night categories have been flagged, as well as those cases with missing data.

The correlation is not strong. The best fit line has a slope of 1.1076×10^{-5} (1.1819×10^{-5})(mb) (ton) (kj^{-1}) with a correlation of .556 (.537). The probabilities of these correlations occurring by chance with the sample sizes of 23 and 29 are both less than one-tenth

of a per cent. Nonetheless, this is not a strong correlation, even if it is statistically significant. It is not strong enough to explain all the increase in Residue for the Weather cases.

The assumption of increase in Residue magnitude with convection looks reasonable, but my hope for a clear dividing line is defeated by the large variances in the Residues.

The Day-Night distinction appears clearly in Table IX. A test for significance on the residue magnitudes for the Day and Night categories shows a $<5\%$ ($<25\%$) probability of this occurring by chance, meaning this separation is less significant than the Weather-No Weather separation. This is undoubtedly due to the large variances obtained by combining Weather and No Weather Residues under the Day and Night categories.

If we look at a scattergram of algebraic mean residues versus omegas (Figure 24), the sheep and the goats seem to segregate very clearly; with the exception of one night case, a heavy diagonal line will separate the Day cases from the Night cases. The physics of this is easy to grasp; Night cases can be characterized by smaller or more negative residues due to nocturnal long-wave radiative cooling and the absence of solar heating. The reason for the dominance of negative omegas (indicating ascent) for both Weather and No Weather cases is not clear.

Having seen some favorable trends in the means over all 19 layers in the model, let us now get one step closer to the data by looking at vertical composites of the four categories. The residues at each layer were averaged for all cases in each category. The results are shown as Figures 26 and 27 and listed in Table XI.

What can we expect to see in these composites? Other than the noise level, the major forces are solar and longwave radiation and sub-grid-scale motions.

The two major types of radiative effects I look for are longwave radiative cooling of the atmosphere and absorption of solar radiation. At night only the longwave cooling is operative, while the daytime net heating or cooling is the sum of the two effects. Further, the radiative heating or cooling of the ground will manifest itself in the lowest layers of the atmosphere through molecular conduction and microscale eddy transport.

Johnson and Shen (1968) have documented the vertical variations of radiative cooling in the presence and absence of clouds for several winter cases in 1961. Longwave radiative cooling averages about 1° to 2° Kelvin per day (about .023 kj ton^{-1} sec^{-1} in my units) below the tropopause. In the presence of clouds, strong deviations from this average were noted, with intensified cooling above stratiform cloud decks and heating below, in one case finding a warming of

as much as +4° K/day below a middle cloud deck. This confirms the theory reviewed in Houghton (1954) and Dopplick (1972). Dopplick (1972) computed seasonal mean radiational cooling profiles based on observed mean concentrations of water vapor, ozone, and carbon dioxide. His mean longwave cooling profile at 40°N for June through August is tabulated in Table X and plotted on Figure 25. This profile varies between -1.4°K and -2.0°K up to about 300 mb, the approximate tropopause level.

Johnson and Shen indicate a layer of heating centered near or above the tropopause, in one case at a rate of +3°K per day. Dopplick's profile shows cooling up to above 50 mb, with a maximum of heating rate of -0.2°K/day at 100 mb. This "peak" is attributed to the fact that the lowest temperatures are found in this area, and hence the rate of energy loss by radiation (which varies directly with the fourth power of the temperature) will be a minimum.

The earth's surface at night radiates more strongly than the layers above, hence cools more (in the absence of low clouds). This will have the effect, by conduction and convection, of cooling the lowest layers of the atmosphere more than the Dopplick profile indicates. The dashed curve suggests the effect in Figure 25.

The daytime radiation profile will be a combination of this longwave cooling profile and the heating absorption of solar radiation,

plus heat transfer from the heated ground. Dopplick (1972) has also calculated seasonal mean cross-sections for the solar heating, excluding heat transfer effects from the ground. This profile, at 40°N for June through August is also tabulated in Table X and plotted on Figure 25. The maximum near 500 mb is attributed to middle and high cloud absorption.

The effects of heat transfer from the ground are less well documented. London (1957) computed a mean solar absorption by the ground at 40°N of 425 ly per day; this value will vary according to solar elevation and cloud cover. Assuming a daylight length of 12 hours, this amount of absorbed radiation would heat the lowest centimeter of air at the rate of 2.1°K per day if transferred completely to that layer. Using this as a ballpark figure, the straight line on Figure 25 corresponds to a linear decrease (with pressure) of heating due to heat transfer from the ground. Summing the three curves for longwave cooling, solar heating, and ground heat transfer, results in the net daytime curve in Figure 25. This is only a rough measure; the parameterization of the upward transfer of heat from the ground is particularly heavy-handed. And in fact what I am looking for in this study is the detectability of this vertical eddy transport of heat and moisture.

Before comparing these curves to residue profiles, it is well to note that a strict comparison is not possible due to the time periods

over which residues were calculated. The Day periods run from 1200Z to 2400Z, which is all daylight in June through August. However, the Night periods, from 0000Z to 1200Z, actually contain from two to four hours of solar exposure, albeit at low solar elevations. Thus a pure nightime radiation curve could not be expected even if all my assumptions were true.

The effect of convection is assumed to be heating and moistening aloft, and cooling and drying near the ground, in effect wiping out the instability which causes it in the first place. In other words, negative Residues should occur near the ground with compensating positive values at high levels. The magnitude of this effect is indeterminate. It is also in addition to the radiation effects.

Figures 26 and 27 show the vertical composites for the four categories. The curves for composites including the "bum" data are not shown since they differ very little qualitatively from the "pure" data profiles.

Looking first to the No Weather profiles on Figure 26, I am encouraged by the fit to my estimate of the radiation effects. The Day surface layer heating is near .10 kj ton^{-1} sec^{-1}, or about the order of magnitude of the solar absorption (4°C/12 hours). However, there are some problems. First, the Day-No Weather profile crosses from heating to cooling at about 750 mb, rather than 500 mb as on my

radiative heating profile. This might just be due to a bad guess by me as to the depth of eddy heat transfer from the surface; if the top of this effect were lower the curves would match better.

Second, the cooling lobe near 300 mb on the theoretical profile has no match on either the Day or Night No Weather profiles. Other than this, the Night curve is a good match, for shape and magnitudes, to the nighttime profile in Figure 25.

The Weather profiles are encouraging. The Night curve exhibits the proper shape with respect to the No Weather-Night curve--additional cooling near the ground up to 650 mb with warming above 650 mb to 250 mb. The Day curve is somewhat disappointing; the cooling is slightly less than the No Weather-Day curve below 850 mb, and erratic but warming above 850 mb. A bit more consistency would have been desirable.

All four profiles exhibit the high level (100 mb to 250 mb) warming lobe. The magnitude of this lobe is about .12 kj ton^{-1} sec^{-1}, or equivalent to a heating rate of about 10 degrees/day. This cannot be water vapor injection or the effects of neglecting the presence of ice in the model since it is equally prominent in the No Weather profiles.

What is this peak then? It cannot be the ozone absorption of ultraviolet radiation. Fleagle and Businger (1963) place that layer

much higher, near 25 km (25 mb). Also, the ozone peak should be no larger than about 10% of the incoming solar radiation, or .015 kj ton^{-1} sec^{-1} in my units (Willett and Sanders--1959). The best guess is error: Figure 20 shows the tropopause to be at about the same pressure as this peak. If we assume, for a moment, dry air at the altitude of this peak:

$$Res = C_p\left[\frac{\partial \bar{T}}{\partial t} + \overline{\nabla \cdot \underset{\sim}{V} T} + \frac{\partial}{\partial p}(\bar{\omega}\bar{T})\right] - \frac{R\bar{\omega}\bar{T}}{p}$$

$$= C_p\left[\frac{\partial \bar{T}}{\partial t} + \overline{\underset{\sim}{V} \cdot \nabla T} + \bar{\omega}\frac{\partial \bar{T}}{\partial p} - \frac{R}{C_p}\frac{\bar{T}}{p}\bar{\omega}\right]$$

$$= C_p\left[\frac{\partial \bar{T}}{\partial t} + \overline{\underset{\sim}{V} \cdot \nabla T} + \bar{\omega}\left(\frac{\partial \bar{T}}{\partial p} - \frac{\alpha}{C_p}\right)\right]$$

and for dry adiabatic motions:

$$C_p\, dT - \alpha\, dp = 0$$

So:

$$\left.\frac{dT}{dp}\right]_{ad} = \frac{\alpha}{C_p}$$

and:

$$Res = C_p\left[\frac{\partial \bar{T}}{\partial t} + \overline{\underset{\sim}{V} \cdot \nabla T} + \bar{\omega}\left(\frac{\partial \bar{T}}{\partial p} - \left.\frac{dT}{dp}\right]_{ad}\right)\right]$$

A quick calculation of the last term will yield a Residue from ascent in the 200 to 100 mb layer of +.08 kj ton^{-1} sec^{-1}, about the order of magnitude of the unexplained peak. That is, weak ascent in the stable

air above the tropopause would produce a net computed cooling not actually observed, and hence a positive residue of about the right size. If the actual omegas are zero in this height range, in other words, this peak would occur as it has. My best guess, therefore, is that in my zeal to have an upper boundary above the effects of the largest cumulus, I overshot. The $\omega = 0$ level is probably closer to 100 mb or 150 mb than to 50 mb, and hence the omegas are all off by the value of ω at 50 mb, which can be estimated from Figure 19 to be +.0002 mb/sec, a descent of about 2 mb/3 hours. The correction for this error would account for the weak ascent shown in the No Weather-Night omega profile below 350 mb on Figure 19; this should actually be weak descent on the order of .0001 to .0003 mb/sec.

The relationship of the Weather to the No Weather curves in Figure 26 was encouraging enough that one further experiment was attempted. Assume that the No Weather curves accurately reflect the radiation and noise profiles for all days. Then by subtracting these profiles from the corresponding Weather case profiles I should see only the effects of convection, plus any noise increase due to the convection. Figure 27 shows these Day and Night difference profiles. The assumption that the radiation profiles are the same in fair weather and foul is shaky, and Johnson and Shen (1968) have shown that the profiles in fact are <u>not</u> similar, at least for stratiform

cloud systems. Nevertheless, I press on.

As before, the correspondence with theory is heartening. The profile is negative below 650 mb at Night and 850 mb during Day periods. Strong warming occurs above these levels except for the strange negative dip in the Day profile at 150 mb. The magnitude of the cooling/warming for the Night profile is about the solar absorption value and about three times the longwave radiative cooling value.

The positive variations in the Day profile are striking, with a strong maximum at 750 mb and a lesser from 550 to 350 mb. At the risk of drawing conclusions from what may only be random variations due to a small sample size (four Weather-Day cases), some conjecture can be made as to the nature of these. The lesser peak (550 to 350 mb, or 5 to 8.5 km) corresponds well with a similar peak on the Night curve, and corresponds to the tops of cumulonimbus towers, showers or thunderstorms. The strongest peak, on the other hand, is at about the height (2.5 km) of the stratocumulus and building cumulus towers which accompany their much larger brethren. Perhaps we see here the difference in the amount of cumulus tops in the layer between 850 and 650 mb between daytime and nighttime convection. Perhaps some digging needs to be done to see if nighttime thunderstorms occur without a surrounding retinue of smaller cumuli

of varying heights. How much difference in coverage of these smaller cumulus is there between Day and Night Weather cases?

After all this analysis of data, one wonders how these results compare to other similar efforts. The closest work of this nature has been done by Ninomiya (1968; 1971) although there are numerous differences. Ninomiya's 1971 article was a major inspiration of this part of my study, and a comparison will yield a further cross-check of my results.

Ninomiya (1971) undertook a case study of a severe thunderstorm complex over the central Appalachians in April 1968, using satellite and conventional data. A part of this study was an analysis of the vertical distribution of a quantity very similar to my Residue (10.19), with the objective of defining the vertical heat transfer due to convection in this case. Ninomiya's study volume was based on the quadrangle bounded by the rawinsonde stations at Pittsburgh, Huntington, West Virginia, Greensboro, North Carolina, and Dulles Airport, Washington, D. C. This quadrangle has an area of 10.1×10^4 km^2 versus my volume's base area of 17.0×10^4 km^2. Although the thunderstorm complex tops reached into the layer between 300 and 200 mb, Ninomiya chose his upper boundary at 200 mb and used a 100 mb layer thickness.

Ninomiya's budget equations are identical to (10.14a and b) except

that heating due to radiation and freezing does not appear. The reason for neglecting radiation is not stated, even though it appears in the derivation of these equations in the 1968 article. Ninomiya simplified the computation in this case by substituting for the partial derivatives $\frac{\partial \bar{T}}{\partial t}$ and $\frac{\partial \bar{q}}{\partial t}$ using the space-time transformation:

$$\frac{\partial}{\partial t} \approx -C \frac{\partial}{\partial \ell}$$

where C is the observed speed of movement (assumed constant) of the thunderstorm complex and ℓ is distance in the direction parallel to the complex's movement. This approximation allowed him to compute his "residue" using data from only one sounding time rather than by integrating his budget equations over a twelve hour period as I did. If $\underset{\sim}{C}$ is approximately equal to the mean winds (that is, if the system is moving with the upper flow), then:

$$\frac{d}{dt} \approx \omega \frac{\partial}{\partial p}$$

and (10.14a and b) would become

$$C_p \omega \frac{\partial T}{\partial p} - \frac{R \omega T}{p} = \mathcal{R} + L_v (C - E) + L_f (F - M)$$

$$\omega \frac{\partial q}{\partial p} = E - C$$

That is, the major changes to the budgets of heat and water vapor

would be due to vertical motions.

Having discarded radiation, Ninomiya further simplified his "Residue" down to:

$$\frac{\partial}{\partial p}\left(C_p \overline{\omega' T'} + L_v \overline{\omega' q'}\right)$$

by discarding terms such as $\frac{R\overline{\omega' T'}}{p}$ from (10.19), and was thus able to integrate his "residue" from the upper boundary down to get a value of the sum of the eddy fluxes ($C_p\overline{w'T'} + L_v\overline{w'q'}$) at fixed pressure. Ninomiya was fortunate in that he did his analysis on evening data (0000Z 24 April 1968). At this time the sun angle was low and heating due to solar absorption should have been zero at most levels. In fact, one of his charts in this paper shows the terminator passing through the east edge of the quadrangle at 2300Z 23 April 1968. This would leave only the effects of longwave radiation to contend with.

Ninomiya computed his vertical velocity from divergences found by a boundary integral just as I did. His omega profile for this case is very similar to my Weather-Day profile of omega (Figure 19). His profile has a broad peak of ascent from 650 to 300 mb with values near -5 mb/hour (1.4×10^{-3} mb sec^{-1}) while mine shows the peak from 300 mb with values near 1.8×10^{-3} mb sec^{-1}. The reason my mean peak value is larger than his single-case peak value is probably the too-high upper boundary previously discussed; this would tend to inflate

upward omega values.

Comparison with Ninomiya's "residues" is more difficult. Since he has taken a "snapshot" at 0000Z by using the space-time transformation, solar radiation absorption should be zero compared to other factors, hence his profile of residue is equivalent to my Weather-Night profile in Figure 26. Ninomiya's profile shows the strongest cooling at the surface, with strongest heating in the 400 to 300 mb layer. The profile crosses zero at about 500 mb. My profile has strongest cooling near the ground at 950 mb, strongest heating at 150 mb (due to the too-high upper boundary) and a cross-over at 600 mb with an unexplained negative dip at 300 mb. The magnitudes of these peaks do not agree, however; Ninomiya's extrema are -13 ly/hour (.0299 kj ton^{-1} sec^{-1}) and +24 ly/hour (.0552 kj ton^{-1} sec^{-1}) while mine are -.23 kj ton^{-1} sec^{-1} and +.12 kj ton^{-1} sec^{-1}. At least the shapes of the profiles are similar.

Why does Ninomiya's curve agree so well with theory on one shot? Perhaps his approximations, being different from mine, gave better results from the data. I think not. The space-time transformation itself is very shaky, and the use of 200 mb as an upper boundary is somewhat suspicious considering the heights of the cells in the thunderstorm complex. I think Ninomiya was fortunate enough to pick a case where the data was good and where a strong convective system

forced the upward heat transfer to stand out in his "residues."

If my results are this encouraging, why haven't I shown the individual cases as Ninomiya did? Aside from the volume of the case results, the plain fact is that the cases individually look very little like the composites. The scatter in, for example, the mean residue magnitudes is magnified in looking at the Residues layer by layer for a group of four to eight cases. Even the shape of the Residue profile for a case bears little resemblance to the shape of the composite profile. Figure 28 shows the profiles for two cases in the Day-Weather category along with the composite profile for that category. It seems clear that the noise in the observation and computation of parameters all but obscures the phenomena we are looking for except through statistical study of a number of cases, as was done here.

Just how bad the noise or difficulties can get is illustrated by the Day-Weather case of 1200Z 4 August 1972 to 0000Z 5 August 1972. During this period weak shower activity ended shortly after the period began and a cooling, drying wind from the northwest set in more strongly at all levels below the tropopause. Temperatures below 500 mb fell 3 to 5 degrees in the twelve hours and the mixing ratio fell by 3-4 gm/kg to about half its initial value. The individual terms compute out these effects well, but when the terms are summed

there is still a net cooling on the order -.17 kj ton^{-1} sec^{-1}, or about 30% more than the negative of the solar constant! This is, furthermore, a daytime case.

The only glitch in the data for this case was missing winds above 400 mb in the Caribou, Maine, RAOB for 1200Z August 4. Caribou contributes only about .25 of the variance to the values of the parameters for the extreme northeast grid point in the volume, and to no other grid point; thus this can hardly be the cause of variations in the residue of this order. The variations must be chalked up to observational error and motions not accounted for in my model, or to the error in omega, previously discussed, caused by placing the upper boundary too high.

Admittedly, there are shortcomings in my model and its programming, primarily in the methods used for interpolating missing data.

The handling of the high levels is particularly suspect. The use of one-half the 100 mb wind for the 50 mb wind is very suspect, since the climatological winds there are easterly rather than westerly, the crossover coming at about 100 mb. The fallbacks for temperature are reasonable enough (temperature at level below, temperature twelve hours prior, and -60°C), but the handling of humidity could be improved. The Asheville 645 decks and the teletype RAOB reports cease reporting relative humidity or dewpoint at about 300 to 250 mb. This

is not due to a very low mixing ratio but to the temperature limitations of the dewpoint detector. Mastenbrook (1971) indicates that the assumption of a nearly constant mixing ratio of 2-3 x 10^{-6} at these heights is supported by frost point observations in the mid-latitude stratosphere. Furthermore, Kuhn and Stearns (1973) and Shlanta and Kuhn (1973) have detected increases in the mixing ratio at these heights due to thunderstorms on the order of 40 to 50% as measured with instrumented WB-57F aircraft. While these changes may not contribute all that much to the Residue (they didn't at lower altitudes) it would be nice to have included them all the same. Perhaps with a correction of the upper boundary to fix the omegas, the mixing ratio changes would assume more significance.

The best change to the model would be an improvement in the interpolation for missing data. The present scheme, while simple to program, caused so many lost cases that the convenience was not worth the reduction in sample size. The best fix for any missing parameter at one station would be to "bogus" the parameter using the regression equation for that station and the observed values of the parameter at the other stations. This is a complicated bit of logic to program, but would be worth the effort, particularly in the upper levels for missing stratospheric winds.

In summary, the residue model provides some confirmation of the

theory of the effects of small-scale convection on large scale parameters. However, the signal level is so near the noise level that the model cannot be used diagnostically on individual cases unless some improvements are made in the physics or mathematics of its development.

14. Conclusions:

In Both Parts I and II we have seen the presence of a phenomenon suggested by the available data but not defined well enough for careful study or diagnostic application. In Part I the phenomenon was a mesoscale pressure pattern associated with lines of thunderstorms over New England. More and better data are needed for successful exploitation of this study. In Part II the effects of small scale convection on large scale systems were discovered to be detectable in the synoptic-scale rawinsonde data but was too near the noise level to allow day-by-day study of convection.

ACKNOWLEDGEMENT

The author is deeply indebted to the U. S. Air Force for funding his studies under the Air Force Institute of Technology, Civilian Institutions program. Research costs for data and data processing were funded by the National Science Foundation and the National Weather Service (National Oceanic and Atmospheric Administration, Department of Commerce), under joint grants to Professor Frederick Sanders' Severe Convective Storms Project (NSF Grant A36107; NOAA Grant 04-3-022-26).

The author feels a deep personal debt to Professor Sanders for his inspiration, supervision, guidance and patience during this research. Special thanks are also due to Spiros Geotis for help in interpreting radar imagery. This thesis would not have been possible without the help of Edward Nelson, David Katz, and Roger Edson who assisted with data extraction and map plotting. The manuscript was typed by Robin Adams. The charts and drawings are the fine work of Isabelle Kole.

REFERENCES

Arakawa, A., 1971: A parameterization of cumulus convection and its application to numerical simulation of the tropical general circulation. Paper presented at the Seventh Technical Conference on Hurricanes and Tropical Meteorology, Barbados, W.I., December, 1971.

Austin, P. M., and Houze, R. A. Jr., 1972: Analysis of the structure of precipitation patterns in New England. Journal of Applied Meteorology, 11, 926-935.

Baker, Dennis G., 1970: A study of high pressure ridges east of the Appalachian Mountains. Ph.D. Thesis, Department of Meteorology, Massachusetts Institute of Technology, August, 1970, 127 pp.

Bosart, L. F., 1973: Detailed analysis of precipitation patterns associated with mesoscale features accompanying United States East Coast Cyclogenesis. Monthly Weather Review, 101, January, 1973, 1-12.

Bosart, L. F., Vando, C. J., and Helsdon, J. H. Jr., 1972: Coastal frontogenesis. Journal of Applied Meteorology, 11, December, 1972, 1236-1258.

Bullock, Horn, and Johnson, 1969: The contribution of infrared cooling to the vertical motion field. Monthly Weather Review, 97, May, 1969, 371-381.

Businger, J. A., and Kuhn, P. M., 1960: On the observation of total and net atmospheric radiation. Journal of Meteorology, 17, 400-405.

Chien, H., and Smith, P. J., 1973: On the estimation of kinematic parameters in the atmosphere from radiosonde wind data. Monthly Weather Review, 101, March, 1973, 252-261.

Dopplick, Thomas G., 1972: Radiative heating of the global atmosphere. Journal of the Atmospheric Sciences, 29, October, 1972, 1278-1294.

Eddy, Amos, 1967: The statistical objective analysis of scalar data fields. Journal of Applied Meteorology, 6, August, 1967, 597-609.

Fankhauser, J. C.: Convective processes resolved by a mesoscale rawin network. Journal of Applied Meteorology, 8, October, 1969, 778-798.

Fleagle, R. G., and Businger, J. A., 1963: An Introduction to Atmospheric Physics. New York, Academic Press, 346 pp.

Hamilton, R. E., 1971: Use of detailed radar intensity data in mesoscale surface analysis. NOAA Tech Memo NWS ER-40, March, 1971, 15 pp.

Houghton, H. G., 1954: On the annual heat balance of the Northern Hemisphere. Journal of Meteorology, 11, February, 1954, 1-9.

Israeli, M., and Sarachik, E. S., 1973: Cumulus parameterization and CISK. Journal of the Atmospheric Sciences, 30, May, 1973, 582-589.

Johnson, D. R., and Shen, W. C., 1968: Profiles of infrared irradiance and cooling through a jet stream. Monthly Weather Review, 96, August, 1968, 559-572.

Kondrat'yev, K. Ya., 1965: Radiative Heat Exchange in the Atmosphere. London, Pergamon Press, 411 pp.

Kuhn, P. M., and Stearns, L. P., 1973: Radiometric observations of atmospheric water vapor injection by thunderstorms. Journal of the Atmospheric Sciences, 30, April, 1973, 507-509.

Leary, C., and Thompson, R. O. R. Y., 1973: Shortcomings of an objective analysis scheme. Journal of Applied Meteorology, 12, June, 1973, 589-594.

London, J., 1957: A study of the atmospheric heat balance. Final Report AFC-TR-57-287, OTS PB 129551, Department of Meteorology and Oceanography, NYU, 99 pp.

Lorenz, Edward N., 1969: The nature and theory of the general circulation of the atmosphere. World Meteorological Organization, 218, TP 115, 161 pp.

Mastenbrook, H. J., 1971: The variability of water vapor in the stratosphere. Journal of the Atmospheric Sciences, 28, 1495-1501.

Ninomiya, K., 1968: Heat and water budget over the Japan Sea and the Japan Islands in winter season - with special emphasis on the relation among the supply from sea surface, the convective transfer and the heavy snowfall. Journal of the Meteorological Society of Japan, 46, 343-372.

_____, 1971: Dynamical analysis of outflow from tornado-producing thunderstorms as revealed by ATS III pictures. Journal of Applied Meteorology, 10, April, 1971, 275-294.

O'Brien, J. J., 1970: Alternative solutions to the classical vertical velocity problem. Journal of Applied Meteorology, 9, April, 1970, 197-203.

Ogura, Y., 1972: Cumulus modelling and parameterization. Reviews of Geophysics and Space Physics (in press).

_____, and Cho, Han-Ru, 1973: Diagnostic determination of cumulus cloud populations from observed large-scale variables. Journal of the Atmospheric Sciences, 30, October, 1973, 1276-1286.

Owens, John J. Jr., 1966: Distribution of air mass thunderstorms in New England. S.M. Thesis, Department of Meteorology, Massachusetts Institute of Technology, June, 1966, 117 pp.

Phillips, Norman A., 1972: Introduction to dynamical meteorology. Massachusetts Institute of Technology Class Notes for 19.61.

Sanders, Frederick, 1970: Dynamical forecasting of tropical storm tracks. Transactions of the New York Academy of Science, 32, 495-508.

Saucier, W. J.: Principles of Meteorological Analysis. Chicago, University of Chicago Press, 1955.

Shaw, Lawrence, 1973: Personal correspondence with the author. March and July, 1973.

Shlanta, A., and Kuhn, P. M., 1973: Ozone and water vapor injected into the stratosphere from two isolated thunderstorms. Journal of Applied Meteorology , 12, December, 1973, 1375-1378.

Smith, P. J., 1971: An analysis of kinematic vertical motions. Monthly Weather Review, 99, October, 1971, 715-724.

United States Department of Commerce/Weather Bureau: Manual of Barometry (WBAN), First Edition, 1963.

United States Environmental Data Service, June 1971: Climatological Data.

_____, July 1971: Climatological Data.

_____, August 1971: Climatological Data.

_____, July 1972: Climatological Data.

_____, August 1972: Climatological Data.

Environmental Data Service, NOAA, June 1971: Storm Data.

_____, July 1971: Storm Data.

_____, August 1971: Storm Data.

_____, July 1972: Storm Data.

_____, August 1972: Storm Data.

VonderHaar and Suomi, 1969: Satellite observations of the earth's radiation budget. Science, 163, 667-669.

Willett, H. C., and Sanders, F., 1959: Descriptive Meteorology, 2 Ed., New York, Academic Press, 355 pp.

Williams, Forrest R., 1972: Application of the SANBAR barotropic hurricane forecast model. S.M. Thesis, June 1972, Massachusetts Institute of Technology, Department of Meteorology, 39 pp.

Yanai, M., Esbensen, S., and Chu, J., 1972: Determination of bulk properties of tropical cloud clusters from large-scale heat and moisture budgets. Preprint, Department of Meteorology, University of California, Los Angeles.

TABLE I

LIST OF PROFESSOR SANDERS' INITIAL CASES

8 June 1971	1800 - 2400Z
21 June 1971	1800 - 2400Z
1 July 1971	1800 - 2400Z
17 - 18 July 1971	2100 - 0300Z
7 August 1971	2100 - 2300Z
11 August 1971	1600 - 2100Z

TABLE II

FINAL LIST OF CASE PERIODS

Case Nr.	From	To
1	1200Z, 3 Jun	1200Z, 4 Jun 1971
2	1200Z, 8 Jun	1200Z, 9 Jun 1971
3	1200Z, 21 Jun	1200Z, 22 Jun 1971
4	1200Z, 24 Jun	1200Z, 25 Jun 1971
5	1200Z, 1 Jul	1200Z, 2 Jul 1971
6	1200Z, 17 Jul	1200Z, 18 Jul 1971
7	1200Z, 11 Aug	1200Z, 12 Aug 1971
8	2400Z, 22 Aug	2400Z, 23 Aug 1971
9	1200Z, 21 Jul	1200Z, 22 Jul 1972
10	1200Z, 3 Aug	1200Z, 4 Aug 1972

TABLE III

SUMMARY OF CASE ANALYSES

Case Number	Mesoscale Amplitude	Radar Echo Character	Echo Coverage	Severe Weather (Storm Data)
1	½	Line	<.1	None
2	1	Cell-Area Line-LEWP	.1-.2	Fryeburg, ME, wind damage Statewide: CN, MA, NH (Southern) RI, VT
3	1	Line-Area	.2-.3	Statewide: ME, MA (Northern), NH (Southern)
4	½	Line-Area	<.1	None
5	1	Area-Lines LEWP	.2-.4	Woodland, ME, tornado Oxford, ME, funnel Littleton-Haveshill, MA, tornado Milford, MA, tornado Statewide: CN, ME, MA, NH, VT
6	½	Line-Area	.1-.2	Lewiston-Auburn, ME, lightening damage Greenwood, ME, wind damage Chicopee, MA, wind damage Orange, MA, tornado Plaistow, NH, lightening damage
7	1	Lines	.1-.3	Fryeburg, Bridgeton, and Bingham, ME, tornadoes Sebago Lake, ME, waterspouts Worcester County, MA, TSTM damage Statewide: CN, ME, NH (Central)
8	0	Line-Area	.1	None
9	½	Cell-Areas	.1	Middletown, CN, tornado Tyngsboro-Chelmsford, MA, tornado Lynnfield, MA, tornado

TABLE III, Continued

SUMMARY OF CASE ANALYSES

Case Number	Mesoscale Amplitude	Radar Echo Character	Echo Coverage	Severe Weather (Storm Data)
9 Continued	½	Cell-Areas	.1	Enfield, NH, tornado Hudson, NH, funnel cloud Statewide: MA (Northeast)
10	½	Line-Areas	.1	Statewide: CN (Southern), RI

TABLE IV

CHARACTERISTICS OF MIT WR-66 WEATHER RADAR

Wavelength	10.5 cm
Beam Width	1.3°
Transmitted Power	600 kw

(after Austin and Houze -1972-)

TABLE V

Table of Symbols and Units

x, y, z	orthogonal coordinates in earth frame of reference (meters)
t	time (sec)
p	pressure, vertical coordinate (mb)
$u = \frac{dx}{dt}$, $v = \frac{dy}{dt}$, $w = \frac{dp}{dt}$	three components of wind velocity vector in frame of reference (m^{-1})
$\underset{\sim}{V} = \hat{i}u + \hat{j}v$	horizontal velocity vector
$\nabla = \hat{i}\frac{\partial}{\partial x} + \hat{j}\frac{\partial}{\partial y}$	horizontal gradient operator
T	temperature (°Kelvin)
q	water vapor mixing ratio (kg/kg)
l	liquid water mixing ratio (kg/kg)
i	ice mixing ratio (kg/kg)
ρ	density of air (kg m^{-3})
α	specific volume ($m^3 kg^{-1}$)
(E-C)	net change of water vapor content due to evaporation and condensation, per unit mass per unit time (kg kg^{-1} ton^{-1} sec^{-1})
(F-M)	net change of ice content due to freezing and melting, per unit mass per unit time (kg kg^{-1} ton^{-1} sec^{-1})
Q	rate of heating per unit time per unit mass (kj ton^{-1} sec^{-1})

TABLE V, Continued

Table of Symbols and Units

ω_{fl} ..... fall velocity function of the liquid water in a volume of air. Function of x, y, p, t, and l. ($mb\ sec^{-1}$)

ω_{fi} ..... fall velocity function of the solid water (ice) phase particles in a volume of air. Function of x, y, p, t, and i.

C_v ..... Specific heat of air at constant volume ($717\ kj\ ton^{-1}\ deg^{-1}$)

R ..... gas constant for air ($287\ kj\ ton^{-1}\ deg^{-1}$)

C_p ..... specific heat of air at constant pressure ($1004\ kj\ ton^{-1}\ deg^{-1}$)

L_v ..... latent heat of vaporization of water ($2.501 \times 10^6\ kj\ ton^{-1}$)

L_f ..... latent heat of fusion of water ($0.334 \times 10^6\ kj\ ton^{-1}$)

$\mathscr{s}$ ..... specific entropy

$\theta = T\left(\frac{P_{oo}}{p}\right)^{K}$ ..... potential temperature (°K)

$K = R/C_p = 2/7$

$s = C_pT + gz$ ..... dry static energy ($kj\ ton^{-1}$)

TABLE V, Continued

Table of Symbols and Units

$h = s + L_v q$ ..... moist static energy (kj ton^{-1})

g ..... gravitational acceleration ($9.8\ m\ sec^{-2}$)

$\mathcal{R}$ ..... heating or cooling by radiation (kjoules $ton^{-1}\ sec^{-1}$)

$\underset{\sim}{dl}$ ..... small element of boundary (m)

ds ..... small element of surface (m^2)

TABLE VI

REGRESSION EQUATIONS USED IN OBJECTIVE ANALYSIS

Rawinsonde Stations			Grid Points and Coefficients							
Location	WMO Number	Latitude (°N) Longitude (°W)	41.0 74.0	41.0 72.5	41.0 71.0	41.0 69.5	42.1 74.0	42.1 72.5	42.1 71.0	42.1 69.5
Chatham, Massachusetts	74494					.383053			.706878	.357982
Nantucket, Massachusetts	72506			.388104	.718318	.591213		.398646		.363854
Albany, New York	72518		.245308				.646838	.640362	.319290	
Portland, Maine	72606									.286428
New York, New York	74486		.749850	.641131	.302123		.358333			
Maniwaki, Ontario	72722									
Caribou, Maine	72712									

TABLE VI, Continued

REGRESSION EQUATIONS USED IN OBJECTIVE ANALYSIS

Rawinsonde Stations			Grid Points and Coefficients							
Location	WMO Number	Latitude (°N) Longitude (°W)	43.2 74.0	43.2 72.5	43.2 71.0	43.2 69.5	44.3 74.0	44.3 72.5	44.3 71.0	44.3 69.5
Chatham, Massachusetts	74494									
Nantucket, Massachusetts	72506									
Albany, New York	72518		.861647	.605584	.275562	.307363	.496483	.286381		
Portland, Maine	72606			.419983	.736072	.692401	.194132	.526791	.859770	.767359
New York, New York	74486									
Maniwaki, Ontario	72722		.155416				.411663	.291006	.184046	
Caribou, Maine	72712									.267275

"BOGUSING" EQUATION:

(Maniwaki) = .689862 (Albany) - .285747 (New York) + .313354 (Moosinee, Ont.) + .729232 (Buffalo, N.Y.)
- .461812 (Pittsburgh, PA) + .272157 (Caribou) - .270716 (Chatham)

TABLE VII

RESULTS OF UNIFORM WIND TESTS

Model Year	Input Wind Speed (m/sec)	Input Wind Direction	Output u or v (m/sec)	Uncorrected Divergence (sec^{-1})	Uncorrected Omega (mb/sec)
1971	10	270	10.27	-5.89×10^{-7}	$+5.60 \times 10^{-4}$
	10	180	10.27	$+1.121 \times 10^{-7}$ $(+4.96 \times 10^{-7})$*	-1.064×10^{-4} (-4.91×10^{-4})*
1972	10	270	10.06	$+4.82 \times 10^{-7}$	-4.57×10^{-4}
	10	180	10.06	-1.451×10^{-6} (-1.07×10^{-6})*	$+1.38 \times 10^{-3}$ (1.013×10^{-3})*

* Quantities in parentheses are values of error from the expected south wind divergence of -3.84×10^{-7} sec^{-1}.

TABLE VIII

VERTICAL COMPOSITES OF AREA MEAN PARAMETERS

NO WEATHER CASES

(a) DAY

Level Number	Pressure	u (m/sec)	v (m/sec)	omega (mb/sec) x104	T (°C)	q (g/kg)
1	50	-1.329	-0.629	0	-55.08	0
2	100	11.284	-1.849	-2.97	-59.26	0
3	150	20.016	-3.842	-3.25	-58.22	0
4	200	25.408	-2.309	-1.55	-55.28	.002
5	250	23.901	-2.631	+1.52	-48.64	.042
6	300	21.221	-3.524	4.77	-38.96	.106
7	350	18.521	-3.307	6.56	-30.62	.232
8	400	16.204	-3.923	7.80	-23.40	.353
9	450	13.744	-3.394	8.58	-17.18	.639
10	500	12.064	-3.444	3.32	-11.69	.801
11	550	10.658	-3.538	7.95	-6.88	1.162
12	600	9.526	-3.501	7.13	-2.98	1.412
13	650	8.335	-3.388	7.09	+0.24	1.950
14	700	7.216	-3.458	6.99	2.70	2.888
15	750	6.354	-3.819	6.67	4.74	3.804
16	800	4.568	-3.686	6.31	7.80	4.766
17	850	3.151	-2.494	4.98	10.87	5.904
18	900	1.167	-2.604	3.81	14.18	6.552
19	950	-0.074	-2.506	1.60	16.63	7.229
20	Surface	+0.011	-1.071	0	18.11	9.254

TABLE VIII, Continued

VERTICAL COMPOSITES OF AREA MEAN PARAMETERS

NO WEATHER CASES, Continued

(b) NIGHT

Level Number	Pressure	u (m/sec)	v (m/sec)	omega (mb/sec) $\times 10^4$	T (°C)	q (g/kg)
1	50	-2.619	-0.878	0	-55.22	0
2	100	8.553	-2.995	-1.11	-59.36	0
3	150	17.407	-6.531	-0.81	-58.72	0
4	200	22.378	-8.281	+0.86	-54.52	.002
5	250	20.848	-9.159	+2.64	-48.26	.049
6	300	18.625	-6.421	2.45	-38.95	.120
7	350	17.001	-5.367	+1.07	-30.45	.260
8	400	15.539	-4.996	-0.19	-23.40	.487
9	450	14.053	-4.070	-1.12	-17.12	.844
10	500	12.532	-4.358	-9.48	-11.72	1.051
11	550	11.422	-4.289	-2.03	-6.82	1.368
12	600	10.232	-4.296	-1.80	-2.75	1.787
13	650	8.578	-4.609	-1.84	+0.65	2.066
14	700	7.157	-4.300	-2.02	2.88	2.984
15	750	5.721	-4.096	-2.39	5.48	3.900
16	800	4.505	-3.461	-2.42	7.88	5.490
17	850	3.742	-2.200	-1.68	11.09	6.275
18	900	2.191	-1.890	-0.39	14.61	6.565
19	950	0.946	-0.871	+0.61	16.97	7.432
20	Surface	0.106	+0.386	0	17.84	9.702

TABLE VIII, Continued

VERTICAL COMPOSITES OF AREA MEAN PARAMETERS

WEATHER CASES

(c) DAY

Level Number	Pressure	u (m/sec)	v (m/sec)	omega (mb/sec) $\times 10^4$	T (°C)	q (g/kg)
1	50	-3.641	-3.579	0	-56.31	0
2	100	7.455	-4.861	-2.70	-62.67	0
3	150	16.795	-6.165	-2.64	-61.84	0
4	200	23.118	-9.525	-3.71	-56.81	.009
5	250	21.829	-5.695	-7.96	-45.68	.106
6	300	19.704	-3.522	-12.12	-35.23	.213
7	350	18.798	-4.272	-15.80	-26.72	.386
8	400	17.526	-3.741	-17.96	-20.00	.687
9	450	16.909	-2.338	-17.26	-14.21	1.103
10	500	15.739	-2.078	-16.88	-9.08	1.681
11	550	14.849	-1.904	-17.34	-4.95	2.425
12	600	13.856	-1.242	-16.06	-1.10	3.171
13	650	12.755	-1.045	-14.18	2.37	4.168
14	700	11.662	-0.695	-20.66	5.80	5.534
15	750	11.216	-0.484	-12.85	8.56	6.271
16	800	10.116	-0.505	-10.41	11.78	7.960
17	850	8.782	-0.395	-6.44	15.03	9.282
18	900	7.690	-0.478	-4.34	18.14	9.986
19	950	5.600	1.936	-2.06	19.84	11.349
20	Surface	1.362	2.111	0	19.81	12.406

TABLE VIII, Continued

VERTICAL COMPOSITES OF AREA MEAN PARAMETERS

WEATHER CASES, Continued

(d) NIGHT

Level Number	Pressure	u (m/sec)	v (m/sec)	omega (mb/sec) $\times 10^4$	T (°C)	q (g/kg)
1	50	-2.471	-1.679	0	-55.49	0
2	100	9.886	-3.915	-1.38	-61.19	0
3	150	18.807	-6.278	-1.60	-60.72	0
4	200	22.590	-6.000	-1.48	-55.45	.006
5	250	22.281	-4.317	-2.23	-45.44	.071
6	300	20.372	-4.502	-3.98	-34.47	.152
7	350	19.323	-5.196	-7.25	-24.75	.312
8	400	17.951	-5.753	-9.57	-20.32	.510
9	450	16.838	-6.041	-9.87	-14.43	.951
10	500	16.121	-5.797	-9.48	-9.35	1.372
11	550	15.050	-5.628	-9.40	-5.16	1.903
12	600	14.034	-5.148	-8.85	-1.40	2.367
13	650	12.882	-4.807	-7.81	1.91	3.371
14	700	11.884	-4.574	-7.15	5.12	4.510
15	750	10.771	-4.296	-6.93	8.10	5.312
16	800	9.428	-3.984	-5.68	10.78	6.600
17	850	7.426	-3.738	-4.85	13.56	8.161
18	900	5.657	-3.531	-2.91	16.24	8.916
19	950	4.348	-2.717	-1.64	18.34	10.025
20	Surface	2.003	-0.780	0	20.09	11.497

TABLE IX

CASE BREAKDOWN

WEATHER CASES

Omegas in mb/sec; Residues in kj/ton/sec
*Bad (incomplete) data case

(a) DAY (1200-2400Z)

Date	Mean Residue	Mean Residue Magnitude	Mean Omega	Mean Omega Magnitude
8 June 1971	.06000	.08262	-.001522	.001567
25 June 1971	.03972	.14914	-.002698	.002947
21 July 1972	.07905	.13630	+.000104	.000693
3 August 1972	.09180	.10312	-.000244	.001239
*4 June 1971	+.08840	.09267	-.002396	.002409
*4 August 1972	-.01677	.16975	.002251	.002252
MEANS 4(6) Cases	.06764	.11780	-.001090	.001612
	(.05703)	(.12227)	(-.000751)	(.001851)

TABLE IX, Continued

CASE BREAKDOWN

WEATHER CASES, Continued

Omegas in mb/sec; Residues in kj/ton/sec
*Bad (incomplete) data case

(b) NIGHT (0000-1200Z)

Date	Mean Residue	Mean Residue Magnitude	Mean Omega	Mean Omega Magnitude
5 June 1971	-.06160	.11870	-.001486	.001559
9 June 1971	-.06380	.18300	-.000686	.002155
22 June 1971	-.08360	.08360	-.000284	.000878
26 June 1971	-.11200	.12940	-.001146	.001462
22 July 1972	-.01873	.13991	-.000515	.000798
23 July 1972	+.06250	.10930	+.000007	.000564
3 August 1972	-.01930	.11100	+.000120	.000875
*4 August 1971	-.04088	.13760	+.000800	.002259
MEANS 7(8) Cases	-.04236	.12499	-.000570	.001184
	(-.04218)	(.12656)	(-.000398)	(.001319)

TABLE IX, Continued

CASE BREAKDOWN

NO WEATHER CASES

Omegas in mb/sec; Residues in kj/ton/sec
*Bad (incomplete) data case

(c) DAY (1200-2400Z)

Date	Mean Residue	Mean Residue Magnitude	Mean Omega	Mean Omega Magnitude
1 June 1971	.01457	.06495	.000780	.000840
9 June 1971	-.03863	.11003	.002018	.002103
16 June 1971	-.03722	.07573	.001215	.001260
22 June 1971	.03391	.04049	-.000008	.000610
23 June 1971	.10641	.10641	.000533	.000940
22 July 1972	.06542	.08787	-.000177	.000761
2 August 1972	.05096	.06875	-.000066	.000683
MEANS 7 cases	.02792	.07918	.000614	.001028

TABLE IX, Continued

CASE BREAKDOWNS

NO WEATHER CASES, Continued

Omegas in mb/sec; Residues in kj/ton/sec
*Bad (incomplete) data case

(d) NIGHT (0000-1200Z)

Date	Mean Residue	Mean Residue Magnitude	Mean Omega	Mean Omega Magnitude
10 June 1971	-.03822	.07598	.001141	.001554
16 June 1971	-.09764	.10600	.001073	.001103
23 June 1971	.00307	.09557	-.001016	.001031
25 June 1971	-.09821	.14719	-.002387	.002576
21 July 1972	-.03603	.11222	.000842	.001035
*4 June 1971	.00120	.11080	-.001959	.001961
*8 June 1971	-.02548	.08372	.000272	.000635
*20 June 1971	-.03268	.05290	.001040	.001401
MEANS 5(8) Cases	-.05341	.10739	-.000069	.001460
	(-.04050)	(.09805)	(-.000124)	(.001412)

TABLE IX, Continued

CASE BREAKDOWN

(e) CUMULATIVE

	Sample Size	Mean Residue Magnitude	Variance Squared
All Weather	11 (14)	.12237 (.12472)	.0007913 (.0008561)
All No Weather	12 (15)	.09093 (.08924)	.0007205 (.0006998)
All Days	11 (13)	.09322 (.09906)	.0009238 (.0011981)
All Nights	12 (16)	.11766 (.11231)	.0007861 (.0009227)
All Cases	23 (29)	.10597 (.10637)	.001001 (.001089)

STANDARD DEVIATION = .0321 (.0330)

TABLE X

Radiational Heating Rates (after Dopplick - 1972)

Heating Rate in Degrees Kelvin Per Day

Level	Number Pressure (mb)	Longwave Radiation	Solar Absorption	Total Due to Radiation
1	50	-0.7	0.30	0.20
2	100	-0.2	0.25	0.20
3	150	-0.4	0.25	0.0
4	200	-1.0	0.3	-0.5
6	300	-2.0	0.6	-1.3
8	400	-2.0	0.9	-1.1
10	500	-1.7	1.2	-0.6
14	700	-1.4	0.8	-0.7
17	850	-1.8	0.6	-1.3
20	Surface	-2.0	0.4	-1.5

TABLE XI

VERTICAL COMPOSITES OF LAYER RESIDUES

Residues are in $kj \cdot ton^{-1} \cdot sec^{-1}$

(a) WEATHER CASES

LAYER		DAY		NIGHT	
Number	Pressure Limits (mb)	Clean Data	All Data	Clean Data	All Data
2	50-100	.11565	.07018	.07847	.10050
3	100-150	.04693	-.01886	.10782	.12210
4	150-200	.04204	-.04967	.09389	.09148
5	200-250	-.01853	-.03645	.04240	.01894
6	250-300	.03674	-.00560	-.02480	-.04449
7	300-350	.05112	-.02859	.02406	.01864
8	350-400	.04591	.010205	.02380	.00086
9	400-450	.05360	.04660	.02088	.02723
10	450-500	.06828	.06767	.03871	.04518
11	500-550	.10984	.10407	.04392	.04946
12	550-600	.01670	.00089	.01976	.03064
13	600-650	-.00142	-.04472	-.05278	-.05673
14	650-700	.14693	.06864	-.08272	-.09375
15	700-750	.23236	.14940	-.08921	-.08527

TABLE XI, Continued

VERTICAL COMPOSITES OF LAYER RESIDUES

Residues are in $kj \cdot ton^{-1} \cdot sec^{-1}$

(a) WEATHER CASES, Continued

LAYER		DAY		NIGHT	
Number	Pressure Limits (mb)	Clean Data	All Data	Clean Data	All Data
16	750-800	.02757	.02266	-.13222	-.11869
17	800-850	.05892	.04292	-.13563	-.12118
18	850-900	.05964	.03311	-.18208	-.16989
19	900-950	.08427	.05590	-.21673	-.21955
20	950-SFC	.10862	.07627	-.20624	-.20679
Algebraic Mean of Residues		.067640	.029717	-.033089	-.032174
Mean Magnitude of Residues		.069740	.049078	.085059	.085335

TABLE XI, Continued

VERTICAL COMPOSITES OF LAYER RESIDUES

Residues are in $kj \cdot ton^{-1} \cdot sec^{-1}$

(b) NO WEATHER CASES

LAYER		DAY	NIGHT	
Number	Pressure Limits (mb)	All Data	Clean Data	All Data
2	50-100	.09618	.06562	.08146
3	100-150	.14351	.08528	.08887
4	150-200	.07613	.03788	.06522
5	200-250	-.00923	-.02568	.00566
6	250-300	-.02429	-.04853	-.03049
7	300-350	-.01618	-.07042	-.04743
8	350-400	-.02134	-.06851	-.04283
9	400-450	-.00987	-.04384	-.02862
10	450-500	-.01957	-.04913	-.03165
11	500-550	-.01998	-.04943	-.03483
12	550-600	-.00328	-.04444	-.03454
13	600-650	-.01041	-.05494	-.05147
14	650-700	-.01131	-.06774	-.05018
15	700-750	+.00289	-.07016	-.07483

TABLE XI, Continued

VERTICAL COMPOSITES OF LAYER RESIDUES

Residues are in $kj \cdot ton^{-1} \cdot sec^{-1}$

(b) NO WEATHER CASES, Continued

LAYER		DAY	NIGHT	
Number	Pressure Limits (mb)	All Data	Clean Data	All Data
16	750-800	+.01374	-.11954	-.08698
17	800-850	.04577	-.11057	-.10812
18	850-900	.07344	-.10147	-.08616
19	900-950	.10972	-.15913	-.15528
20	950-SFC	.11449	-.13869	-.15660
Algebraic Mean of Residues		.027916	-.054407	-.040989
Mean Magnitude of Residues		.043228	.074279	.066380

TABLE XI, Continued

VERTICAL COMPOSITES OF LAYER RESIDUES

Residues are in $kj \cdot ton^{-1} \cdot sec^{-1}$

(c) WEATHER MINUS NO WEATHER

LAYER		DAY		NIGHT	
Number	Pressure Limits (mb)	Clean Data	All Data	Clean Data	All Data
2	50-100	.01947	-.02600	+.01285	+.01904
3	100-150	-.09658	-.16237	+.02254	+.03323
4	150-200	-.03409	-.12580	+.05601	+.02626
5	200-250	-.00930	-.02722	+.06806	+.01328
6	250-300	+.06103	+.01869	+.02373	-.01400
7	300-350	+.06730	-.01241	+.09448	+.06607
8	350-400	+.06725	+.031545	+.09231	+.04369
9	400-450	+.06347	+.05647	+.06472	+.05585
10	450-500	+.08785	+.08724	+.08784	+.07683
11	500-550	+.12982	+.12405	+.09335	+.08429
12	550-600	+.01998	+.00417	+.06420	+.06518
13	600-650	+.00899	-.03431	+.00216	-.00526
14	650-700	+.15824	+.07995	-.01498	-.04357
15	700-750	+.22947	+.14651	-.01905	-.01044

TABLE XI, Continued

VERTICAL COMPOSITES OF LAYER RESIDUES

Residues are in $kj \cdot ton^{-1} \cdot sec^{-1}$

(c) WEATHER MINUS NO WEATHER, Continued

LAYER		DAY		NIGHT	
Number	Pressure Limits (mb)	Clean Data	All Data	Clean Data	All Data
16	750-800	+.01383	+.00892	-.01268	-.03171
17	800-850	+.01315	-.00285	-.02506	-.01306
18	850-900	-.01380	-.04033	-.08061	-.08373
19	900-950	-.02545	-.05382	-.05760	-.06427
20	950-SFC	-.00587	-.03822	-.06755	-.05019
Algebraic Mean of Residues		+.039724	+.001801	+.021318	+.008815

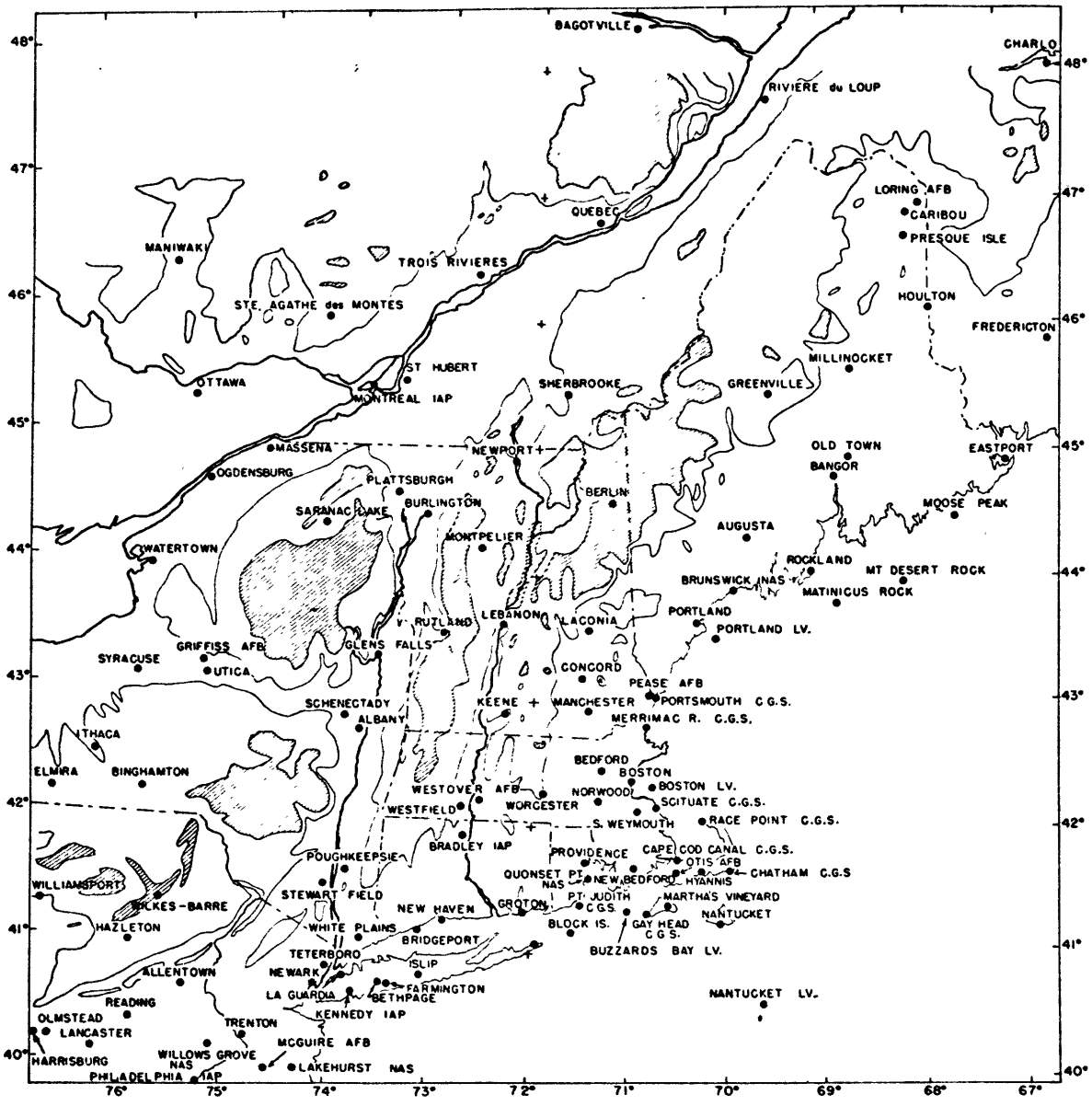

Figure 1: Analysis Area and Surface Observing Stations - Topographic contours are 1000 and 2000 feet MSL. Terrain above 2000 feet is hatched. Terrain field hand smoothed by author from MIT New England Area Chart. Abbreviations: IAP - International Airport, CGS - Coast Guard Station, AFB - Air Force Base, NAS - Naval Air Station.

Figure 2

PRESSURE EFFECTS

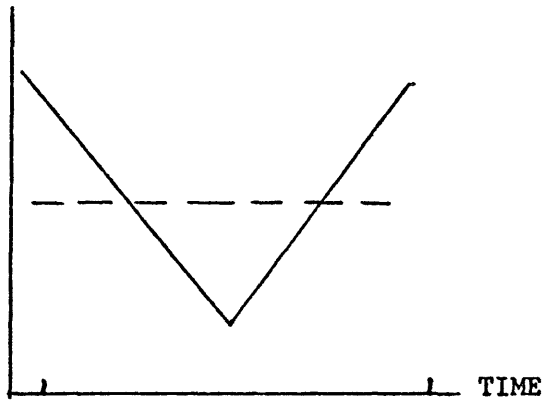

(a) Showing level of time-mean pressure when frontal passage (fropa-minimum pressure is near center of averaging period).

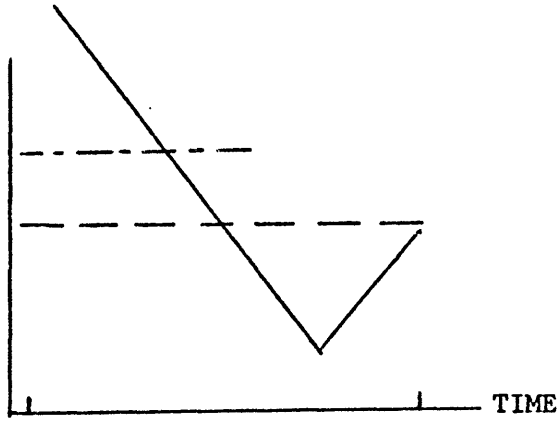

(b) Showing lower time mean pressure when fropa is near end of averaging period.

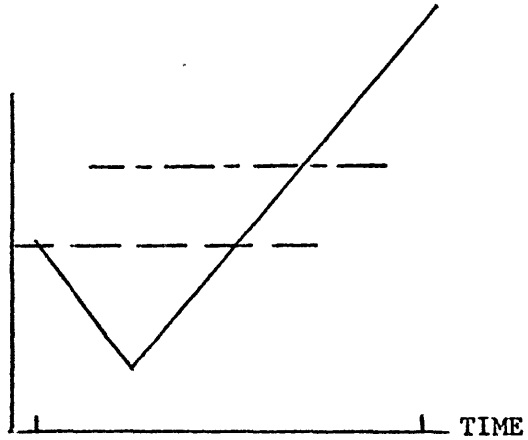

(c) Showing lower time mean pressure when fropa is near beginning of averaging period.

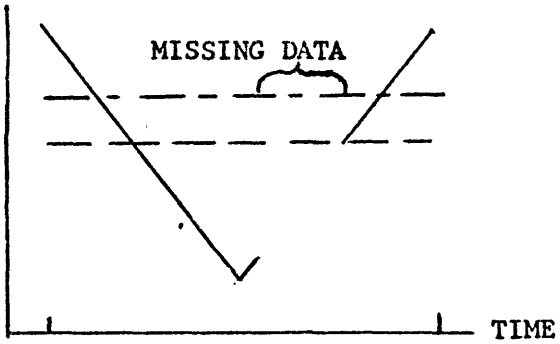

(d) Showing effects on time mean pressure when pressure observations are missing.

— — — — TRUE WAVE MEAN

— · — · — PERIOD MEAN

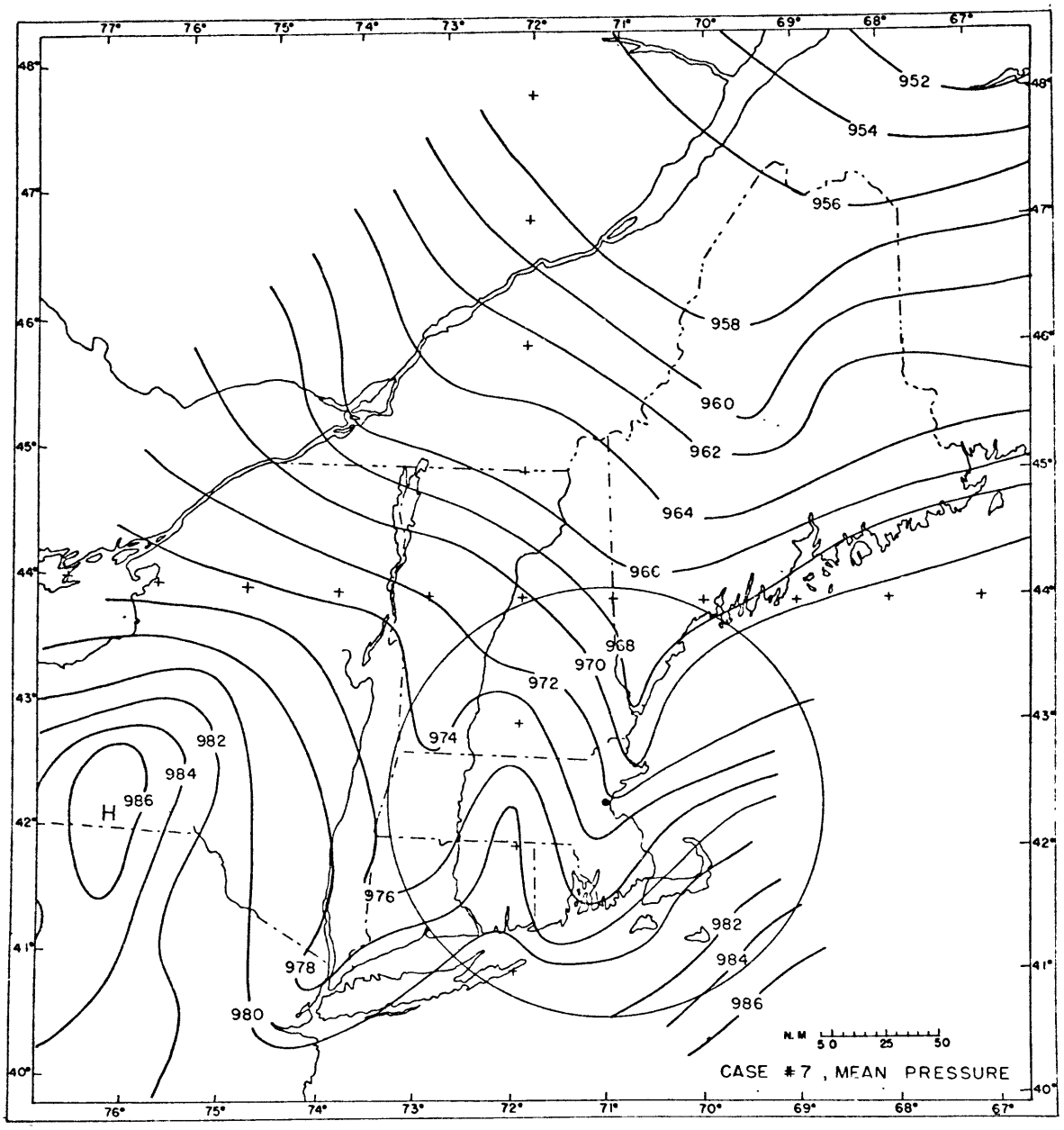

Figure 3: Case #7 Mean Pressure Analysis - Contours are mean pressure minus 20 inches times 100. Circle is 100 NM. range circle from MIT radar.

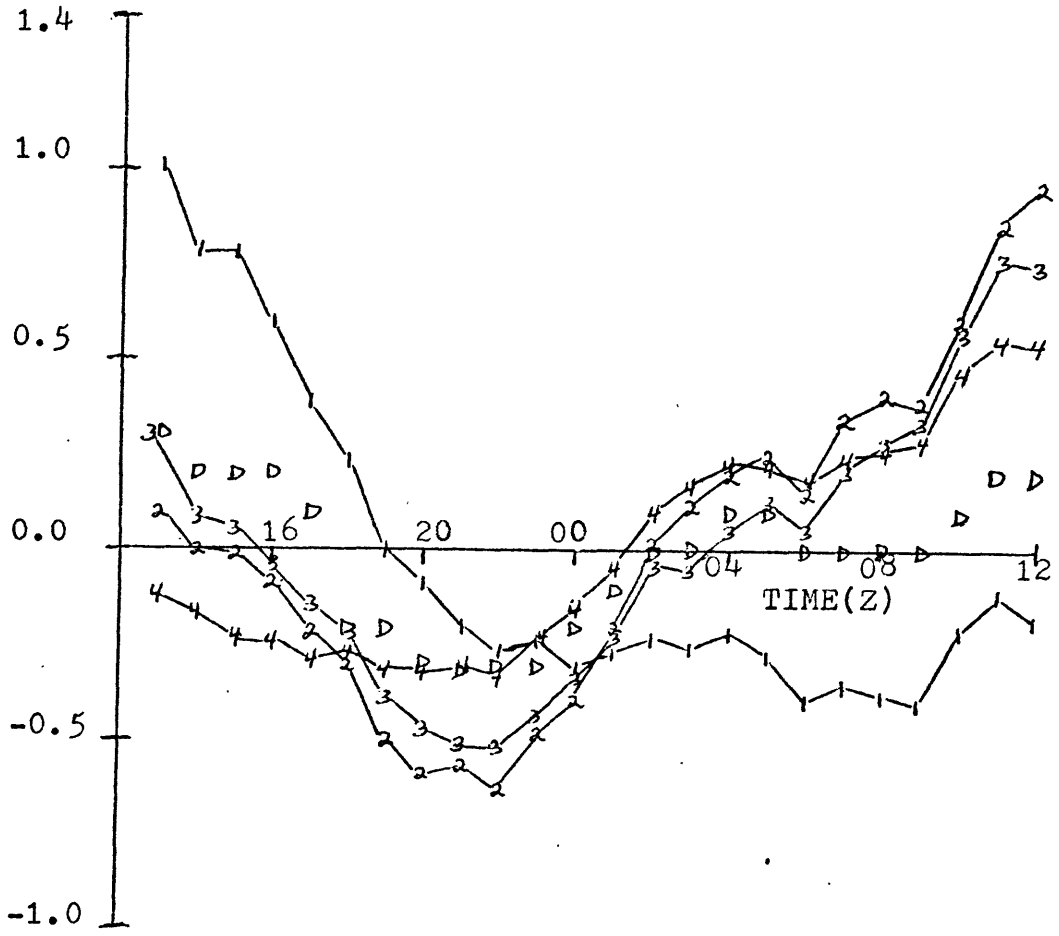

Figure 4: Variation of Map Mean Pressures-June Cases - Ordinate is tenths of inches of mercury. D - dashed curve is diurnal variation of prèssure for Westover AFB, Massachusetts. (Shaw, 1973).

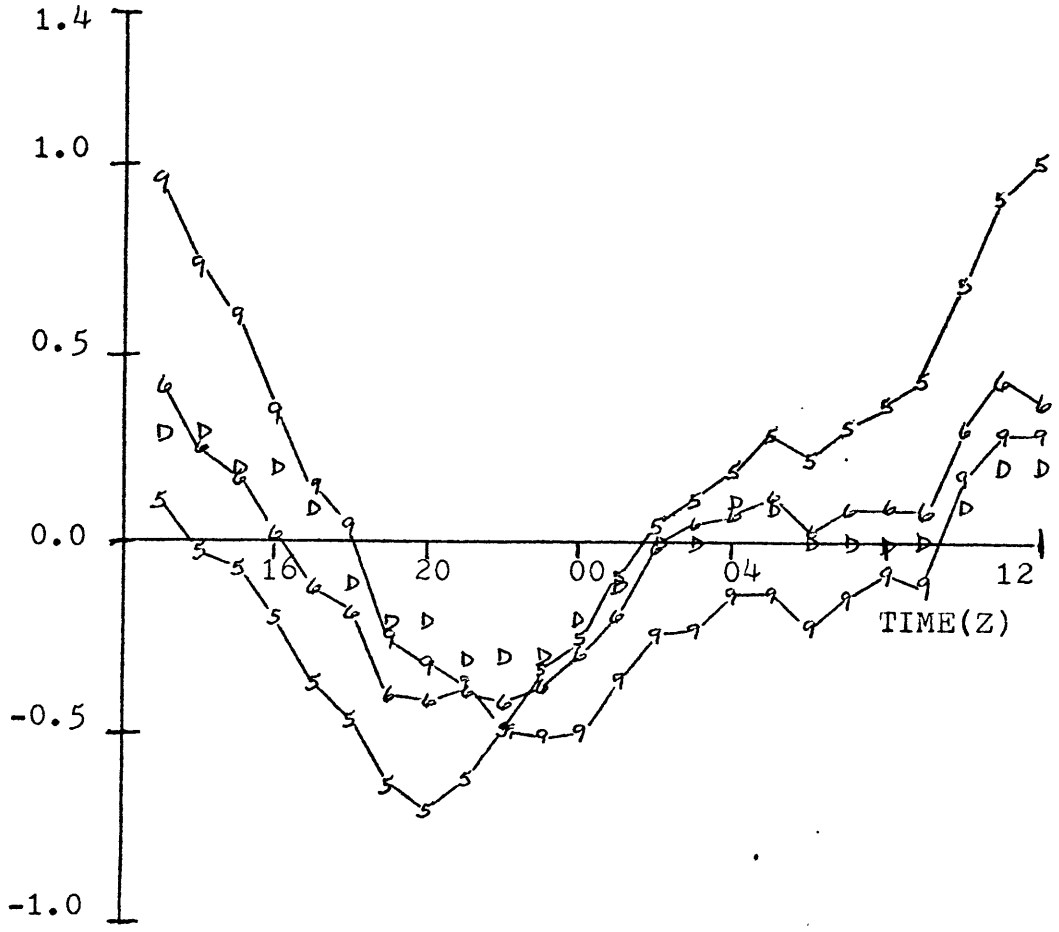

Figure 5: Variation of Map Mean Pressures-July Cases - Ordinate is tenths of inches of mercury. D - dashed curve is diurnal variation of pressure for Westover AFB, Massachusetts. (Shaw, 1973).

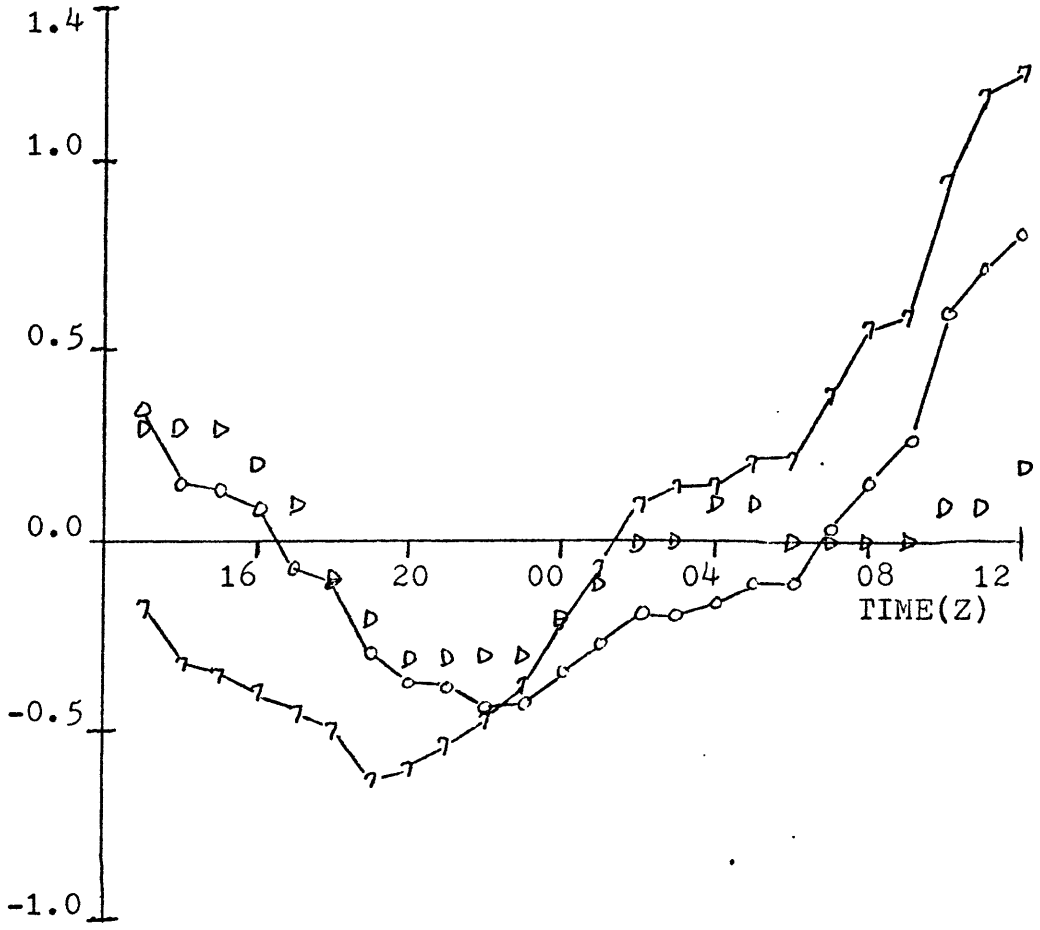

Figure 6: Variation of Map Mean Pressure-August Cases - Ordinate is tenths of inches of mercury. D - dashed curve is diurnal variation of pressure for Westover AFB, Massachusetts. (Shaw, 1973).

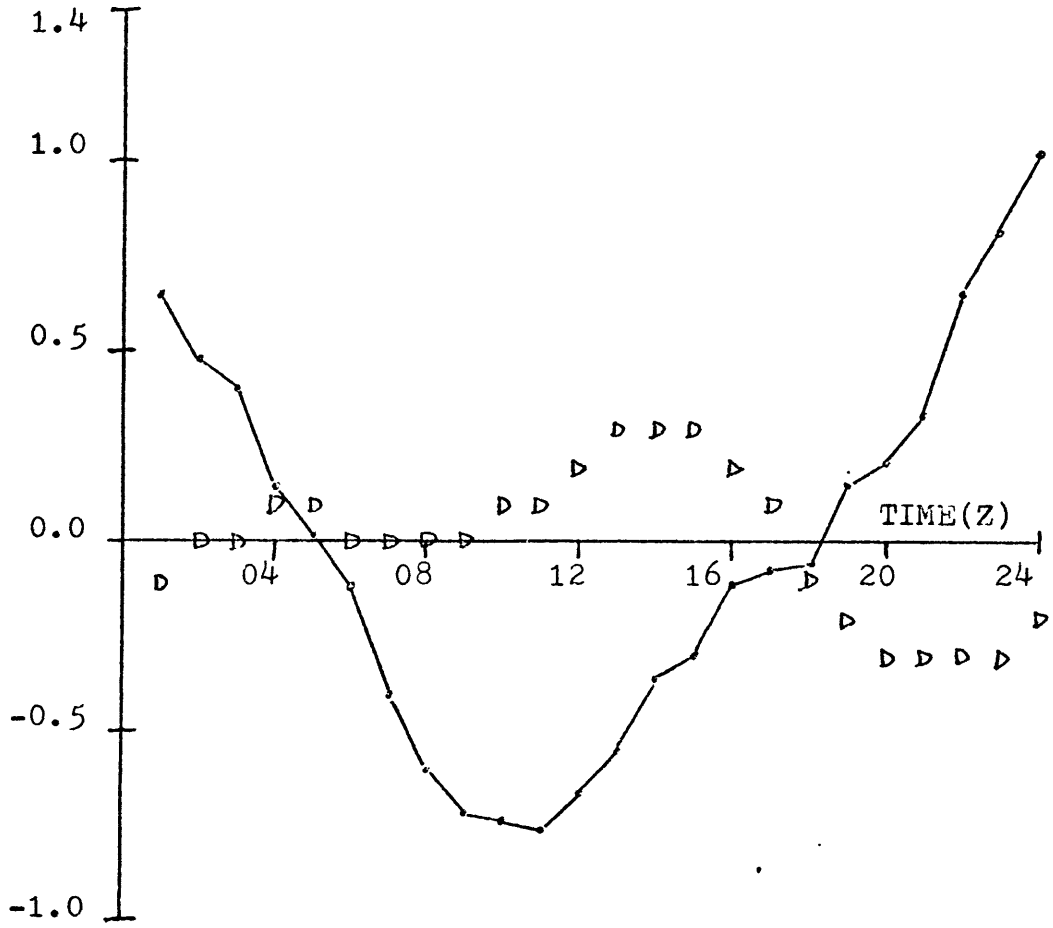

Figure 7: Variation of Map Mean Pressure-Case #8 - Ordinate is tenths of inches of mercury. D - dashed curve is diurnal variation of pressure for Westover AFB, Massachusetts. (Shaw, 1973).

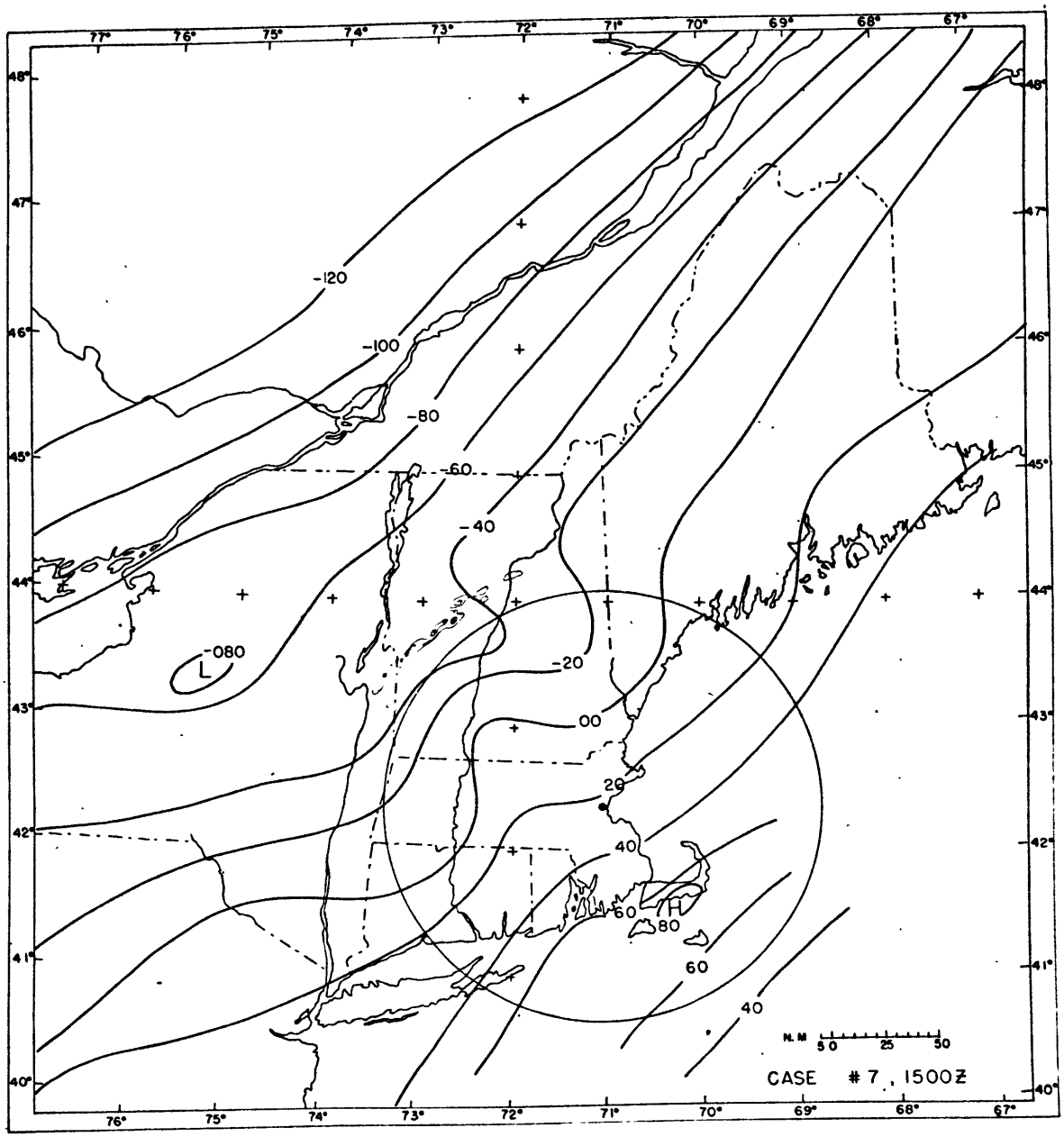

Figure 8: Residual Pressure Analysis-Case 7, 1500Z, 11 August 1971 - Isobars are labeled in thousandths of inches. Radar intensity isolines (fine lines) are for 2, 5, 7, 8, 9, and 10 db. Circle is 100 NM range from M.I.T. radar.

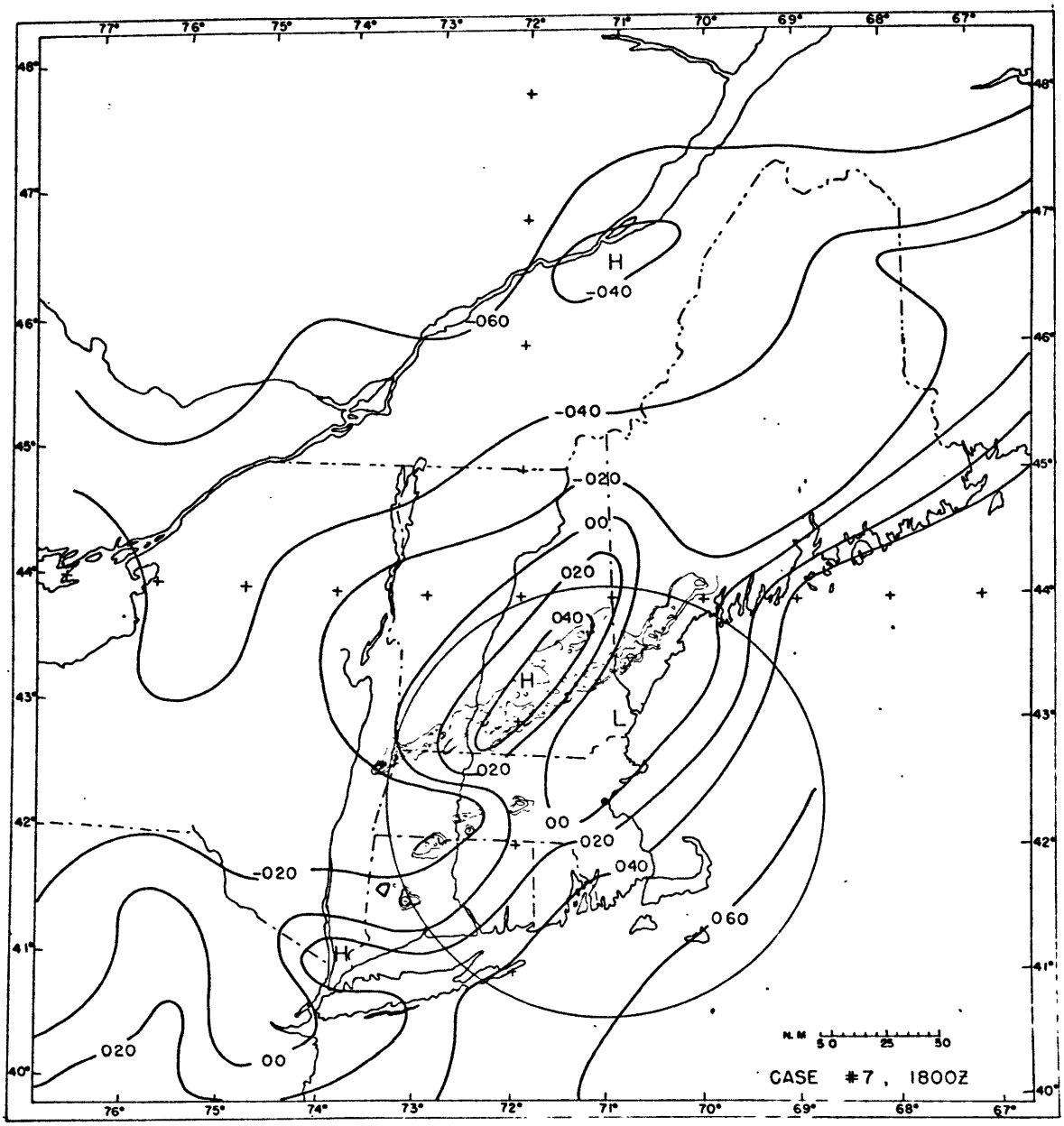

Figure 9: Residual Pressure Analysis-Case 7, 1800Z, 11 August 1971 - Isobars are labeled in thousandths of inches. Radar intensity isolines (fine lines) are for 2, 5, 7, 8, 9, and 10 db. Circle is 100 NM range from M.I.T. radar.

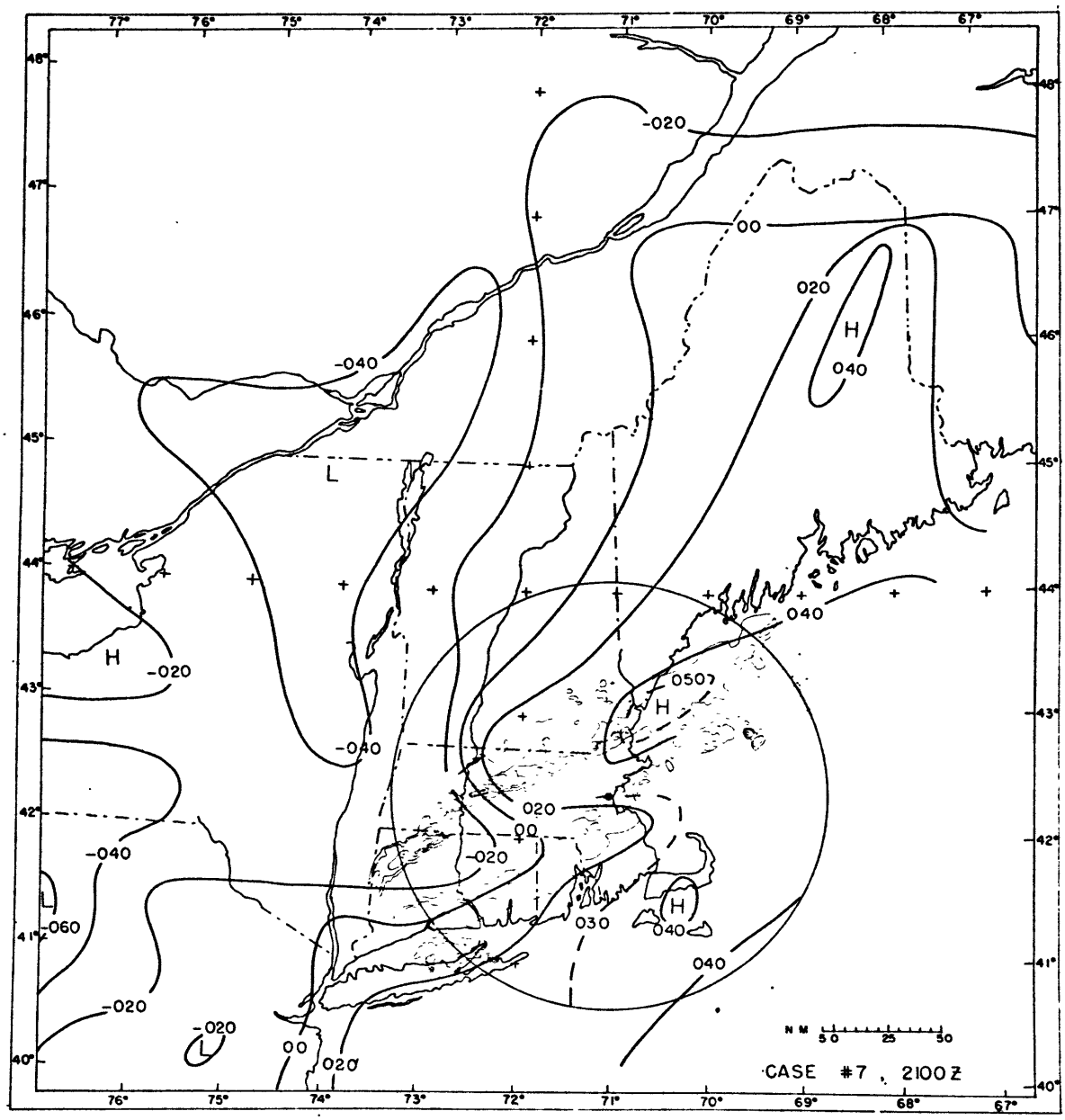

Figure 10: Residual Pressure Analysis-Case 7, 2100Z, 11 August 1971 - Isobars are labeled in thousandths of inches. Radar intensity isolines (fine lines) are for 2, 5, 7, 8, 9, and 10 db. Circle is 100 NM range from M.I.T. radar.

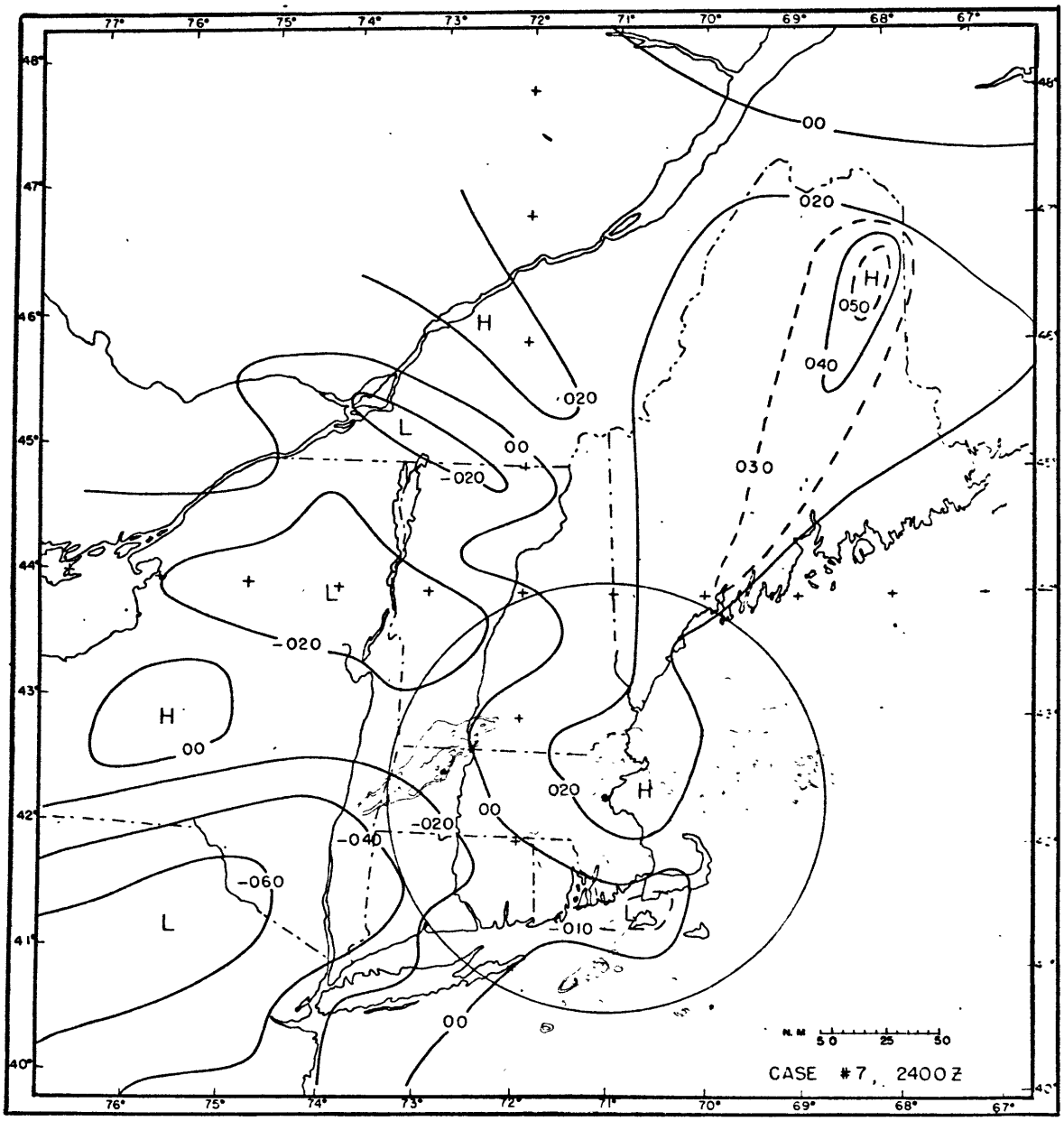

Figure 11: Residual Pressure Analysis-Case 7, 2400Z, 11 August 1971 - Isobars are labeled in thousandths of inches. Radar intensity isolines (fine lines) are for 2, 5, 7, 8, 9, and 10 db. Circle is 100 NM range from M.I.T. radar.

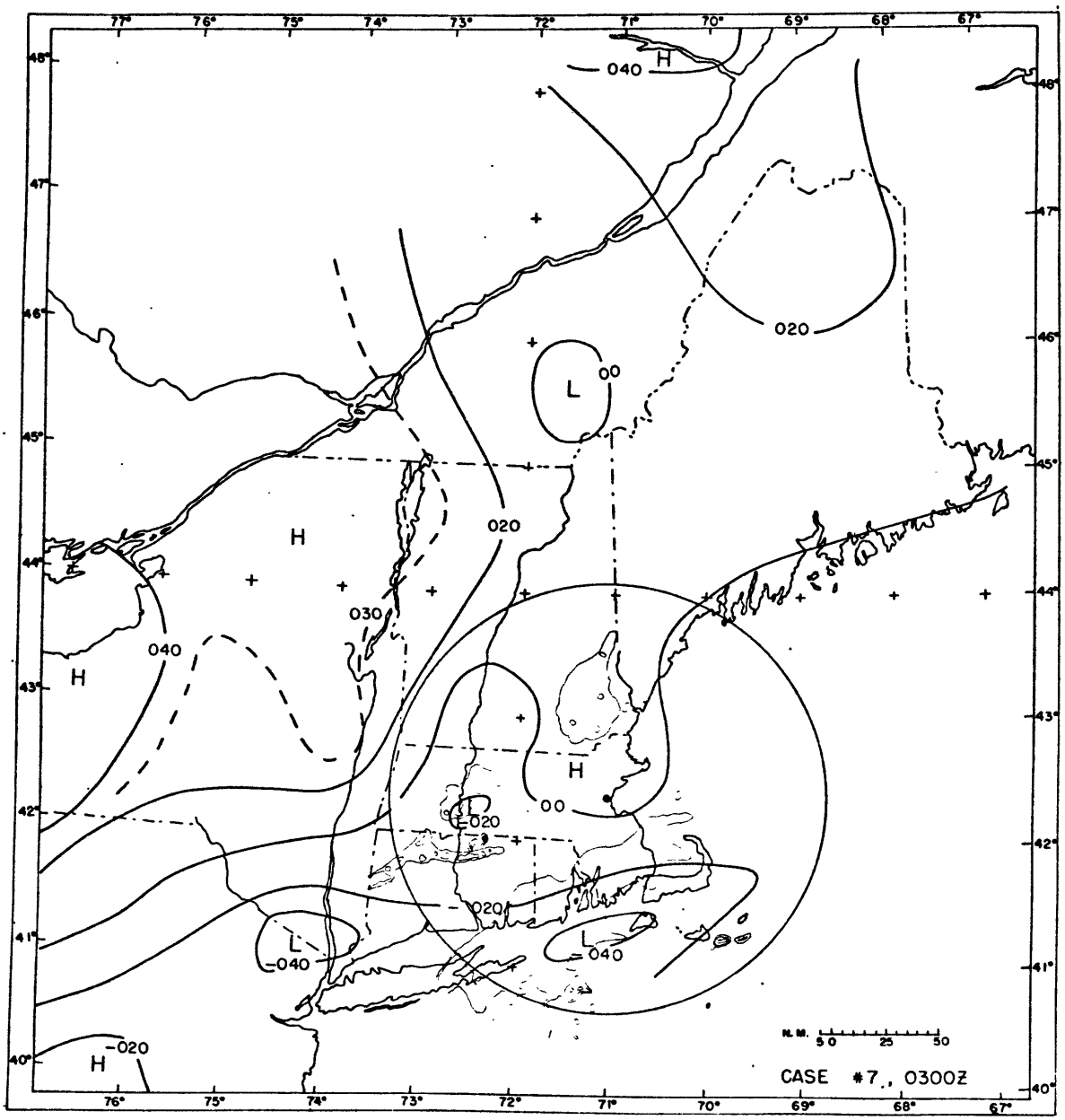

Figure 12: Residual Pressure Analysis-Case 7, 0300Z, 12 August 1971 - Isobars are labeled in thousandths of inches. Radar intensity isolines (fine lines) are for 2, 5, 7, 8, 9, and 10 db. Circle is 100 NM range from M.I.T. radar.

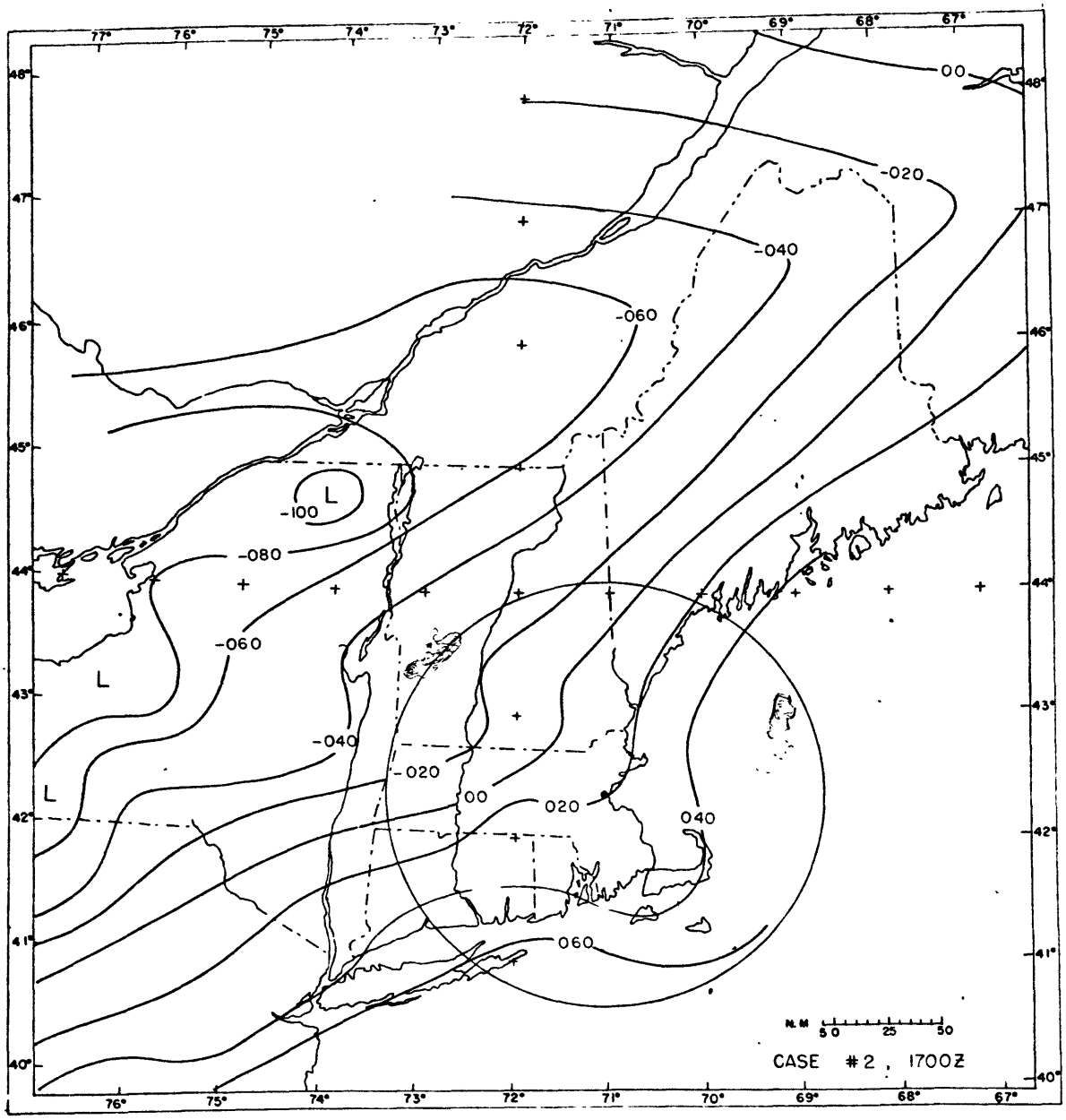

Figure 13: Residual Pressure Analysis-Case 2, 1700Z, 8 June 1971 - Isobars are labeled in thousandths of inches. Radar intensity isolines (fine lines) are for 2, 5, 7, 8, 9, and 10 db. Circle is 100 NM range from M.I.T. radar.

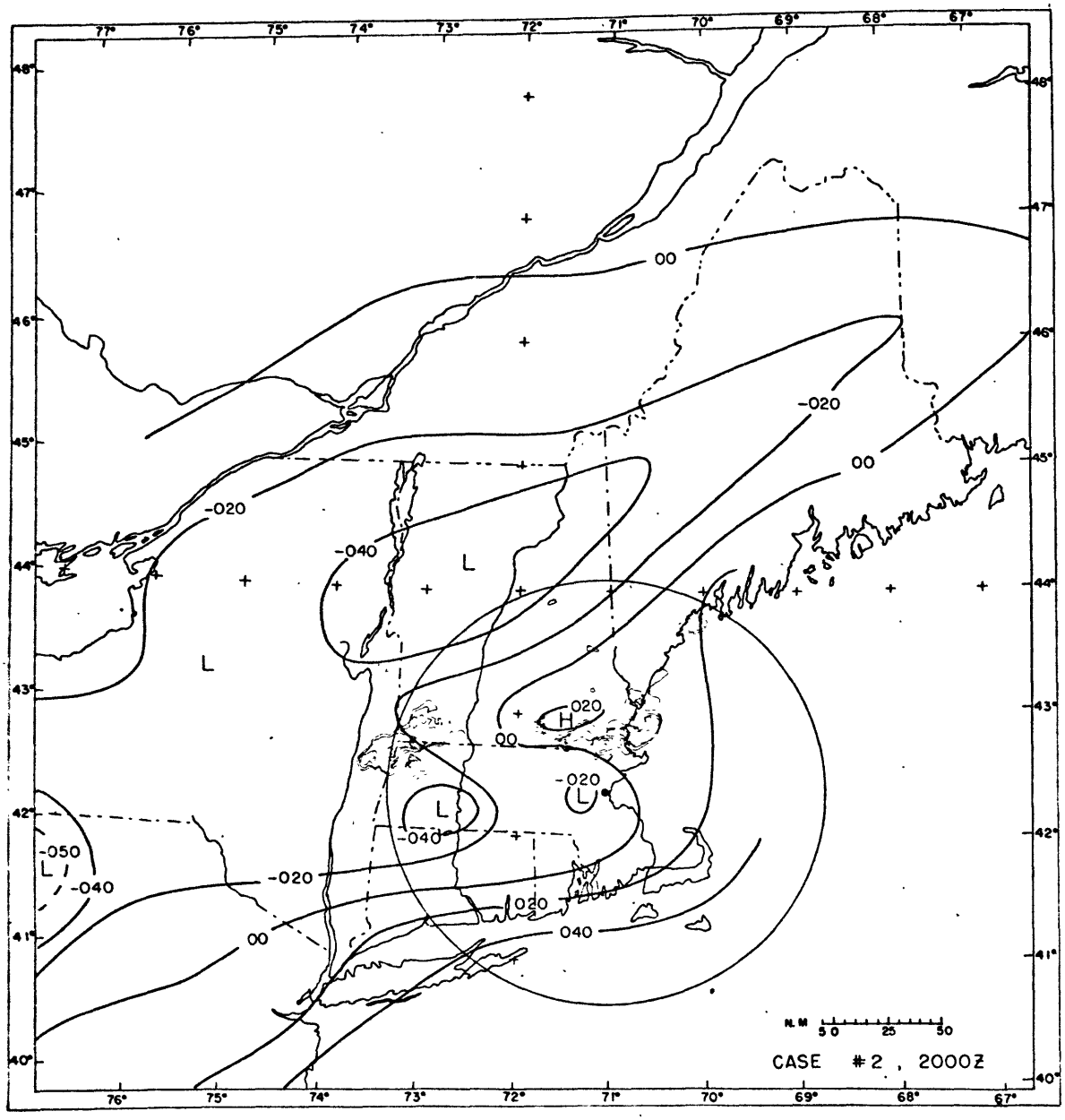

Figure 14: Residual Pressure Analysis-Case 2, 2000Z, 8 June 1971 - Isobars are labeled in thousandths of inches. Radar intensity isolines (fine lines) are for 2, 5, 7, 8, 9, and 10 db. Circle is 100 NM range from M.I.T. radar.

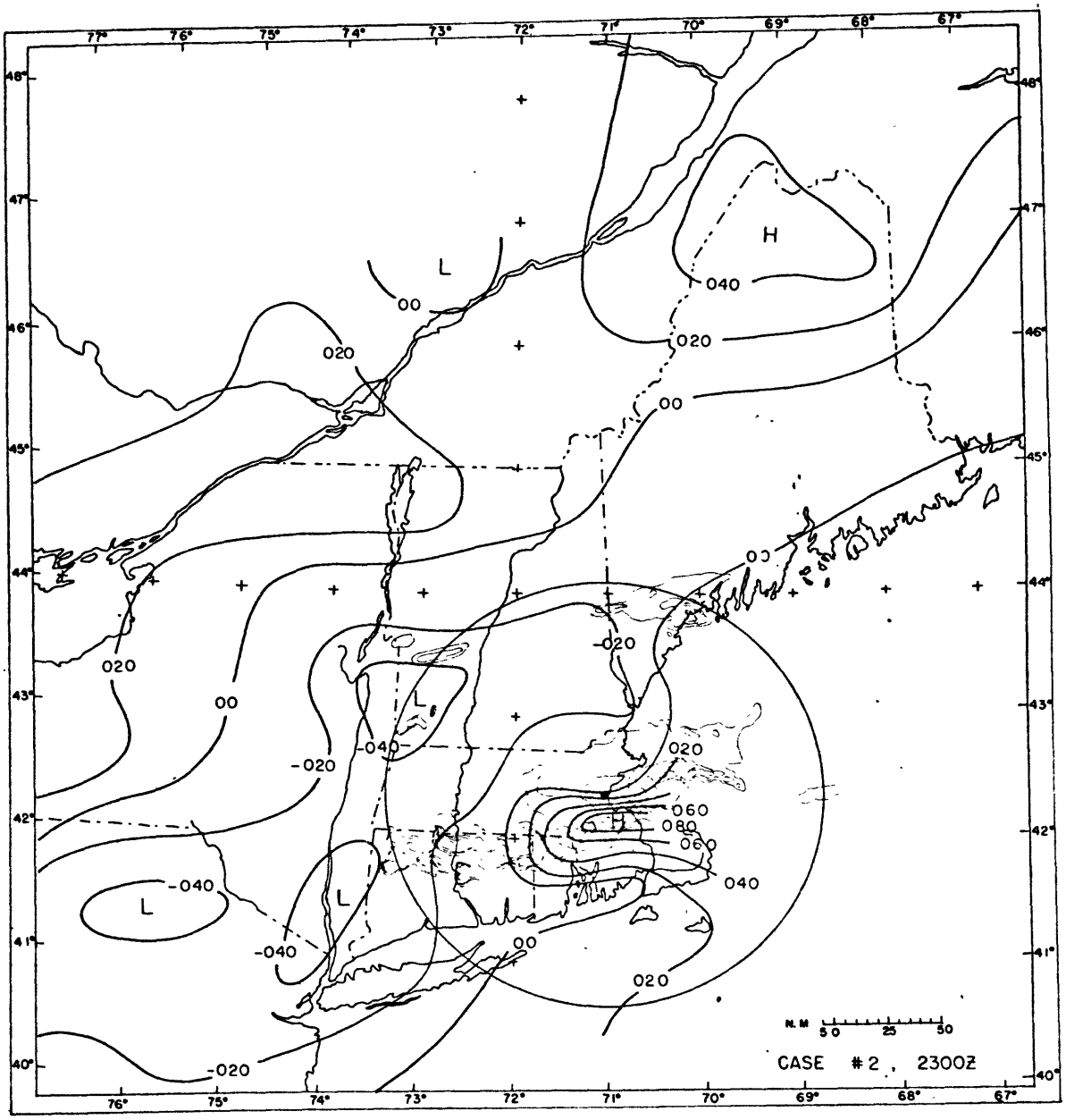

Figure 15: Residual Pressure Analysis-Case 2, 2300Z, 8 June 1971 - Isobars are labeled in thousandths of inches. Radar intensity isolines (fine lines) are for 2, 5, 7, 8, 9, and 10 db. Circle is 100 NM range from M.I.T. radar.

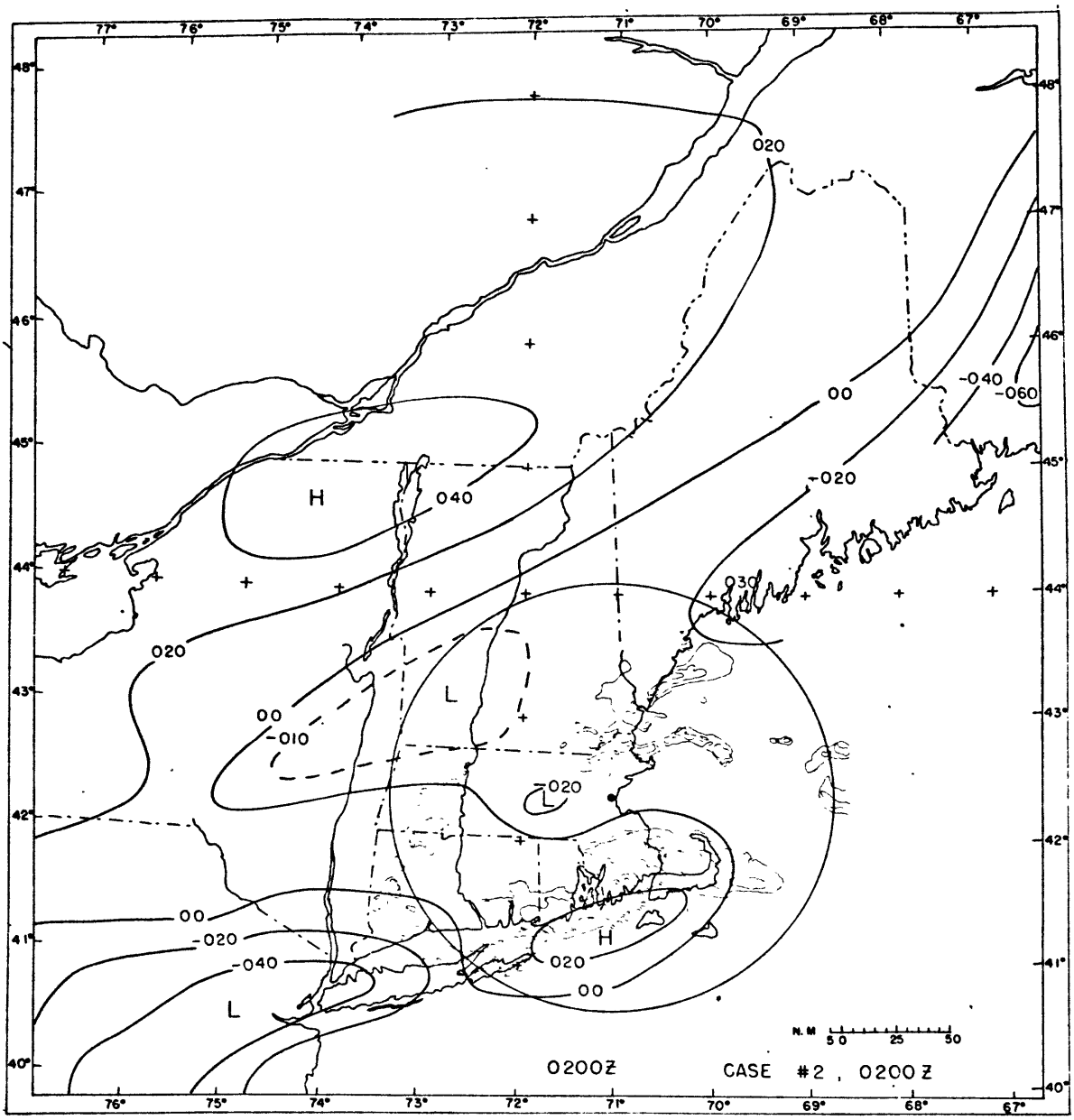

Figure 16: Residual Pressure Analysis-Case 2, 0200Z, 9 June 1971 - Isobars are labeled in thousandths of inches. Radar intensity isolines (fine lines) are for 2, 5, 7, 8, 9, and 10 db. Circle is 100 NM range from M.I.T. radar.

FIGURE 17

AREA MEAN PARAMETERS FOR TIME 7106260

LVL	UBAR (m/sec)	VBAR (m/sec)	SFC PRES (millibars)	TBAR (^{o}K)	QBAR (kg/kg)	DIV (m^2/sec)	PBAR(DIV) (sec^{-1})	OMEGA (mb/sec)
1	-0.99	0.19	656.18	218.03	0.0	-0.3456E+07	0.0	0.0
2	11.62	-0.74	4813.32	212.39	0.0	0.3289E+06	-0.1068E-04	0.5340E-03
3	24.38	2.06	2946.86	208.25	0.0	0.4238E+06	0.7256E-06	0.4977E-03
4	28.83	4.09	1624.70	216.95	0.0	0.2766E+07	0.7889E-05	0.1033E-03
5	23.71	5.57	555.14	227.43	0.0001325	0.5114E+07	0.2168E-04	-0.9805E-03
6	20.33	3.21	7038.44	237.85	0.0002720	0.2178E+07	0.1995E-04	-0.1978E-02
7	21.81	3.05	6233.11	245.99	0.0005812	0.3530E+07	0.1529E-04	-0.2743E-02
8	22.05	0.92	5509.56	252.99	0.0010386	0.2493E+07	0.1622E-04	-0.3554E-02
9	22.76	0.85	4856.01	258.77	0.0013167	-0.1048E+07	0.2760E-05	-0.3692E-02
10	20.26	1.33	4259.03	264.03	0.0016202	-0.4769E+06	-0.5971E-05	-0.3393E-02
11	18.08	1.22	3709.37	268.26	0.0023759	0.1155E+07	0.5073E-06	-0.3419E-02
12	16.69	3.24	3211.36	271.14	0.0034638	-0.1092E+07	-0.1302E-05	-0.3354E-02
13	15.95	1.51	2726.38	275.06	0.0045333	-0.1097E+07	-0.7923E-05	-0.2957E-02
14	15.02	2.06	2281.87	278.66	0.0053123	-0.5414E+06	-0.6374E-05	-0.2642E-02
15	15.51	4.25	1861.85	281.68	0.0063830	-0.1050E+07	-0.6167E-05	-0.2334E-02
16	13.55	6.20	1464.40	284.71	0.0075069	-0.2189E+07	-0.1101E-04	-0.1783E-02
17	10.81	6.31	1087.00	287.77	0.0092259	-0.1509E+07	-0.1236E-04	-0.1166E-02
18	8.35	7.94	726.94	290.82	0.0098610	-0.1296E+07	-0.9732E-05	-0.6789E-03
19	4.40	7.04	383.58	292.67	0.0106367	-0.5938E+06	-0.7041E-05	-0.3268E-03
20	-0.41	2.64	1004.13	292.46	0.0116250	-0.1295E+07	-0.7038E-05	-0.6286E-08

DIV is the level divergence multiplied by the area of study (1.7×10^{10} m^2).

PBAR(DIV) is the corrected average of the divergences at the levels bounding the layer.

0.99643E+03	0.49237E+02	-0.14974E-12	-0.18814E-12	0.20075E-02
-0.26428E-07	0.89763E-05	Surface Omega before correction to zero (mb/sec)	Average of the Level Omegas (mb/sec)	Average Magnitude of the Level Omegas (mb/sec)

Base pressure of Boundary Layer (mb)

Thickness of the Boundary Layer for the time span ending at this Z time (mb)

Average of the Layer Divergences (sec^{-1})

Average Magnitude of Layer Divergences (sec^{-1})

PAST WEATHER FROM SYNOPTIC OBS

	26/ 00Z	26/ 06Z
BOSTON,MA	1	9
CONCORD,NH	6	9

RESIDUE ARRAY FOR 12 HOUR PERIOD FROM 71062512 TO 71062600

FIGURE 18

LVL	C (DELTBAR / P(DELTIME	+ DIV(VT)	+ DEL(WT) / DELP)	-ADIABATIC COOLING	+L (DELQBAR / V(DELTIME	+ DIV(VQ)	+ DEL(WQ) / DELP)	= RES	P INTEGRAL OF RESIDUE
1	0.0	0.0	0.0	0.0	0.0	0.0	0.0	0.0	0.0
2	-0.01486	-3.97084	3.93382	-0.28117	0.0	0.0	0.0	-0.33304	-16.652
3	-0.02971	-0.76163	0.73697	-0.50373	0.0	0.0	0.0	-0.55809	-44.557
4	-0.00764	3.93519	-3.75246	-0.25538	0.0	0.0	0.0	-0.08030	-48.571
5	0.02246	7.50939	-7.63494	0.15521	0.00284	0.00122	-0.00540	0.05478	-45.833
6	0.02996	6.50262	-7.03825	0.51973	0.00865	0.00003	-0.01626	0.00648	-45.509
7	0.03424	4.87339	-5.51282	0.72117	0.01755	-0.00329	-0.04397	0.08626	-41.196
8	0.04246	3.83121	-4.49764	0.81812	0.02613	-0.01101	-0.11164	0.09764	-36.313
9	0.05111	0.80424	-1.43102	0.82485	0.02694	-0.02688	-0.08474	0.16450	-28.088
10	0.05535	-0.58017	0.05344	0.75961	0.02516	-0.04110	-0.06467	0.20763	-17.707
11	0.05415	-0.98306	-0.54879	0.69328	0.02956	-0.03512	-0.16064	0.11559	-11.927
12	0.03442	-1.01843	0.62164	0.63251	0.04916	-0.10668	-0.15732	0.05532	-9.161
13	0.02422	-2.03838	1.65519	0.55611	0.09698	-0.21611	-0.31706	0.16094	-6.114
14	0.04009	-1.78060	1.51754	0.48105	0.14626	-0.25379	-0.32157	0.12897	0.334
15	0.06687	-2.24168	2.04835	0.41274	0.18957	-0.26191	-0.30784	0.23611	10.640
16	0.09341	-3.67293	3.45098	0.33566	0.17395	-0.27726	-0.17193	-0.06813	7.234
17	0.09825	-4.55923	4.31225	0.24813	0.16752	-0.31127	0.15263	0.10827	12.647
18	0.07951	-4.43317	4.24692	0.16388	0.22049	-0.33298	0.24341	0.18805	22.050
19	0.05701	-3.95014	3.85255	0.09224	0.22596	-0.29019	0.18682	0.17424	30.762
20	0.05443	-3.97062	3.94116	0.02999	0.14773	-0.32339	0.26112	0.13939	37.625

0.39717E-01
Mean of the Layer Residues

0.14914E+00
Mean Magnitude of Layer Residues

Residues and their components in kj/ton/sec

Integral of Residues in mb·kj/ton/sec

PAST WEATHER FROM SYNOPTIC OBS

TIME	25/ 12Z	25/ 18Z	26/ 00Z	26/ 06Z
BOSTON, MA	1	Ø	1	9
CONCORD, NH	1	1	6	9

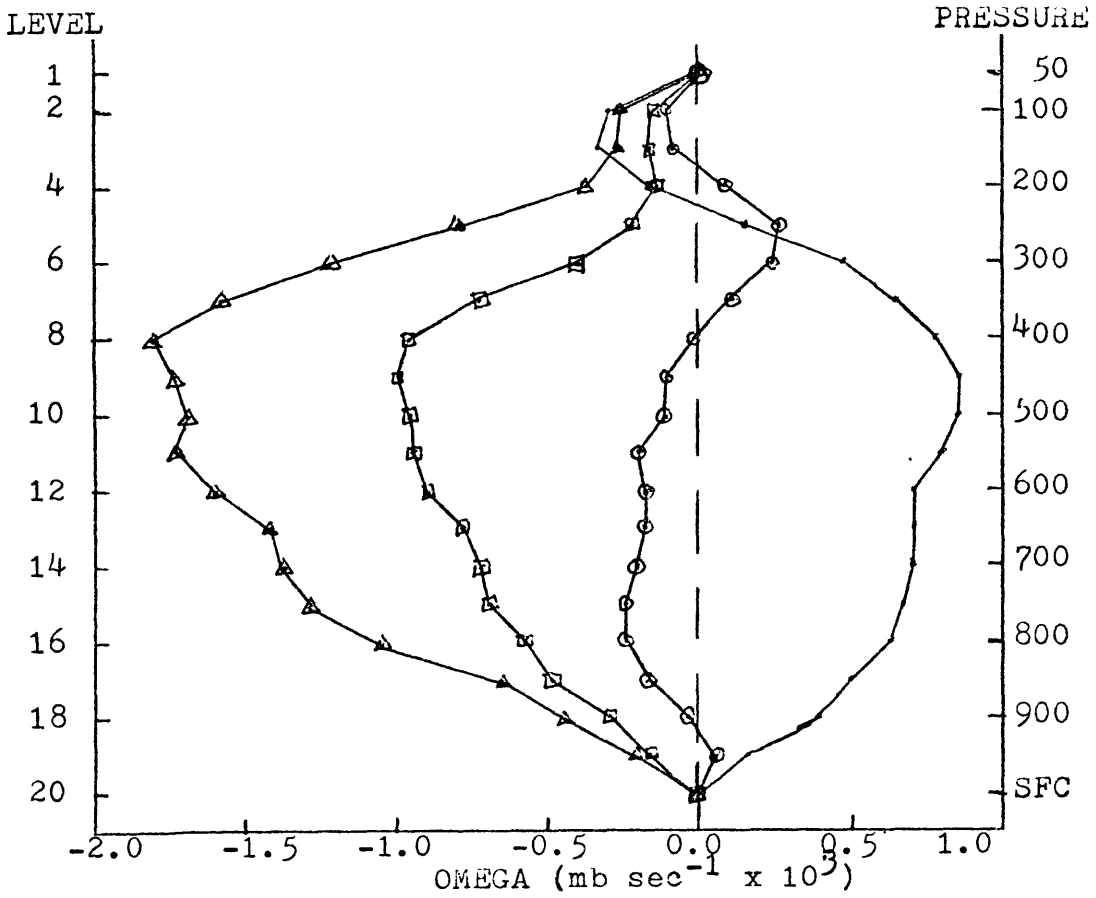

Figure 19: Vertical Composite Omega Profiles - • No Weather Day, ⊙ No Weather Night, △ Weather Day, ⊡ Weather Night.

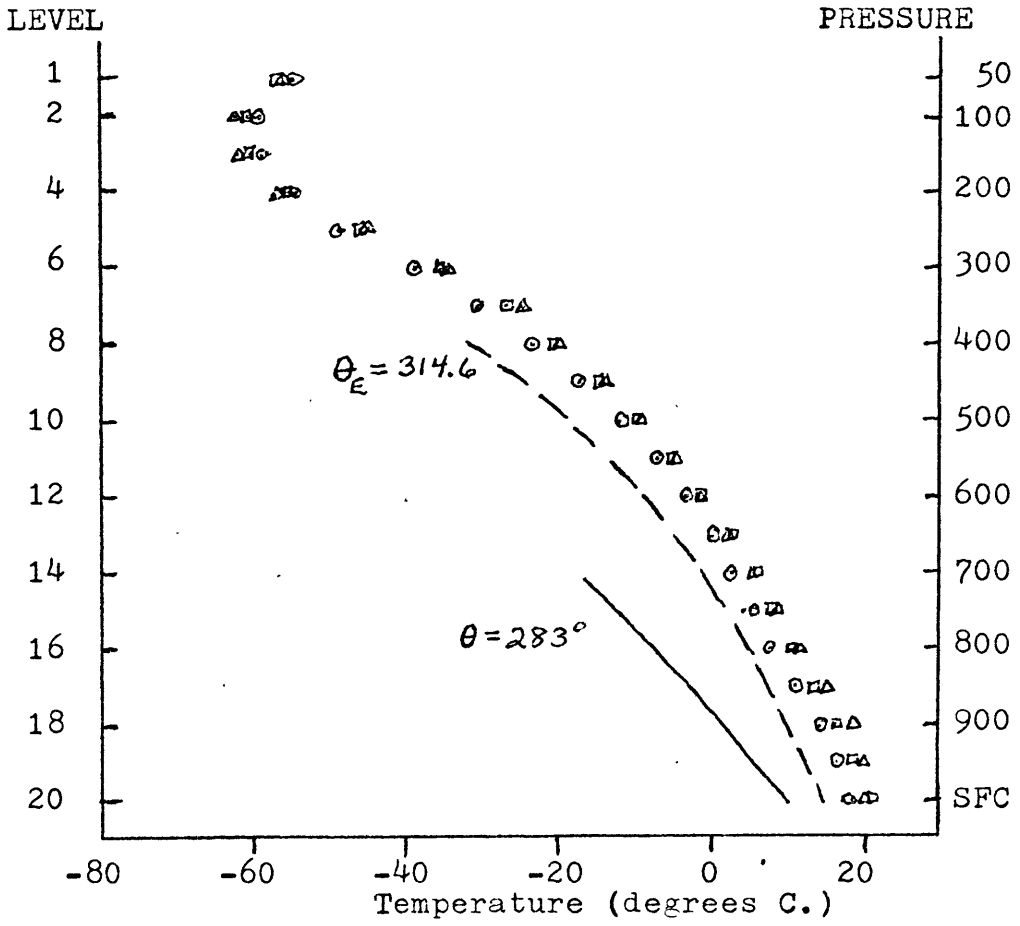

Figure 20: Vertical Composite Temperature Profile - • No Weather Day, ⊙ No Weather Night, ◬ Weather Day, ⊡ Weather Night.

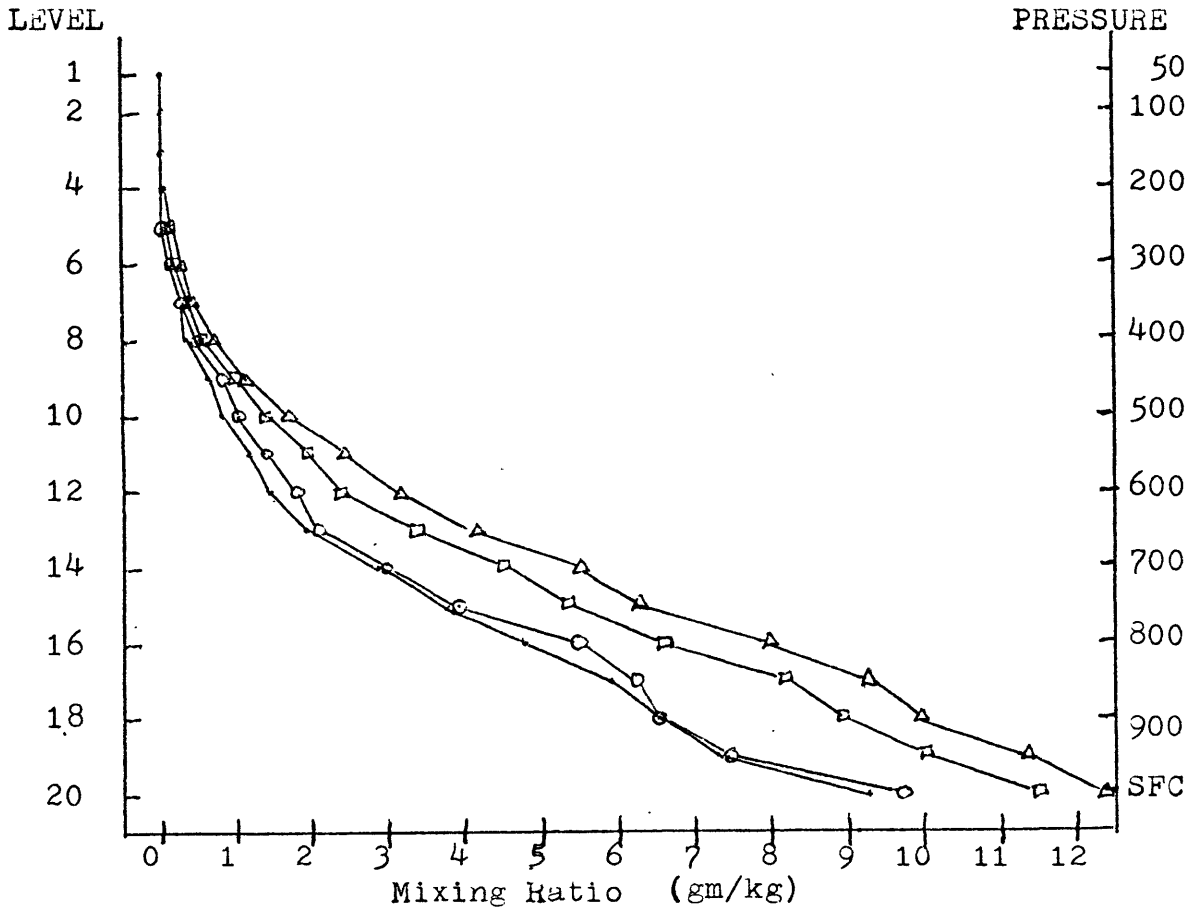

Figure 21: Vertical Composite Mixing Ratio Profiles - • No Weather Day, ⊙ No Weather Night, ▲ Weather Day, ▣ Weather Night.

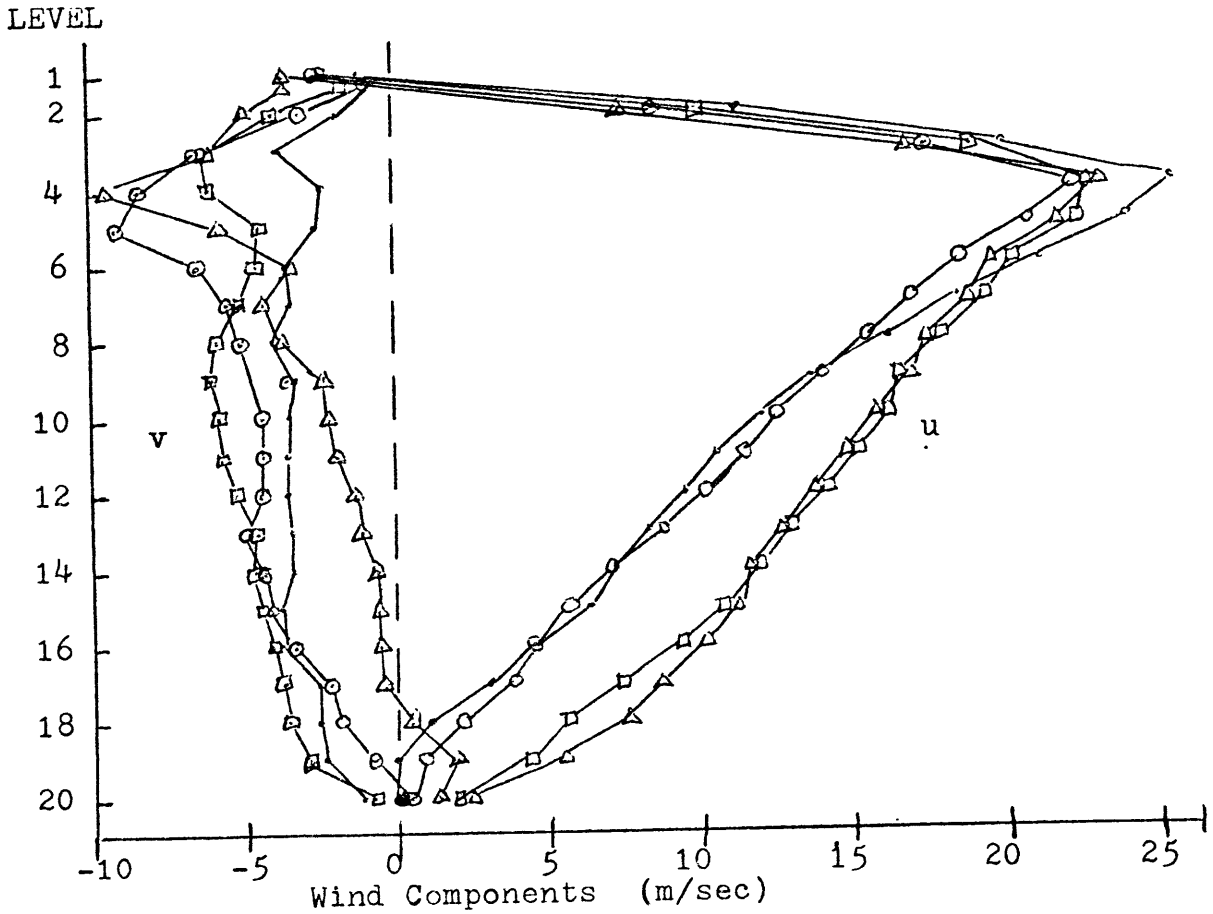

Figure 22: Vertical Composite Wind Component Profiles - • No Weather Day, ⊙ No Weather Night, ▲ Weather Day, ▣ Weather Night.

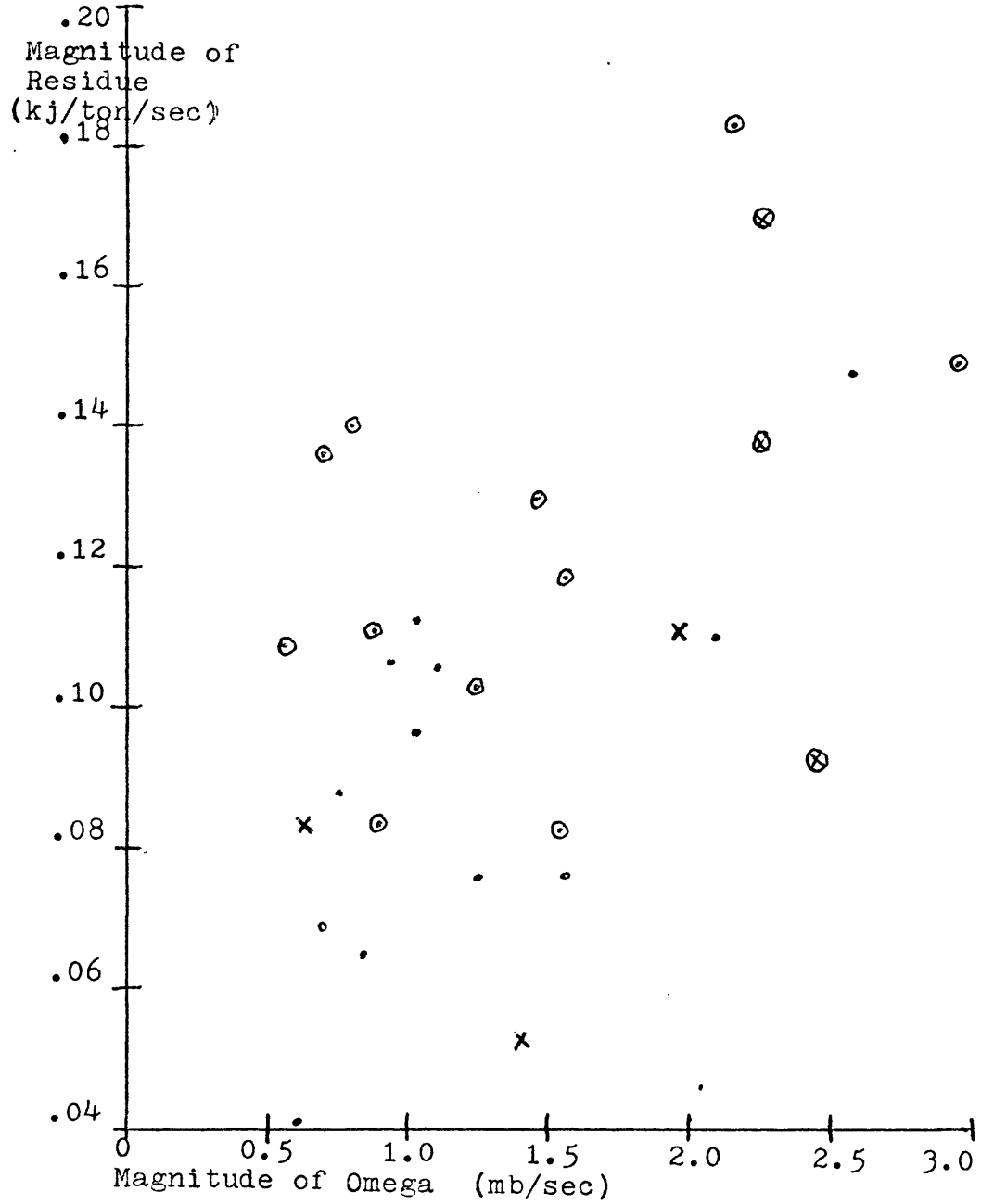

Figure 23: Scattergram of Residue and Omega Mean Magnitudes - • Clean Data, X Incomplete data, circled = Weather case, uncircled = No Weather case.

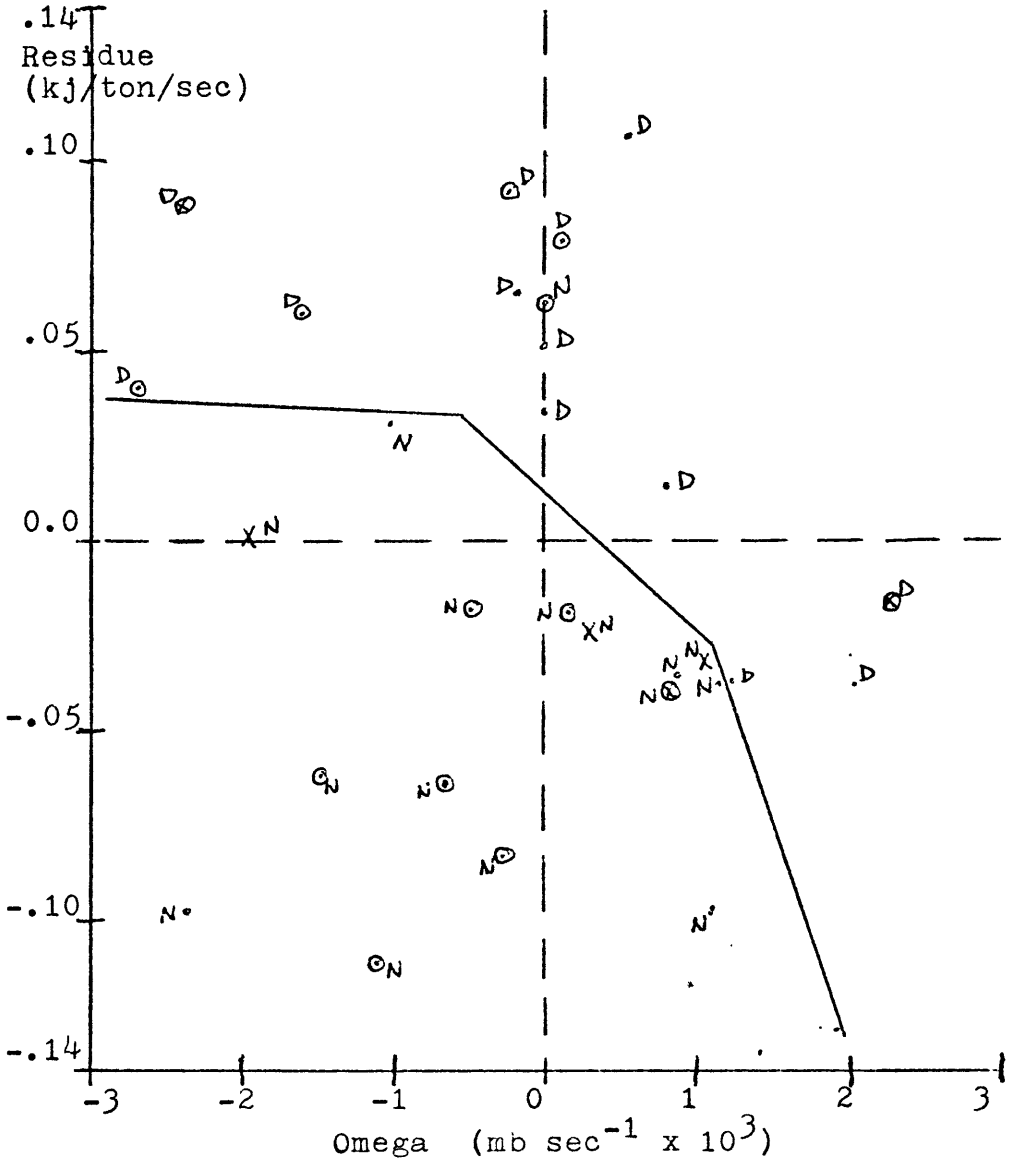

Figure 24: Scattergram of Residue and Omega Algebraic Means - • Clean Data, X Incomplete data, circled = Weather case, uncircled = No Weather case, D = Day case, N = Night case.

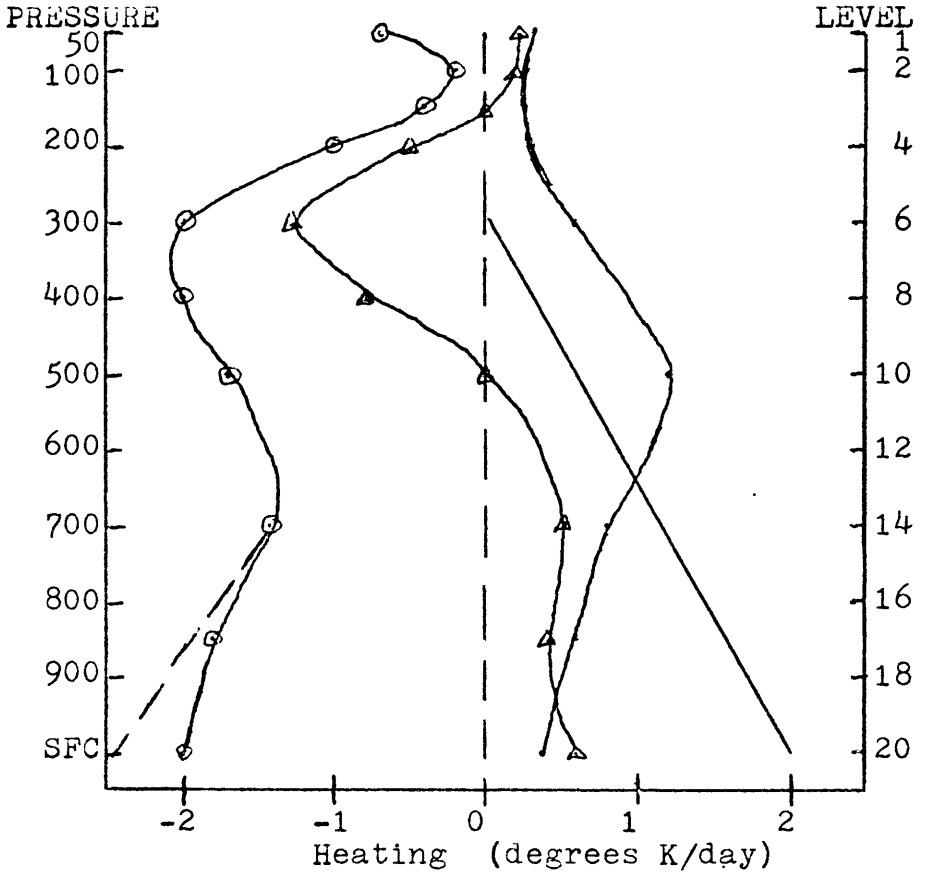

Figure 25: Radiational Heating Profiles - see text for references to sources; ⊙ nightime radiational heating, • solar absorption heating, ▲ total daytime heating; dashed lines are estimated heating by transfer from the ground.

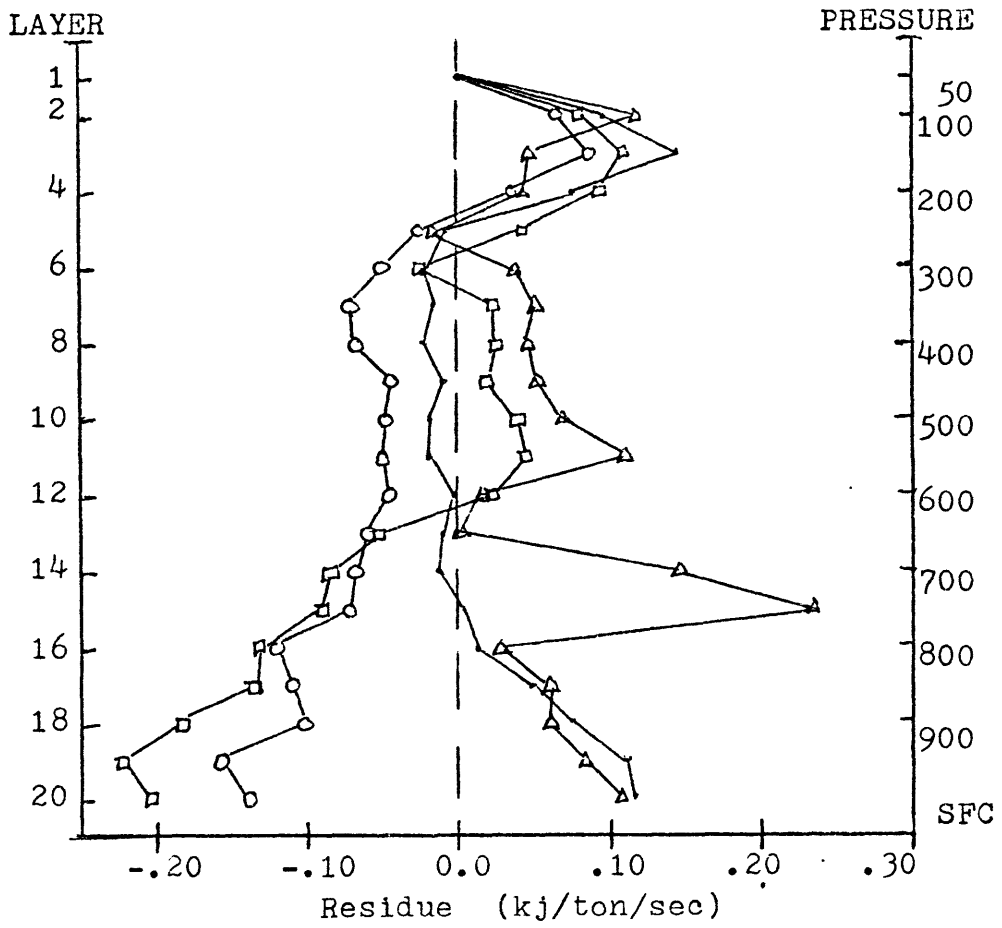

Figure 26: Vertical Composite Residue Profiles - • No Weather Day, ⊙ No Weather Night, ⧋ Weather Day, ⧈ Weather Night.

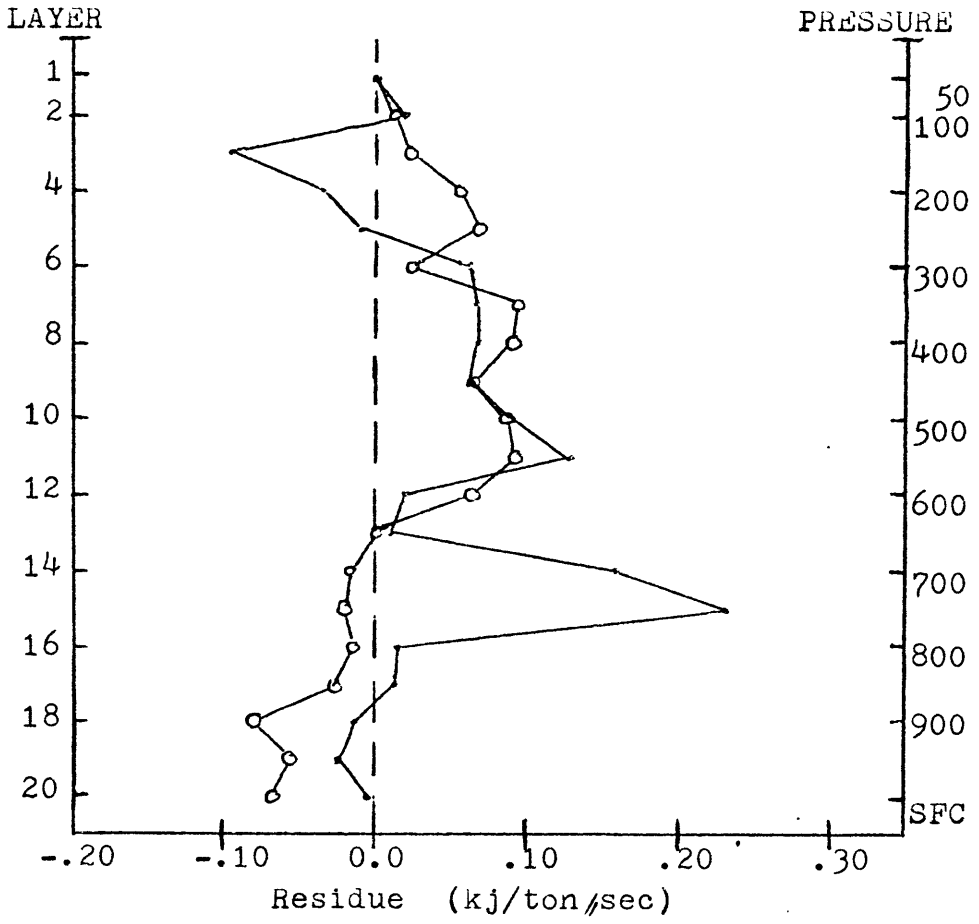

Figure 27: Vertical Composite Profiles of Residue Differences - • Day profile, ⊙ Night profile.

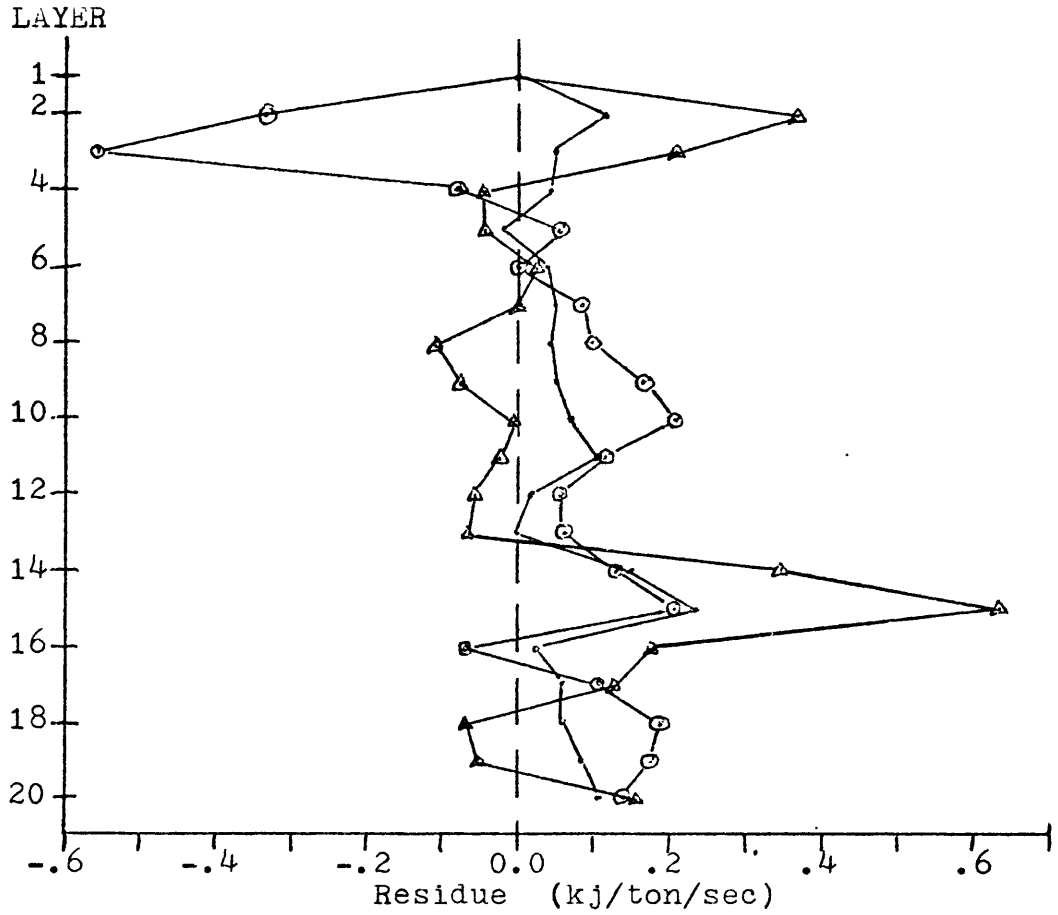

Figure 28: Individual Case Residue Profiles - · Composite profile for Weather Day cases, ⊙ profile for case of 1200Z-2400Z 25 June 1971, △ profile for case of 1200Z-2400Z 21 July 1972.